Online Monitoring of Loading-Space Instability in Large Factor Models via Self-Normalized DFT Spectral Scores

Jiajing Sun* Yongmiao Hong†

March 2, 2026

Abstract

We propose an online (sequential) procedure for detecting factor loading–space instability in large approximate factor models using discrete Fourier transform (DFT) spectral scores. After estimating baseline loadings on a clean Phase I window, each incoming panel observation is projected onto the frozen loading space to produce a DFT spectral score curve, which is mapped to a fixed-dimensional real score vector by low-frequency grid vectorization or frequency-domain functional principal component analysis. To avoid bandwidth-sensitive long-run variance estimation and bootstrap calibration in sequential settings, we develop two tuning-lean self-normalized monitors: a Shao-type quadratic self-normalized statistic (SSMS) and an adjusted-range self-normalized statistic (RSMS). For each we provide Kolmogorov–Smirnov (KS)-type and Cramér–von Mises (CvM)-type stopping rules, establish pivotal null limits and power properties, and show how to obtain critical values by simulating the limiting Brownian-motion functionals. Monte Carlo experiments under abrupt, smooth, heterogeneous, and staggered loading changes show that self-normalization delivers substantially more stable false-alarm control than heteroskedasticity and autocorrelation consistent studentization, which can be severely oversized at short horizons. Among KS-type rules, RSMS improves late-break detection and shortens conditional detection delays; for CvM-type rules, SSMS with a late-emphasis weight offers a favorable size–power compromise. Additional experiments indicate that adjusted-range self-normalization is more resilient when the training window is mildly contaminated. An empirical illustration using the Federal Housing Finance Agency (FHFA) metro house price index panel signals an alarm at 2005Q1 and reveals heterogeneous metro-level shifts in factor exposures.

Keywords: approximate factor model; sequential monitoring; discrete Fourier transform; self-normalization; loading instability.

JEL: C12; C22; C33; C38; R31.

*MOE Social Science Laboratory of Digital Economic Forecasts and Policy Simulation, and School of Economics and Management, University of Chinese Academy of Sciences, Zhongguancun Nanyitiao, Haidian District, Beijing 100190, China. Correspondence author. Email: jiajing.sun@gmail.com.

†Academy of Mathematics and Systems Science, Chinese Academy of Sciences, No. 55 Zhongguancun East Road, Haidian District, Beijing 100190, China. Email: yh20@cornell.edu.

1 Introduction

Large-dimensional factor models are a workhorse for summarizing information in macroeconomic and financial panels: a small number of latent forces can explain the co-movement of hundreds of series, enabling forecasting, nowcasting, and policy analysis. Canonical diffusion-index and principal component analysis (PCA) approaches exploit this idea and have become standard in empirical work (e.g. Stock and Watson, 2002a,b; Bai and Ng, 2002; Bai, 2003). A maintained assumption in much of the literature is that the factor loading space is stable over time. In practice, however, the mapping from observables to latent factors can evolve with policy regime shifts, crises, financial innovation, or measurement changes; such loading instability can distort PCA-based factor extraction and weaken downstream inference and prediction (e.g. Stock and Watson, 2009; Bai and Han, 2016; Fu et al., 2023).

This paper focuses on loading instability detection in a sequential/online setting: given a clean training window, we monitor streaming panel observations and stop as soon as there is evidence that the loading space has changed. From a practitioner's perspective, factor models are rarely an end in themselves: once estimated, they are typically deployed as plug-in inputs for real-time forecasting and nowcasting systems, risk monitoring, and policy analysis. In these applications, the key issue is not only how well the model fits the training window, but also when the estimated mapping from observables to latent forces ceases to be reliable. If the loading space drifts, factor extraction based on the pre-estimated loadings can become contaminated, leading to silent forecast deterioration and potentially misleading counterfactuals or scenario assessments. This motivates an online change-detection perspective: as new panel observations arrive, we continuously test the validity of the trained loading space and raise an alarm as soon as there is statistically meaningful evidence of change. Such an alarm provides an objective trigger to update the factor representation—e.g., re-estimating loadings and factors, revising the set of series, or switching to an alternative specification—thereby enabling adaptive forecasting and more credible real-time policy and stress/scenario analysis. A sequential testing rule is particularly attractive because it formalizes the trade-off between rapid detection and false alarms, which is central in real-time model maintenance. Methodologically, our approach combines two complementary compressions: the factor structure aggregates information across the cross section to boost signal-to-noise, while Fourier projections aggregate information over time in an orthogonal multi-scale basis, producing a compact but information-rich score stream for sequential monitoring.

A frequency-domain viewpoint is particularly natural for instability detection. The DFT is an orthogonal (unitary) change of basis: it reorganizes the entire time-domain score path into frequency components, so any departure from stability—whether an abrupt break, a smooth drift, or more oscillatory misspecification—must leave a footprint in at least some Fourier coefficients. This yields a genuinely multi-scale, omnibus diagnostic that does not privilege a particular break date and avoids selecting a finite lag order.

DFTs and periodogram-based residual diagnostics are classical tools in time-series analysis (e.g. Durbin, 1969; Brillinger, 1969). In econometrics, Hong (1996, 1999, 2000) develop a generalized

spectral framework—built on Fourier transforms and empirical characteristic functions—that yields omnibus Kolmogorov–Smirnov (KS)/Cramér–von Mises (CvM)-style diagnostics without selecting a finite lag order; see also Hong and Lee (2003, 2005) for influential extensions. More recently, Fu and Hong (2019) show that discrete Fourier transforms can also be used to construct consistent tests for structural change, providing global sensitivity to both abrupt and smooth departures while sidestepping unknown break dates. In large factor models, Fu et al. (2023) further establish a sharp "zero vs. nonzero spectrum" dichotomy for factor-weighted residuals: under stable loadings the DFT empirical process is asymptotically centered, whereas loading variation induces systematic Fourier components. These features make Fourier-score objects especially attractive online: they provide low-dimensional, nearly orthogonal summaries whose null behavior is amenable to pivotal self-normalized sequential calibration.

The sequential setting introduces additional challenges: (i) we need a stopping rule with controlled false-alarm probability over a monitoring horizon, and (ii) we want to avoid long-run variance (LRV) estimation (kernel/bandwidth/block choices), which is notoriously unstable in early monitoring and in high dimensions. Standard sequential cumulative sum (CUSUM)-type monitors typically rely on studentization by a heteroskedasticity and autocorrelation consistent (HAC) estimator of the LRV, which can be sensitive to tuning choices and persistent dependence (Newey and West, 1987; Andrews, 1991; Kiefer and Vogelsang, 2005; Müller, 2007).

Self-normalization (SN) offers a tuning-lean alternative by replacing the unknown LRV with a data-dependent self-normalizer that is (asymptotically) stochastically proportional to it, yielding pivotal or near-pivotal null limits. The idea traces back to Student's t statistic (Student, 1908): although the sample variance is not a perfect proxy for the population variance, it is randomly proportional to it and hence can self-normalize the statistic. For dependent data, SN development long lagged behind HAC inference because econometric practice largely focused on improving HAC-type LRV estimators and their asymptotics. A modern time-series SN theory was initiated by Shao (2010); see Shao (2015) for a review and further references. Since its introduction, time-series SN has become a widely used device for inference without explicit LRV estimation. It has been applied to confidence interval construction, tests for autocorrelation and model specification, and inference in the presence of structural change. The core idea has also been extended beyond standard time series to more complex settings, including censored outcomes, functional and spatial data, and alternating- or regime-switching dependence structures. Applications now span economics and finance as well as a range of environmental and health-science domains; see Hong et al. (2024) for a concise literature review.

Despite its size robustness, classical SN based on the quadratic variation of partial sums (Shao's (2010) SN) can suffer from the familiar "better size but less power" phenomenon, and can even exhibit non-monotonic power for KS-type change-point statistics because the SN factor may inflate rapidly as shifts grow (Shao and Zhang, 2010; Hong et al., 2024). These power issues are especially consequential online: repeated testing makes it difficult to guarantee a perfectly clean training window, so mild contamination by undetected (borderline) changes—and the accompanying Type II

errors—is practically hard to avoid and can delay alarms.

Adjusted-range-based self-normalization (AR-SN) addresses this issue by replacing the quadratic SN factor with the squared adjusted range of partial sums (Hong et al., 2024, 2025). Because range-type normalizers rely on extrema of partial sums rather than quadratic aggregation, they are often viewed as more robust in heavy-tailed environments, including settings where second moments may be unstable or infinite (Mandelbrot, 1972, 1975). In the retrospective setting, Hong et al. (2024) show that adjusted-range self-normalized KS statistics avoid the non-monotonicity of Shao and Zhang (2010) while delivering power comparable to their proposed G-type change-point statistic, but with far simpler computation and without estimating the number of breaks. Subsequent work has expanded AR-SN to censored-dependent-data inference (Sun et al., 2022), autocorrelation testing (Sun et al., 2025), and structural stability of functional data (Sun et al., 2025); in the sequential setting, Zhu et al. (2025) provide theory and simulation evidence that adjusted-range KS monitors achieve materially higher power and shorter detection delays, especially when the training window is mildly contaminated.

The contribution of this paper is as follows. First, we develop a sequential monitoring framework for online factor instability built around frequency-domain information: we construct a streaming DFT spectral score curve by projecting each incoming panel observation onto the baseline loading space estimated from a Phase-I window, and we provide practical dimension-reduction schemes—either frequency-grid vectorization or (recommended) frequency-domain functional principal component analysis (fPCA)—that map the score curve into a fixed-dimensional real score vector suitable for online monitoring. Second, to avoid bandwidth and lag choices inherent in LRV estimation, we introduce two tuning-lean self-normalized sequential monitoring statistics, namely the sequential monitoring statistic based on Shao's (2010) quadratic SN (SSMS) and the sequential monitoring statistic based on adjusted-range SN (RSMS), and for each we develop both KS-type (supremum) and CvM-type (integrated) stopping rules to let practitioners trade off fast detection against power for late or diffuse changes. Third, we establish pivotal null limit theory and characterize power properties for the proposed sequential procedures, and we provide a practical calibration strategy based on Monte Carlo simulation of the associated Brownian-motion functionals; simulation experiments and an Federal Housing Finance Agency (FHFA) house-price panel illustration further indicate that SN yields markedly more reliable false-alarm control than HAC studentization in sequential settings while offering strong late-break performance when paired with adjusted-range SN or with appropriate CvM weighting. Fourth, motivated by the fact that offline screening can miss small instabilities, we study robustness to mild Phase-I contamination: we give a simple sufficient condition under which local training contamination does not affect the pivotal null limits, and we provide targeted Monte Carlo evidence (Appendix E.2) showing that adjusted-range SN remains closer to the clean-training benchmark and preserves post-break detection in this borderline regime, where training-window changes are small enough to be plausibly included by accident. Fifth, we discuss the open-end benchmark $T = \infty$ in Appendix B: we show how the finite-horizon Brownian-motion limits extend as $T \to \infty$ for KS- and CvM-type rules, and we clarify the role of

horizon-decaying weights in preventing inevitable false alarms for open-end CvM monitoring.

The remainder of the paper is organized as follows. Section 2 introduces the factor-model setting, the sequential hypotheses, and the DFT spectral-score construction. Section 3 presents the self-normalized SSMS/RSMS monitoring rules, including KS- and CvM-type variants. Section 4 establishes pivotal null limits and power results, and discusses implementation details. Sections 5–6 provide simulation studies and an empirical illustration, respectively. Finally, Section 7 concludes and outlines future directions of research.

2 Model and monitoring objective

This section formalizes the monitoring problem. We introduce the approximate factor-model setting, state the sequential null and alternatives (stable loadings in the training window and potential loading instability thereafter), and construct the DFT-based spectral score objects that feed our monitoring statistics. We also describe how to reduce the score curve to a fixed-dimensional real vector so that the subsequent self-normalized monitoring theory applies directly.

We work in the standard large-N approximate factor-model regime with a fixed number of factors. We impose a set of sufficient conditions—largely standard in the factor-model and frequency-domain literature—that justify the PCA training-step and the DFT-score construction used below (see, e.g., Bai and Ng, 2002; Bai, 2003; Fu et al., 2023).

Assumption 1 (Factors). *$\{F_t\}$ is weakly stationary with $\mathbb{E}F_t = 0$, $\mathbb{E}(F_t F_t^\top) = \Sigma_F$ positive definite, and $\sup_t \mathbb{E}\|F_t\|^{4+\delta} < \infty$ for some $\delta > 0$.*

Assumption 2 (Pervasive loadings and identification). *The baseline loadings $\Lambda_0 = (\lambda_{10}, \ldots, \lambda_{N0})^\top$ satisfy $\max_{1\le i\le N} \|\lambda_{i0}\| \le C$ and $N^{-1}\Lambda_0^\top\Lambda_0 \to \Sigma_\Lambda$ with Σ_Λ positive definite. Moreover, the eigenvalues of $\Sigma_F\Sigma_\Lambda$ are distinct, so the loading space is identified up to rotation.*

Assumption 3 (Idiosyncratic component). *$\{\varepsilon_t\}$ has $\sup_{i,t} \mathbb{E}|\varepsilon_{it}|^{4+\delta} < \infty$ for some $\delta > 0$ and weak dependence (serial and cross-sectional) sufficient for a functional central limit theorem for the score vectors constructed below. In particular, cross-sectional dependence is weak enough that $N^{-1}\sum_{i=1}^N \varepsilon_{it}^2 = O_p(1)$ uniformly in t, and factor–idiosyncratic interactions admit central limit theorem (CLT)-type behavior.*

Assumption 4 (Fourier weights). *The weight $W : \mathbb{R} \to \mathbb{R}_+$ used to define the frequency-domain inner product is symmetric, continuous, and integrable with $\int_{\mathbb{R}} |u|^4 W(u)\, du < \infty$.*

Assumption 2 is the usual pervasiveness condition: each factor loads on many series, so the leading eigenvectors of the training covariance identify the loading space. Assumptions 1 and 3 impose weak dependence and moments to ensure that (i) PCA estimation error is small on the training window and (ii) the resulting DFT-based score vectors satisfy an invariance principle. Assumption 4 ensures the Fourier-score curves belong to the relevant L^2 space and that frequency-domain projections (grid reduction or fPCA) are well behaved.

2.1 Approximate factor model and sequential hypotheses

Let $\{X_t\}_{t\geq 1}$ be an N-dimensional panel observed sequentially, with

$$X_t = \Lambda_t F_t + \varepsilon_t, \qquad t = 1, 2, \ldots, \tag{1}$$

where $F_t \in \mathbb{R}^K$ is the latent factor vector, $\Lambda_t \in \mathbb{R}^{N\times K}$ is the loading matrix, and $\varepsilon_t \in \mathbb{R}^N$ is the idiosyncratic component. The factor dimension K is fixed as $N \to \infty$.[1] We allow weak cross-sectional and serial dependence in ε_t.

We assume a training sample of size m is stable:

$$\Lambda_t = \Lambda_0, \qquad t = 1, \ldots, m.$$

Starting from time $t = m + 1$, we monitor whether Λ_t remains stable. The monitoring horizon is mT for some fixed $T \in (0, \infty]$. In most applications the monitoring period is specified in advance and therefore $T < \infty$ (closed-end monitoring); this is also the empirically relevant case in our simulations, where we consider horizons up to $T = 10$. The open-end case $T = \infty$ (monitoring indefinitely without a pre-specified terminal time) is mainly a theoretical benchmark and is discussed in Appendix B; because indefinite monitoring is typically unrealistic in practice, we restrict attention in the main text to finite-T asymptotics. A change-point occurs at $t^\star = m + k^\star$ (unknown), after which Λ_t may change:

$$H_0 : \ \Lambda_t = \Lambda_0 \ \ \forall t \leq m + mT \qquad \text{vs} \qquad H_1 : \ \Lambda_t \neq \Lambda_0 \ \ \text{for some } t > m.$$

Both abrupt and smooth loading changes are permitted.

2.2 A Fourier viewpoint: "zero vs nonzero spectrum"

A useful starting point is the frequency-domain DFT empirical-process representation of factor-weighted residuals studied by Fu et al. (2023). Related DFT-based structural-change tests for time series models are developed in Fu and Hong (2019). Under the no-change null, estimate a factor model (e.g. by PCA), obtaining factor estimates $\widehat{F}_t$ and residuals $\widehat{\varepsilon}_{it}$. For a frequency parameter $u \in \mathbb{R}$, define a complex Fourier regressor (demeaned across t)

$$\varphi_t(u) \equiv e^{\mathrm{i}2\pi ut/T} - T^{-1}\sum_{s=1}^{T} e^{\mathrm{i}2\pi us/T},$$

[1] The factor number K can be selected from the training window via information criteria (e.g. Bai and Ng, 2002) or a fixed economic choice. For the DFT frequency-grid vectorization in Section 2.3, a modest number of frequencies (e.g. $J \in \{3, \ldots, 10\}$) often works well; for larger J, frequency-domain fPCA is recommended.

and the complex-valued DFT empirical process

$$\widehat{A}(u) \equiv \frac{1}{NT} \sum_{i=1}^{N} \sum_{t=1}^{T} \widehat{F}_t \, \widehat{\varepsilon}_{it} \, \varphi_t(u) \in \mathbb{C}^K. \tag{2}$$

Under loading stability, $\widehat{A}(u)$ has an asymptotically "zero spectrum" in the sense that its mean vanishes (after accounting for estimation error), whereas under time-varying loadings it exhibits nonzero spectral features. The frequency-domain representation is appealing because Fourier regressors form an (approximately) orthogonal basis on the observation grid: projecting factor-weighted residuals onto sinusoids provides a global scan for a wide range of departures (abrupt breaks, smooth drifts, or mixtures) without pre-specifying break dates or local windows. Fu et al. (2023) aggregate this spectrum via an integrated energy statistic

$$\widehat{D} \equiv NT \int_{\mathbb{R}} \left\| \widehat{A}(u) \right\|^2 W(u) \, du, \tag{3}$$

for a weighting function $W : \mathbb{R} \to \mathbb{R}_+$ (e.g. Gaussian/Laplace density). Offline calibration of such integrated spectrum statistics is generally nonpivotal and often relies on resampling. Our approach in Section 2.3 uses a time-indexed version of (2) as an online spectral-score curve and monitoring statistics its finite-dimensional reductions using pivotal SN.

Let $X_{1:m} = [X_1, \ldots, X_m]^\top \in \mathbb{R}^{m \times N}$ denote the training panel. We estimate the baseline loading space using PCA on the training window. Let

$$\widehat{\Sigma}_m = \frac{1}{m} X_{1:m}^\top X_{1:m} \in \mathbb{R}^{N \times N},$$

and let $\widehat{U}_K \in \mathbb{R}^{N \times K}$ be the matrix of eigenvectors corresponding to the largest K eigenvalues $\widehat{\lambda}_1 \geq \cdots \geq \widehat{\lambda}_K$. Define

$$\widehat{\Lambda}_0 = \widehat{U}_K \widehat{\Gamma}_K^{1/2}, \qquad \widehat{\Gamma}_K = \mathrm{diag}(\widehat{\lambda}_1, \ldots, \widehat{\lambda}_K). \tag{4}$$

This normalization yields $\widehat{\Lambda}_0^\top \widehat{\Lambda}_0 = \widehat{\Gamma}_K$ (diagonal).

For any new observation X_t (including in training), define the out-of-sample projected factor and residual using the baseline loadings:

$$\widetilde{F}_t = (\widehat{\Lambda}_0^\top \widehat{\Lambda}_0)^{-1} \widehat{\Lambda}_0^\top X_t = \widehat{\Gamma}_K^{-1/2} \widehat{U}_K^\top X_t, \qquad \widetilde{\varepsilon}_t = X_t - \widehat{\Lambda}_0 \widetilde{F}_t. \tag{5}$$

These are computationally light: $\widetilde{F}_t$ costs $O(NK)$ per time point.

Remark 1 (Rotation)**.** *Factor models are identified only up to a $K \times K$ rotation. The monitoring scores below can be designed to be rotation-robust (e.g. by "square-first" aggregation), so sequential procedures do not depend on a particular factor rotation.*

A key design choice is a low-dimensional score vector $\psi_t \in \mathbb{R}^q$ (q fixed) whose mean is (approximately) zero under H_0 and becomes nonzero under loading instability. This transforms a

high-dimensional structural change problem into sequential monitoring of a fixed-dimensional time series.

2.3 Fourier/DFT spectral score curves

We now construct the online DFT spectral-score curves used for monitoring. Define a (horizon-dependent) demeaned Fourier regressor for $u \in \mathbb{R}$ by

$$\varphi_{t,mT}(u) \equiv e^{\mathrm{i}2\pi ut/(mT)} - (mT)^{-1} \sum_{s=1}^{mT} e^{\mathrm{i}2\pi us/(mT)}.$$

Using the frozen training-window projection (5), define the K-dimensional complex spectral score curve

$$\eta_t(u) \equiv \frac{1}{N} \sum_{i=1}^{N} \widetilde{F}_t \, \widetilde{\varepsilon}_{it} \, \varphi_{t,mT}(u), \qquad u \in \mathbb{R}. \tag{6}$$

Under H_0 and suitable conditions, $\mathbb{E}\eta_t(\cdot) \approx 0$ ("zero spectrum"); under H_1, $\mathbb{E}\eta_t(\cdot)$ carries Fourier coefficients of loading variation.

Define the running-average DFT score curve, for each monitoring time $k = 1, 2, \ldots, mT$,

$$\widehat{A}_m(k, u) \equiv \frac{1}{k} \sum_{t=m+1}^{m+k} \eta_t(u). \tag{7}$$

One could also monitor an integrated spectrum-energy functional such as $Nk \int_{\mathbb{R}} \left\| \widehat{A}_m(k,u) \right\|^2 W(u)\, du$, but its null distribution is typically nonpivotal. Instead, we apply self-normalized sequential monitoring to finite-dimensional reductions of the curve-valued score process.

To implement self-normalized monitoring, we convert the (possibly complex-valued) DFT score curves into a q-dimensional real vector ψ_t using either frequency-grid vectorization or frequency-domain functional PCA.

Choose frequencies $u_1, \ldots, u_J$ and define the complex vector $\boldsymbol{\eta}_t = (\eta_t(u_1)', \ldots, \eta_t(u_J)')' \in \mathbb{C}^{KJ}$. Convert to real form by stacking real and imaginary parts, yielding $\psi_t \in \mathbb{R}^q$ with $q = 2KJ$.

View $\eta_t(\cdot)$ as an element of a weighted Hilbert space $\mathbb{H}$ with inner product $\langle f, g \rangle_{\mathbb{H}} \equiv \int_{\mathbb{R}} f(u)^* g(u)\, W(u)\, du$, where * denotes complex conjugate transpose. Let $\mathcal{C}$ be the covariance operator of η_t under H_0, with eigenfunctions $\{v_\ell\}$ and eigenvalues $\{\kappa_\ell\}$. Estimate (v_ℓ, κ_ℓ) from the training window and define complex principal component scores

$$\xi_{t\ell} \equiv \langle \eta_t, \widehat{v}_\ell \rangle_{\mathbb{H}}, \qquad \ell = 1, \ldots, q_0.$$

Stack $\Re(\xi_{t\ell})$ and $\Im(\xi_{t\ell})$ to obtain a real $q = 2q_0$-vector ψ_t. Because eigenfunctions are orthogonal, the score covariance is approximately diagonal, which is convenient for RSMS.

From here on, $\{\psi_t\}$ denotes the DFT-based real q-dimensional score sequence obtained from (6) by either frequency-grid vectorization or frequency-domain functional PCA in Section 2.3. All

self-normalized monitoring statistics below apply once ψ_t is fixed.

Define the centered training mean and monitoring partial sums:

$$\bar{\psi}_m = \frac{1}{m}\sum_{t=1}^{m}\psi_t, \qquad \phi_t = \psi_t - \bar{\psi}_m, \qquad S_m(k) = \sum_{t=m+1}^{m+k}\phi_t, \quad k \geq 1. \tag{8}$$

The sequential statistics in Sections 3 depend on $\{S_m(k)\}$ and a self-normalizer estimated from the training window.

3 Self-normalized sequential monitoring

This section builds the sequential stopping rules from the score stream. We first present SSMS, the sequential monitoring statistic based on Shao's (2010) quadratic SN, and then RSMS, the sequential monitoring statistic based on adjusted-range-based SN, together with a training-window prewhitening step for cross-coordinate dependence. We finally introduce CvM/integral-type variants and discuss the roles of the boundary exponent γ and the CvM weight function $w(\cdot)$.

3.1 Shao-type quadratic self-normalization (SSMS)

Quadratic SN uses the training partial sums of ϕ_t to form

$$D_m = \frac{1}{m^2}\sum_{t=1}^{m}\left(\sum_{j=1}^{t}\phi_j\right)\left(\sum_{j=1}^{t}\phi_j\right)^{\top} \in \mathbb{R}^{q\times q}. \tag{9}$$

The SSMS KS-type monitoring statistic at time $m+k$ is

$$\mathcal{M}_m^{\mathrm{S}}(k) = \frac{S_m(k)^{\top}D_m^{-1}S_m(k)}{m(1+k/m)^2\left(\frac{k}{k+m}\right)^{2\gamma}}, \qquad k = 1,\ldots,mT, \quad \gamma \in [0,1/2). \tag{10}$$

Here, γ is a boundary exponent/tuning parameter that controls the amount of early-monitoring downweighting. The factor $\left(\frac{k}{k+m}\right)^{2\gamma}$ stabilizes the statistic for very small k (early monitoring). Setting $\gamma = 0$ recovers the recovers the standard SSMS statistic. The corresponding stopping time is

$$\mathcal{T}_m^{\mathrm{S}} = \inf\left\{1 \leq k \leq mT:\ \mathcal{M}_m^{\mathrm{S}}(k) > c_\alpha^{\mathrm{S}}(T,q,\gamma)\right\}. \tag{11}$$

Crucially, for fixed γ the asymptotic null distribution of $\sup_{1\leq k\leq mT}\mathcal{M}_m^{\mathrm{S}}(k)$ is pivotal and can be tabulated via Brownian-motion simulation for each (T,q,γ).

3.2 Adjusted-range self-normalization (RSMS)

Adjusted-range SN replaces D_m by a componentwise adjusted-range normalizer. Because the self-normalizer is diagonal, pivotality requires (approximate) diagonal instantaneous covariance

across score components. When $\mathrm{Cov}(\phi_t)$ is not diagonal, we recommend a partial prewhitening step based on the training window.

Step 1: estimate component covariance from the training window. Let

$$\widehat{\Sigma}_{\phi,0} = \frac{1}{m}\sum_{t=1}^{m}(\phi_t - \bar{\phi}_m)(\phi_t - \bar{\phi}_m)^\top, \qquad \bar{\phi}_m = \frac{1}{m}\sum_{t=1}^{m}\phi_t. \tag{12}$$

This is a lag-0 covariance estimate and does not require any bandwidth choice.

Step 2: spectral-decomposition-based whitening (orthogonal + scaling). Let $\widehat{\Sigma}_{\phi,0} = \widehat{Q}\widehat{D}\widehat{Q}^\top$ be the eigen-decomposition with $\widehat{D} = \mathrm{diag}(\widehat{d}_1, \ldots, \widehat{d}_q)$ and orthogonal $\widehat{Q}$. Define the whitening matrix

$$\widehat{W}_m = \widehat{D}_\eta^{-1/2}\widehat{Q}^\top, \qquad \widehat{D}_\eta = \mathrm{diag}(\widehat{d}_1 + \eta, \ldots, \widehat{d}_q + \eta), \tag{13}$$

where $\eta > 0$ is a small ridge for numerical stability. Then set

$$\widetilde{\phi}_t = \widehat{W}_m\phi_t, \qquad \widetilde{S}_m(k) = \sum_{t=m+1}^{m+k}\widetilde{\phi}_t. \tag{14}$$

This step removes cross-coordinate contemporaneous dependence (approximately). Serial dependence remains and is handled by SN.

Step 3: adjusted-range self-normalizer (with the $m^{-1/2}$ scaling). Let the centered training partial-sum bridge of component ℓ be

$$\widetilde{B}_{m,\ell}(t) = \sum_{j=1}^{t}\widetilde{\phi}_{j,\ell} - \frac{t}{m}\sum_{j=1}^{m}\widetilde{\phi}_{j,\ell}, \qquad t = 1, \ldots, m,$$

and define the (scaled) adjusted range

$$\widetilde{R}_{m,\ell} = m^{-1/2}\Big(\max_{1\le t\le m}\widetilde{B}_{m,\ell}(t) - \min_{1\le t\le m}\widetilde{B}_{m,\ell}(t)\Big), \qquad \widetilde{R}_m = \mathrm{diag}(\widetilde{R}_{m,1}, \ldots, \widetilde{R}_{m,q}). \tag{15}$$

The RSMS KS-type monitoring statistic is

$$\widetilde{\mathcal{M}}_m^{\mathrm{R}}(k) = \frac{\widetilde{S}_m(k)^\top\widetilde{R}_m^{-2}\widetilde{S}_m(k)}{m(1+k/m)^2\left(\frac{k}{k+m}\right)^{2\gamma}}, \qquad \gamma \in [0, 1/2), \tag{16}$$

and the stopping time is

$$\mathcal{T}_m^{\mathrm{R}} = \inf\Big\{1 \le k \le mT : \ \widetilde{\mathcal{M}}_m^{\mathrm{R}}(k) > c_\alpha^{\mathrm{R}}(T, q, \gamma)\Big\}.$$

The factor $\left(\frac{k}{k+m}\right)^{2\gamma}$ stabilizes very early monitoring (small k) and is standard in sequential adjusted-range SN.

Note that we only prewhiten cross-component contemporaneous covariance using $\widehat{\Sigma}_{\phi,0}$. Serial dependence is handled by SN, so we do not estimate a LRV matrix, instead a sample estimate suffices. This preserves the "no bandwidth/tunning" advantage while restoring approximate pivotality for RSMS in many applications.

3.3 CvM / integral-type sequential monitoring statistics

KS-type monitoring uses a running maximum and often exhibits small detection delay, but quadratic SN may suffer a "better size but less power" phenomenon. An integral-type (CvM-like) sequential statistic accumulates evidence over time and could potentially reduce this power loss.

Throughout this subsection we set the boundary exponent $\gamma = 0$ in the underlying KS-type statistics (i.e., we drop the factor $\left(\frac{k}{k+m}\right)^{2\gamma}$) and focus on the choice of weight function $w(\cdot)$.

3.3.1 CvM-SSMS

Define the integrated SSMS statistic

$$\mathcal{I}_m^{\mathrm{S}}(k) = \frac{1}{m}\sum_{j=1}^{k} w\left(\frac{j}{m}\right)\, \mathcal{M}_m^{\mathrm{S}}(j), \qquad k = 1, \ldots, mT, \tag{17}$$

where $w : [0, T] \to \mathbb{R}_+$ is a deterministic weight function (default $w \equiv 1$ for closed-end monitoring). The CvM-type stopping time is

$$\mathcal{T}_{m,\mathrm{CvM}}^{\mathrm{S}} = \inf\left\{1 \le k \le mT :\ \mathcal{I}_m^{\mathrm{S}}(k) > c_{\alpha,\mathrm{CvM}}^{\mathrm{S}}(T, q)\right\}. \tag{18}$$

3.3.2 CvM-RSMS

Similarly, define

$$\mathcal{I}_m^{\mathrm{R}}(k) = \frac{1}{m}\sum_{j=1}^{k} w\left(\frac{j}{m}\right)\, \widetilde{\mathcal{M}}_m^{\mathrm{R}}(j), \qquad \mathcal{T}_{m,\mathrm{CvM}}^{\mathrm{R}} = \inf\left\{1 \le k \le mT :\ \mathcal{I}_m^{\mathrm{R}}(k) > c_{\alpha,\mathrm{CvM}}^{\mathrm{R}}(T, q)\right\}. \tag{19}$$

Remark 2 (Open-end monitoring and weights)**.** *For $T = \infty$, the unweighted integral typically diverges under H_0. For open-end CvM monitoring, one needs a decaying weight with finite mass, $\int_0^\infty w(s)\, ds < \infty$; for example $w(s) = (1+s)^{-\eta}$ with $\eta > 1$ or $w(s) = e^{-\eta s}$. See Appendix B for a brief theoretical discussion.*

4 Asymptotic theory for DFT-based monitoring

This section gives the null and power theory for the KS- and CvM-type SSMS/RSMS monitoring statistics in Sections 3.1–3.3, specialized to the DFT-based score construction in Section 2.3. Proofs of the results in this section are collected in Appendix D.

Let $\{\psi_t\}$ be the (DFT-based) q-dimensional score vector, and let $\bar{\psi}_m$, ϕ_t, and $S_m(k)$ be defined in (8). Write $\mu := \mathbb{E}(\psi_t)$, which is constant under H_0 (and typically $\mu = 0$ for centered DFT scores).

Assumption 5 (Training-window stability)**.** *The training window is change-free:* $\Lambda_t = \Lambda_0$ *for* $t = 1, \ldots, m$.

Assumption 5 ensures the self-normalizers are computed from a stable baseline and therefore have a fixed (nonrandom) target law under H_0.

Assumption 6 (Sequential invariance principle under H_0)**.** *Under* H_0*, there exists a positive definite matrix* $\Sigma \in \mathbb{R}^{q\times q}$ *and a standard* q*-dimensional Brownian motion* $\{B_q(r) : 0 \le r \le 1+T\}$ *such that*

$$\left\{ \frac{1}{\sqrt{m}} \sum_{t=1}^{\lfloor mr \rfloor} (\psi_t - \mu) \right\}_{0\le r\le 1+T} \Rightarrow \left\{ \Sigma^{1/2} B_q(r) \right\}_{0\le r\le 1+T} \quad \text{in } D([0, 1+T], \mathbb{R}^q). \tag{20}$$

Assumption 6 is the key null requirement. It is a functional CLT for the fixed-dimensional score vectors; it is implied by many weak-dependence conditions and is the minimal input needed for pivotal SN limits.

Assumption 7 (Negligibility of training-based estimation and projection error)**.** *Let* $\psi_t^{(0)}$ *denote the infeasible DFT score vector obtained by replacing* $(\widetilde{F}_t, \widetilde{\varepsilon}_t)$ *and (if used) estimated frequency-domain fPCA objects by their population counterparts under* H_0*. Then, uniformly in* $r \in [0, 1+T]$*,*

$$\sup_{0\le r\le 1+T} \left\| \frac{1}{\sqrt{m}} \sum_{t=1}^{\lfloor mr \rfloor} \left(\psi_t - \psi_t^{(0)} \right) \right\| = o_p(1).$$

Assumption 7 formalizes that training-based estimation (PCA projection; optional frequency-domain fPCA) does not affect $\sqrt{m}$-scale partial sums. It requires that using estimated loadings/factors (and, if applicable, estimated frequency-domain fPCs, i.e., functional principal components) does not affect $\sqrt{m}$-scale partial sums; in large panels this is typically delivered by PCA consistency and the N^{-1} averaging in the score construction.

Assumption 8 (RSMS diagonalization)**.** *Either (i) the long-run covariance matrix* Σ *in Assumption 6 is diagonal, or (ii) RSMS is applied to the partially prewhitened scores* $\widetilde{\phi}_t$ *in* (14) *and the induced long-run covariance of the transformed score array is diagonal, with the whitening error asymptotically negligible at the* $\sqrt{m}$ *scale.*

Assumption 8 is needed only for RSMS, because the adjusted-range self-normalizer is componentwise, (approximate) diagonalization is needed for a coordinatewise pivotal limit. In practice

this is not restrictive: approximate diagonalization can be achieved by a preliminary (partial) prewhitening/orthogonalization step (see, e.g., Hong et al. (2024)), which is closely in spirit to the VAR prewhitening of Andrews and Monahan (1992); after this step, the remaining whitening error is asymptotically negligible at the $\sqrt{m}$ scale.

4.1 Pivotal null limits (KS-type)

Define the q-dimensional Brownian bridge $B_q^0(r) := B_q(r) - rB_q(1)$ for $r \in [0,1]$ and

$$U_q(s) := B_q(1+s) - (1+s)B_q(1), \qquad s \in [0,T].$$

Define the random matrix

$$V := \int_0^1 B_q^0(r)\, B_q^0(r)^\top \, dr,$$

which is almost surely (a.s.) positive definite.

Theorem 1 (SSMS KS-type null limit)**.** *Under Assumptions 5–7, with $T < \infty$ (and setting $\gamma = 0$),*

$$\sup_{1\le k\le mT} \mathcal{M}_m^{\mathrm{S}}(k) \xrightarrow{d} \sup_{0<s\le T} \frac{U_q(s)^\top V^{-1} U_q(s)}{(1+s)^2 \left(\frac{s}{1+s}\right)^{2\gamma}}.$$

In particular, the limit is pivotal (free of Σ), so $c_\alpha^{\mathrm{S}}(T,q,\gamma)$ can be obtained by Brownian-motion simulation.

Theorem 2 (RSMS KS-type null limit (diagonal covariance / after prewhitening))**.** *Assume Assumptions 5–7 and Assumption 8. Then, for $T < \infty$,*

$$\sup_{1\le k\le mT} \widetilde{\mathcal{M}}_m^{\mathrm{R}}(k) \xrightarrow{d} \sup_{0<s\le T} \frac{U_q(s)^\top R^{-2} U_q(s)}{(1+s)^2 \left(\frac{s}{1+s}\right)^{2\gamma}},$$

where $R = \mathrm{diag}(R_1, \ldots, R_q)$ and

$$R_\ell := \sup_{0\le r\le 1} B_\ell^0(r) - \inf_{0\le r\le 1} B_\ell^0(r) > 0 \quad \text{a.s.}$$

The limit is pivotal and $c_\alpha^{\mathrm{R}}(T,q,\gamma)$ can be simulated.

4.2 Pivotal null limits (CvM-type)

Assumption 9 (CvM weight function)**.** *The weight function $w : [0,T] \to \mathbb{R}_+$ in (17)–(19) is bounded and Riemann integrable (e.g. piecewise continuous).*

Assumption 9 is a mild regularity condition on the deterministic CvM weight. It ensures that the discrete CvM sums in (17)–(19) are genuine Riemann approximations to the continuous-time weighted integrals that appear in Theorems 3–4. Boundedness prevents the weight from exploding

(so no single monitoring time can dominate), while Riemann integrability is the minimal condition needed for the usual Riemann-sum/continuous-mapping argument that yields the stated integral limits for fixed $T < \infty$.

Theorem 3 (CvM-SSMS null limit)**.** *Under Assumptions 5–7, with $T < \infty$ (and setting $\gamma = 0$),*

$$\mathcal{I}_m^{\mathrm{S}}(\lfloor ms \rfloor) \xrightarrow{d} \int_0^s w(u)\, \frac{U_q(u)^\top V^{-1} U_q(u)}{(1+u)^2}\, du, \qquad s \in [0,T].$$

Hence the crossing probability $\mathbb{P}(\sup_{0\le s\le T} \mathcal{I}^{\mathrm{S}}(s) > c)$ can be simulated to set $c^{\mathrm{S}}_{\alpha,\mathrm{CvM}}(T,q)$.

Theorem 4 (CvM-RSMS null limit)**.** *Under the conditions of Theorem 2 (with $\gamma = 0$) and Assumption 9, with $T < \infty$,*

$$\mathcal{I}_m^{\mathrm{R}}(\lfloor ms \rfloor) \xrightarrow{d} \int_0^s w(u)\, \frac{U_q(u)^\top R^{-2} U_q(u)}{(1+u)^2}\, du, \qquad s \in [0,T].$$

Theorem 1–Theorem 4 provide pivotal limiting null distributions for the KS-type and CvM-type SSMS/RSMS monitoring statistics. Accordingly, for a given monitoring horizon T, dimension q, and (for KS-type monitoring statistics) boundary exponent $\gamma \in [0, 1/2)$, we set constant decision boundaries as quantiles of the corresponding Brownian-motion functionals. For CvM-type monitoring we set $\gamma = 0$ and the boundary depends on the chosen weight function w in Assumption 9.

4.3 Calibration of simulated critical values

Theorems 1–4 show that, under H_0, the proposed KS-type and CvM-type SSMS/RSMS monitoring statistics admit pivotal limiting distributions that depend only on the monitoring horizon T, the score dimension q, and (for KS-type monitoring) the boundary exponent $\gamma \in [0, 1/2)$. Accordingly, we calibrate constant decision boundaries using simulated quantiles of the corresponding Brownian-motion functionals. Throughout the paper we report KS-type results for $\gamma \in \{0, 0.15\}$, where $\gamma = 0$ is the default and $\gamma = 0.15$ serves as a sensitivity check. For CvM-type monitoring we set $\gamma = 0$ and the null distribution depends on the deterministic weight function $w(\cdot)$ in (17)–(19).

To assess sensitivity to how evidence is accumulated over monitoring time, we consider four common bounded weights. Let $s \in [0,T]$ and define the normalized time $\tau = s/T \in [0,1]$. We use

$$\begin{aligned} w_{\mathrm{U}}(s) &:= 1, \\ w_{\mathrm{Early}}(s) &:= 2(1-\tau), \\ w_{\mathrm{Mid}}(s) &:= 6\tau(1-\tau), \\ w_{\mathrm{Late}}(s) &:= 2\tau, \end{aligned} \qquad s \in [0,T]. \tag{21}$$

All four weights satisfy $\int_0^T w(s)\, ds = T$ (unit average weight), so differences reflect where evidence is emphasized (early / mid / late) rather than a scale change. Importantly, for each choice of $w(\cdot)$

in (21) we simulate a separate CvM critical value $c^{\mathrm{S}}_{\alpha,\mathrm{CvM}}(T,q;w)$ and $c^{\mathrm{R}}_{\alpha,\mathrm{CvM}}(T,q;w)$, because the null distribution of $\sup_{0\le s\le T}\mathcal{I}^{\mathrm{S}}(s)$ and $\sup_{0\le s\le T}\mathcal{I}^{\mathrm{R}}(s)$ depends on $w(\cdot)$.

For each horizon T and each dimension q, we approximate the pivotal limiting Brownian-motion functionals on an equispaced grid. Let the step size be $\Delta = 1/m$ and define $t_j = j\Delta$. In our implementation we keep the monitoring grid length fixed at $k_{\max} = mT = 10{,}000$ points for every horizon T, so the training-grid size is $m = 10{,}000/T$ and the total number of increments is $m + k_{\max} = m(1+T)$.

We simulate a q-dimensional standard Brownian motion $\{B(t)\}$ on $[0, 1+T]$ via independent Gaussian increments $\Delta B_j \sim \mathcal{N}(0, \Delta I_q)$. Equivalently, we draw i.i.d. $Z_j \sim \mathcal{N}(0, I_q)$ and set $\Delta B_j = \sqrt{\Delta}\, Z_j$, so each replication uses $(m + k_{\max}) \times q$ independent standard normal draws. Let $B(1)$ denote the value at the end of the training interval. On $[0,1]$ we form the Brownian bridge $B^0(r) = B(r) - rB(1)$. For SSMS, the quadratic self-normalizer $V = \int_0^1 B^0(r)B^0(r)^\top dr$ is approximated by the Riemann sum $V \approx m^{-1}\sum_{j=1}^{m} B^0(t_j)B^0(t_j)^\top$; when inverting V we add a small ridge term 10^{-10} for numerical stability. For RSMS, we approximate the coordinatewise training ranges $R_\ell = \sup_{0\le r\le 1} B^0_\ell(r) - \inf_{0\le r\le 1} B^0_\ell(r)$ by the corresponding maxima/minima over the training grid.

On the monitoring interval $(0, T]$ we form the bridge process $U(s) = B(1+s) - (1+s)B(1)$ on the grid $s_k = k\Delta$ for $k = 1, \ldots, k_{\max}$. We then evaluate the KS-type limiting statistic by taking the maximum over k of the corresponding normalized quadratic form, using boundary exponent γ. For CvM-type monitoring (with $\gamma = 0$), we approximate the weighted integrated process by the cumulative Riemann sum $\int_0^{s_k} w(u)M(u)\,du \approx m^{-1}\sum_{j=1}^{k} w(s_j)M(s_j)$ and take the maximum over k.

Finally, we repeat the above simulation for 10,000 independent replications and set the decision boundary equal to the empirical $(1-\alpha)$ quantile of the simulated maxima for $\alpha \in \{0.05, 0.10\}$. All KS-type and CvM-type critical values used in the simulation study and empirical illustration (including the HAC benchmark values based on Appendix A) are tabulated in Appendix C. Because the null limits are pivotal, the resulting critical values depend only on (T, q, γ) for KS-type monitoring and on (T, q, w) for CvM-type monitoring, and can therefore be simulated once and reused across applications. In empirical work, however, both the monitoring horizon T (determined by the Phase-I/Phase-II split) and the score dimension q (determined by the chosen score construction) need not match the tabulated grid $T \in \{1, 2, 5, 10\}$ and $q \le 20$ used for our simulation tables. Accordingly, Appendices F and G report additional simulated critical values for the specific (T, q) combinations required in our empirical analysis.

4.4 Consistency and local power

Assumption 10 (Post-change mean shift)**.** *Under H_1, there exists $k^\star = \lfloor ms^\star \rfloor$ with $s^\star \in (0,T)$ and a nonzero vector $\Delta \in \mathbb{R}^q$ such that*

$$\mathbb{E}(\psi_{m+k}) = \begin{cases} \mu, & k < k^\star, \\ \mu + \Delta, & k \geq k^\star, \end{cases} \tag{22}$$

up to $o(1)$ terms. Moreover, $\psi_t - \mathbb{E}\psi_t$ continues to satisfy the same weak dependence/moment conditions as under H_0 (so stochastic fluctuations remain $O_p(\sqrt{m})$).

Assumption 10 encodes a canonical "signal + noise" alternative for the monitored score stream: after a change-point at fraction $s^\star$ of the monitoring horizon, the mean of ψ_{m+k} shifts by a fixed nonzero amount Δ. Since $S_m(k)$ aggregates the centered scores, this produces an (approximately) linear drift term of the form $(k-k^\star)_+\,\Delta$ in $S_m(k)$ (up to the negligible training-mean/estimation effects absorbed by the $o(1)$ terms), while the random fluctuations remain of order $O_p(\sqrt{m})$ under the maintained dependence and moment conditions. This separation of scales is what drives (i) consistency of the stopping rules in Theorem 5 and (ii) the drifted Brownian-motion limits under local alternatives in Theorem 6.

Theorem 5 (Consistency)**.** *Under Assumptions 5, 6, 7, and 10,*

$$\mathbb{P}(\mathcal{T}_m^{\mathrm{S}} \leq mT \mid H_1) \to 1, \qquad \mathbb{P}(\mathcal{T}_m^{\mathrm{R}} \leq mT \mid H_1) \to 1,$$

and similarly for the CvM stopping times $\mathcal{T}_{m,\mathrm{CvM}}^{\mathrm{S}}$ and $\mathcal{T}_{m,\mathrm{CvM}}^{\mathrm{R}}$.

Theorem 5 shows that the proposed stopping rules have asymptotic power one against fixed mean-shift alternatives: with probability tending to one, an alarm is raised within the monitoring horizon mT. Intuitively, after $k^\star$ the partial sums $S_m(k)$ accumulate a linear drift $(k-k^\star)\Delta$, whereas the training-window self-normalizers remain $O_p(1)$; consequently the normalized statistics diverge and must eventually exceed any fixed critical value.

Definition 1 (Local alternatives)**.** *A local alternative has a post-change drift of order $m^{-1/2}$: for $k \geq k^\star$,*

$$\mathbb{E}(\psi_{m+k}) = \mu + \Delta_m, \qquad \Delta_m = \frac{\delta}{\sqrt{m}},$$

for some fixed $\delta \in \mathbb{R}^q$.

Definition 1 introduces a Pitman local alternative sequence in which the post-change mean shift shrinks with the training size. This scaling is chosen so that the induced drift in the monitoring partial sums is of the same order as the $O_p(\sqrt{m})$ stochastic fluctuations under H_0: for $k = \lfloor ms \rfloor$,

$$\mathbb{E}S_m(k) \;\approx\; (k-k^\star)_+\Delta_m \;=\; (k-k^\star)_+\frac{\delta}{\sqrt{m}} \;\sim\; \sqrt{m}\,(s-s^\star)_+\,\delta.$$

Consequently, after the $\sqrt{m}$ normalization used in the null FCLT, the limiting monitoring process becomes a Brownian motion/bridge functional with an added deterministic drift term, yielding a nondegenerate asymptotic local-power characterization (Theorem 6). By contrast, under fixed alternatives with $\Delta \neq 0$, the statistics diverge and the corresponding stopping rules are consistent (Theorem 5).

Theorem 6 (Local power: Brownian motion with drift)**.** *Under Definition 1 and Assumptions 5–7, for fixed $\gamma \in [0, 1/2)$ the SSMS KS-type statistic converges to a Brownian functional with drift:*

$$\sup_{1\le k\le mT} \mathcal{M}_m^{\mathrm{S}}(k) \xrightarrow{d} \sup_{0<s\le T} \frac{\left(U_q(s) + (s-s^\star)_+\delta\right)^\top V^{-1} \left(U_q(s) + (s-s^\star)_+\delta\right)}{(1+s)^2 \left(\frac{s}{1+s}\right)^{2\gamma}},$$

where $s^\star = \lim k^\star/m$ and $(x)_+ = \max(x, 0)$. Analogous drifted limits hold for RSMS and for the CvM functionals by replacing $U_q(s)$ with $U_q(s) + (s - s^\star)_+\delta$ inside the corresponding limit expressions.

Theorem 6 characterizes nontrivial power against local (Pitman) alternatives, where the post-change mean shift is of order $m^{-1/2}$. In this regime the deterministic drift in $S_m(k)$ is of the same order as the $O_p(\sqrt{m})$ stochastic fluctuations, so the monitoring statistic converges to the same Brownian functional as under H_0, but with an added piecewise-linear drift term $(s - s^\star)_+\delta$. This drifted limit provides an asymptotic approximation to finite-sample power against small changes and makes explicit how sensitivity depends on the change location $s^\star$, the boundary exponent γ, and (for CvM-type monitoring) the choice of weight function $w(\cdot)$.

4.5 Algorithm: Factor-Adjusted Score with SSMS and RSMS Monitoring

Algorithm 1 summarizes the full online procedure—covering Phase I training, SSMS/RSMS normalization, and Phase II sequential monitoring—and (optionally) the HAC/LRV benchmark in Appendix A.

4.6 Training-window contamination and practical safeguards

Our asymptotic results are derived under a clean Phase-I training window (Assumption 5), which ensures that the baseline loading space $\widehat{\Lambda}_0$ and the self-normalizers computed from $\{\psi_t\}_{t=1}^m$ are stable under H_0. In empirical monitoring applications, however, a perfectly change-free training window can be difficult to guarantee: borderline instabilities may go undetected, small drifts may accumulate gradually, and repeated testing implies a nontrivial probability of Type II errors. When the training window is mildly contaminated, three practical effects are worth keeping in mind. First, PCA on $\{X_t\}_{t=1}^m$ may estimate a loading space that blends multiple regimes, so the "frozen" projection (5) is no longer anchored to a single baseline loading space. Second, the training mean $\bar{\psi}_m$ used for centering can inherit a small bias, which in turn induces a drift in the monitored partial sums $S_m(k) = \sum_{t=m+1}^{m+k}(\psi_t - \bar{\psi}_m)$ and may lead to premature stopping. Third, the training

self-normalizers (both the quadratic D_m and the adjusted-range self-normalizer $\widetilde{R}_m$) can be inflated by within-training instability, which can delay detection when a new change occurs in Phase II.

To mitigate these risks in practice, we recommend the following. First, before freezing $\widehat{\Lambda}_0$, it is helpful to pre-screen (or validate) the training window by applying an offline stability diagnostic to $\{X_t\}_{t=1}^m$ (or to the resulting score vectors $\{\psi_t\}_{t=1}^m$), and to reselect the Phase-I window if there is evidence of structural breaks/shifts. Second, when the training window is long, a buffer or trimming strategy can reduce the influence of late instabilities: for example, one may estimate $\widehat{\Lambda}_0$ using an early subsample and reserve the remaining observations as a validation buffer, and/or compute the self-normalizers from a trimmed training block (e.g., by dropping the last few observations). Third, in most real-time deployments the monitor is used repeatedly, so after a signal one re-estimates the factor model on a fresh (post-alarm) window and restarts monitoring; this restart logic naturally limits the long-run impact of occasional training contamination and aligns with the goal of maintaining an up-to-date loading space for downstream forecasting/nowcasting systems. Fourth, when training stability is uncertain, it is prudent to favor robust SN: adjusted-range SN has been found to be less prone to the power pathologies of quadratic SN and to deliver shorter delays when the training window is mildly contaminated; see, for example, Zhu et al. (2025) for sequential evidence in related settings. This is because contamination can have an inflating—or even explosive—effect on the quadratic self-normalizer of Shao (2010); this is precisely why KS-type statistics can be ineffective for offline structural-break testing (see Figure 1 in Shao and Zhang (2010)). Accordingly, whether SSMS performs well for change-point detection hinges critically on the Phase-I training sample being clean, i.e., free of change points.

Appendix E.2 complements this discussion with a targeted Monte Carlo experiment that injects mild Phase-I contamination of magnitude b_{train} (comparable to $1/\sqrt{m}$) and quantifies its effect on sequential detection under H_1. The results highlight the practical robustness gains of adjusted-range SN: RSMS stays closer to the clean-training benchmark in the borderline regime, while quadratic SN and HAC can experience substantially higher premature stopping and corresponding losses of post-break detection, especially for late breaks.

We state a simple sufficient condition under which mild (local/vanishing) training-window contamination does not affect the pivotal null limits. The key role of Assumption 5 is to ensure that (i) the training centering $\bar{\psi}_m$ is a consistent estimate of the stable null mean μ and (ii) the training self-normalizers (D_m for SSMS and $\widetilde{R}_m$ for RSMS) converge to fixed Brownian functionals. If the training block is mildly contaminated, $\bar{\psi}_m$ can inherit a small bias that induces a drift in the monitored partial sums $S_m(k) = \sum_{t=m+1}^{m+k}(\psi_t - \bar{\psi}_m)$. Because k can be of order m over the monitoring horizon, the drift is negligible at the $\sqrt{m}$ scale if and only if the training-mean bias is $o(m^{-1/2})$. The proposition below gives a simple sufficient condition.

Proposition 1 (Pivotal limits under mild training-window contamination)**.** *Assume that, under H_0, there exists a "clean" score sequence $\{\psi_t^{(0)}\}_{t\geq 1}$ with mean μ that satisfies Assumptions 6 and 7 (and Assumption 8 if RSMS is used). Suppose that the score vectors used on the training window*

admit the decomposition

$$\psi_t = \psi_t^{(0)} + d_{t,m}, \qquad t = 1, \dots, m,$$

while on the monitoring window $t \geq m+1$ the observed scores coincide with the clean sequence (i.e. $\psi_t = \psi_t^{(0)}$). Assume the (possibly deterministic) contamination array $\{d_{t,m}\}$ satisfies

$$\sup_{0 \leq r \leq 1} \frac{1}{\sqrt{m}} \left\| \sum_{t=1}^{\lfloor mr \rfloor} d_{t,m} \right\| \to 0, \qquad \frac{1}{m} \sum_{t=1}^{m} \|d_{t,m}\|^2 \to 0. \tag{23}$$

If RSMS is implemented with the prewhitening step (13)*, additionally assume that $\frac{1}{m} \sum_{t=1}^{m} \|\psi_t^{(0)}\|^2 = O_p(1)$ and that the whitening map $\widehat{\Sigma}_{\phi,0} \mapsto \widehat{W}_m$ is continuous at the relevant limit (e.g. by using a symmetric inverse square-root, or by an eigen-gap condition for the eigendecomposition in* (13)*). Then the SSMS/RSMS KS- and CvM-type monitoring statistics constructed from $\{\psi_t\}$ have the same null weak limits as in Theorems 1–4.*

The first requirement in (23) controls the entire contamination partial-sum path at the $\sqrt{m}$ scale. This strengthening (relative to controlling only $\| \sum_{t=1}^{m} d_{t,m} \|$) is essential because both D_m and $\widetilde{R}_m$ depend on the full training bridge process. It rules out "large-but-canceling" contaminations—e.g. a sizeable block shift early in training that is offset later—which can substantially inflate the self-normalizers even if the endpoint sum is small. A primitive sufficient condition for the first display in (23) is $m^{-1/2} \sum_{t=1}^{m} \|d_{t,m}\| \to 0$, since $\max_{1 \leq n \leq m} m^{-1/2} \| \sum_{t=1}^{n} d_{t,m} \| \leq m^{-1/2} \sum_{t=1}^{m} \|d_{t,m}\|$. The second requirement in (23) is an "energy" condition ensuring that the overall second-moment contribution of the contamination vanishes, which stabilizes covariance-based operations (e.g. RSMS prewhitening) and prevents systematic inflation of training scales.

A simple special case is a late training break of magnitude Δ_m affecting only the last m_c training observations: $d_{t,m} = \Delta_m$ for $t = m - m_c + 1, \dots, m$ and $d_{t,m} = 0$ otherwise. Then (23) reduces to

$$m_c \|\Delta_m\| = o(\sqrt{m}), \qquad \frac{m_c}{m} \|\Delta_m\|^2 \to 0,$$

which is satisfied, for example, if (i) a fixed-size break affects a vanishing fraction of the training window ($m_c = o(\sqrt{m})$), or (ii) the break magnitude is local/vanishing ($\|\Delta_m\| = o(m^{-1/2})$) while the affected fraction m_c/m is bounded away from zero.

Algorithm 1 Online monitoring of loading instabilities via SSMS/RSMS (with optional HAC benchmark)

Require: Training size m, factor dimension K, monitoring horizon mT, score construction choices (DFT; e.g. frequency grid or fPCA projection), boundary exponent γ (KS-type; set $\gamma = 0$ for CvM-type monitoring), and (if using CvM monitoring) a weight function $w(\cdot)$.

Optional (HAC benchmark): kernel $\mathcal{K}(\cdot)$, bandwidth (truncation lag) h, ridge ε.

Phase I (training): Compute $\widehat{\Lambda}_0$ from PCA on $\{X_t\}_{t=1}^m$ as in (4).
for $t = 1, \ldots, m$ **do**
    Compute $(\widetilde{F}_t, \widetilde{\varepsilon}_t)$ using (5).
    Compute the chosen score ψ_t (DFT-based vectorization/projection from (6) and Section 2.3).
end for
Compute $\bar{\psi}_m$ and $\phi_t = \psi_t - \bar{\psi}_m$ for $t \le m$; initialize $S_m(0) = 0$.
Compute SSMS normalizer D_m in (9).
(RSMS prewhitening): compute $\widehat{W}_m$ in (13) and set $\widetilde{\phi}_t = \widehat{W}_m \phi_t$.
Compute RSMS range normalizer $\widetilde{R}_m$ via (15).
(HAC benchmark): choose kernel $\mathcal{K}(\cdot)$ and bandwidth h, and compute $\widehat{\Sigma}_{m,h}$ in (A.1) (optionally invert $\widehat{\Sigma}_{m,h} + \varepsilon I_q$ with $\varepsilon > 0$).
Choose thresholds $c_\alpha^{\mathrm{S}}, c_\alpha^{\mathrm{R}}, c_{\alpha,\mathrm{CvM}}^{\mathrm{S}}, c_{\alpha,\mathrm{CvM}}^{\mathrm{R}}$ (and, if used, $c_{\alpha,\mathrm{KS}}^{\mathrm{H}}, c_{\alpha,\mathrm{CvM}}^{\mathrm{H}}$) by Brownian simulation; see Section 4.3 and Appendix A.
Phase II (monitoring):
for $k = 1, 2, \ldots, mT$ **do**
    Observe X_{m+k}.
    Compute $(\widetilde{F}_{m+k}, \widetilde{\varepsilon}_{m+k})$ and then the chosen score ψ_{m+k}.
    Form $\phi_{m+k} = \psi_{m+k} - \bar{\psi}_m$ and update $S_m(k) = S_m(k-1) + \phi_{m+k}$.
    Update $\widetilde{\phi}_{m+k} = \widehat{W}_m \phi_{m+k}$ and $\widetilde{S}_m(k) = \widetilde{S}_m(k-1) + \widetilde{\phi}_{m+k}$.
    Compute $\mathcal{M}_m^{\mathrm{S}}(k)$ in (10) and/or $\widetilde{\mathcal{M}}_m^{\mathrm{R}}(k)$ in (16).
    (HAC benchmark): compute $\mathcal{M}_m^{\mathrm{H}}(k)$ in (A.2).
    Update CvM integrals $\mathcal{I}_m^{\mathrm{S}}(k), \mathcal{I}_m^{\mathrm{R}}(k)$ via (17)–(19) (and, if used, $\mathcal{I}_m^{\mathrm{H}}(k)$ via (A.4)).
    if any selected monitoring statistic crosses its threshold **then**
        Stop and signal: report $\widehat{t} = m + k$.
        break
    end if
end for

5 Simulation studies

This section evaluates the finite-sample performance of the proposed monitoring statistics in controlled factor-model experiments. We report null false-alarm rates and, under a range of loading-instability scenarios, detection probabilities and conditional detection delays for both early and late breaks across (N, m, T) configurations. Results are compared with HAC-based benchmarks to illustrate the practical gains from SN. To visualize how detection strength varies with the break magnitude, we also report overall power–versus–b plots in Figures 1–2; scenario-level versions (power versus b within each instability design) and additional graphical diagnostics are collected in Appendix E.1.

5.1 Simulation design

We generate a panel $\{X_{it}\}_{1\le i\le N,\ 1\le t\le m+mT}$ from the approximate factor model

$$X_{it} = \lambda_{it}^{\top} F_t + \varepsilon_{it}, \qquad i = 1, \dots, N,\ t = 1, \dots, m + mT, \tag{24}$$

where $K = 2$ factors are observed through time-varying loadings $\lambda_{it} \in \mathbb{R}^2$ and idiosyncratic errors ε_{it}. The first m observations form the training window and the subsequent mT observations form the monitoring window. Throughout, we set the nominal level to $\alpha = 0.05$ and use 1,000 Monte Carlo replications per configuration.

Let $F_t = (F_{1t}, F_{2t})^{\top}$ follow two independent AR(1) processes

$$F_{1t} = 0.6F_{1,t-1} + z_{1t}, \qquad z_{1t} \overset{iid}{\sim} \mathcal{N}(0, 1 - 0.6^2),$$

$$F_{2t} = 0.3F_{2,t-1} + z_{2t}, \qquad z_{2t} \overset{iid}{\sim} \mathcal{N}(0, 1 - 0.3^2),$$

initialized at $F_{10} = F_{20} = 0$ (equivalently, one may discard a short burn-in; results are qualitatively unchanged).

We draw baseline loadings $\lambda_{i0} \in \mathbb{R}^2$ i.i.d. from $\mathcal{N}(0, I_2)$ and impose stability on the training window:

$$\lambda_{it} = \lambda_{i0}, \qquad t = 1, \dots, m.$$

This enforces Assumption 5 in the theoretical analysis and matches the monitoring interpretation: the baseline loading space is learned from a clean training sample.

In practice, however, it can be hard to guarantee a perfectly change-free Phase-I window, especially when potential instabilities are small enough to evade offline screening. To assess robustness in this empirically relevant "borderline" regime, Appendix E.2 reports an additional simulation that allows mild Phase-I contamination (late-break or drift in the training loadings with magnitude b_{train} on a fine local grid) and studies how sequential power and premature stopping change under the alternative. This robustness check is designed to inform how the choice between quadratic SN and adjusted-range SN matters when training-window cleanliness is uncertain.

We consider three commonly used cross-sectional error designs (independent of $\{F_t\}$):

1. **i.i.d. Gaussian:** $\varepsilon_{it} \overset{iid}{\sim} \mathcal{N}(0,1)$.
2. **Cross-sectional heteroskedasticity:** $\varepsilon_{it} = \sigma_i v_{it}$ where $\sigma_i \overset{iid}{\sim} \mathrm{Unif}(0.5, 1.5)$ and $v_{it} \overset{iid}{\sim} \mathcal{N}(0,1)$.
3. **Cross-sectional dependence:** $\varepsilon_t = (\varepsilon_{1t}, \ldots, \varepsilon_{Nt})^\top \overset{iid}{\sim} \mathcal{N}(0, \Sigma_\varepsilon)$, with $(\Sigma_\varepsilon)_{ij} = \rho^{|i-j|}$ and $\rho = 0.5$.

We study training sizes $m \in \{1000, 2000, 5000\}$, cross-sectional dimensions $N \in \{200, 500\}$, and monitoring horizons $T \in \{1, 2, 5\}$. To evaluate sensitivity to changes occurring early vs. late in the monitoring period, we set the (common) change location

$$k^* \in \Big\{ \lfloor 0.1\, mT \rfloor,\ \lfloor 0.8\, mT \rfloor \Big\}, \qquad t^* = m + k^*,$$

and vary the break magnitude over a grid $b \in \{0.1, 0.2, 0.3, 0.5\}$.

Write $k = t - m \in \{1, \ldots, mT\}$ for monitoring time and define the rescaled post-change time

$$r_k := \frac{k - k^*}{mT - k^*} \in [0,1] \quad \text{for } k > k^*.$$

For $k \le k^*$, we keep $\lambda_{i,m+k} = \lambda_{i0}$. For $k > k^*$, we consider the following instability designs (all are changes in the loading space, not mere factor rotations):

1. **Single abrupt break (pervasive shift).** For $k > k^*$,

$$\lambda_{i,m+k} = \lambda_{i0} + (b_1, b_2)^\top, \qquad (b_1, b_2) = (b,\, 2b),$$

   so both loading components shift after t^*.

2. **Multiple abrupt breaks (non-monotonic piecewise constant).** For $k > k^*$, only the first loading component changes:

$$\lambda_{i,m+k,1} = \lambda_{i0,1} + b \cdot g(r_k), \qquad \lambda_{i,m+k,2} = \lambda_{i0,2},$$

   where

$$g(r) = \begin{cases} 0, & r \in (0.1, 0.2] \cup (0.7, 0.8], \\ +1, & r \in (0.4, 0.5], \\ -1, & \text{otherwise}, \end{cases}$$

   which induces multiple sign-switching breaks after t^*.

3. **Smooth non-monotonic change (logistic multi-transition profile).** Define the smooth

logistic transform

$$G(y;\varsigma,\beta) := \Big[1+\exp\big\{-\varsigma\prod_{\ell=1}^{p}(y-\beta_\ell)\big\}\Big]^{-1}, \qquad (\varsigma,p,\beta) = (0.1,\ 4,\ (1,3,7,9)^\top).$$

For $k > k^*$, we let

$$\lambda_{i,m+k,1} = \lambda_{i0,1} + b\Big(G\big(10r_k;\varsigma,\beta\big) - G(0;\varsigma,\beta)\Big), \qquad \lambda_{i,m+k,2} = \lambda_{i0,2},$$

so the loading evolves smoothly with multiple transitions after t^* and is continuous at $k = k^*$.

4. **Heterogeneous break magnitudes (cross-sectionally varying shifts).** Let $\vartheta_i \overset{iid}{\sim} \mathrm{Unif}(0,1)$ and set $b_i = b\vartheta_i$. For $k > k^*$,

$$\lambda_{i,m+k,1} = \lambda_{i0,1} + b_i \cdot g(r_k), \qquad \lambda_{i,m+k,2} = \lambda_{i0,2},$$

with the same $g(\cdot)$ as in (S2), yielding heterogeneous change sizes across series.

5. **Staggered break dates (cross-sectionally heterogeneous change times).** Let $\vartheta_i \overset{iid}{\sim} \mathrm{Unif}(0,1)$ and define individual break locations

$$k_i^* := k^* + \Big\lfloor \big(0.4 + 0.2\vartheta_i\big)\,(mT - k^*)\Big\rfloor, \qquad t_i^* = m + k_i^*.$$

Then for each i,

$$\lambda_{i,m+k,1} = \begin{cases} \lambda_{i0,1}, & k \le k_i^*, \\ \lambda_{i0,1} + b, & k > k_i^*, \end{cases} \qquad \lambda_{i,m+k,2} = \lambda_{i0,2}.$$

This design produces a dispersed "wave" of loading changes across the cross section.

We implement the DFT score sequence $\{\psi_t\}$ as in Section 2.3. Unless stated otherwise, we use the frequency-grid vectorization with $J = 5$ low frequencies $u_j = jT$ $(j = 1,\dots,5)$, so that $q = 2KJ = 20$ (stacking real and imaginary parts). For the frequency-domain inner product in the fPCA variant, we use the Gaussian weight $W(u) = (2\pi)^{-1/2}\exp(-u^2/2)$. For the KS-type monitoring statistics (SSMS and RSMS) we consider boundary exponents $\gamma \in \{0, 0.15\}$; for RSMS we additionally apply the training-window partial prewhitening described in Section 3.2. For the CvM-type monitoring statistics we set $\gamma = 0$ and consider the four bounded weights in (21): w_{U} (uniform), w_{Late}, w_{Early}, and w_{Mid}.

For the HAC benchmark in Appendix A we use the Bartlett (Newey–West) kernel $\mathcal{K}(x) = \max\{0, 1-|x|\}$ and set the truncation lag to $h = \lfloor m^{1/3}\rfloor$.

5.2 Simulation results

All reported probabilities are estimated by Monte Carlo using 1,000 replications per configuration. The self-normalized (SN) monitoring statistics are calibrated using the simulated asymptotic critical values reported in Tables C.1 and C.2 and Tables C.3–C.10 in Appendix C. For comparison, we also report HAC-based benchmarks (columns H0/H15 for KS and the HAC blocks for CvM), calibrated using the corresponding Monte Carlo critical values in Tables C.11–C.15. To keep the presentation compact while still reporting results separately for each (N, m, T) and break location, we average (within each cell) over the three error designs and over break magnitudes $b \in \{0.1, 0.2, 0.3, 0.5\}$. Under alternatives, we focus on the detection probability $\mathbb{P}(k^* < \mathcal{T}_m \leq mT)$ and the conditional average delay $\mathbb{E}[\mathcal{T}_m - k^* \mid k^* < \mathcal{T}_m \leq mT]$.

In addition to these clean-training experiments, Appendix E.2 reports a new robustness simulation that allows mild Phase-I contamination and traces how post-break detection and premature stopping vary with the contamination magnitude b_{train}. This experiment is intended to mimic borderline training-window instabilities that may slip into Phase I due to Type II errors and highlights that adjusted-range RSMS is more resilient in this regime.

Tables 1–3 report null false-alarm rates for the KS- and CvM-type monitoring statistics. Overall, the results highlight the practical advantage of SN in sequential monitoring: by eliminating explicit LRV estimation—and hence bandwidth/lag choices—SN delivers substantially more stable finite-sample size control across monitoring horizons and dependence designs. By contrast, the HAC benchmarks over-reject sharply, particularly at short horizons, leading to frequent premature signals.

5.2.1 False-alarm control under H_0

For KS-type monitoring (Table 1), the HAC benchmark is strongly oversized: the null rejection probabilities are around 0.09–0.30 at $T = 1$ (H0/H15) and remain well above 0.05 even at $T = 5$ (about 0.08–0.20). The SN procedures substantially improve false-alarm control. At $T = 1$, RSMS-KS with $\gamma = 0$ (R0) ranges from about 0.027–0.080, while SSMS-KS with $\gamma = 0$ (S0) is more liberal (0.058–0.090). As m and N increase, the null rejection probabilities for the SN procedures move closer to the nominal level, whereas HAC remains far too liberal. As the horizon increases, the SN procedures become conservative (especially RSMS), with R0 around 0.003–0.015 at $T = 5$. Increasing the boundary exponent from $\gamma = 0$ to $\gamma = 0.15$ (S15/R15) systematically increases rejection rates, which can partially alleviate SN conservativeness for long horizons but may over-reject at $T = 1$.

For CvM-type monitoring (Tables 2–3), the weight function has a clear and systematic impact on size: the early-emphasis weight w_{Early} is the most liberal and the late-emphasis weight w_{Late} is the most conservative. Again, HAC-CvM is highly oversized across weights (often exceeding 10% and reaching roughly one third at $T = 1$), while SN-CvM provides substantially better (though still imperfect) size control. Across (T, N, m), SSMS-CvM with w_{Late} is typically closest to the nominal 5% level, whereas RSMS-CvM is more conservative, especially for longer horizons.

Table 1: Null false-alarm probabilities (KS-type, $\alpha = 0.05$, $q = 20$). Entries are $\mathbb{P}(\mathcal{T}_m \leq mT)$ based on 1,000 Monte Carlo replications per configuration and averaged over the three error designs. Column labels: **S0** = SSMS-KS ($\gamma = 0$), **S15** = SSMS-KS ($\gamma = 0.15$), **R0** = RSMS-KS ($\gamma = 0$), **R15** = RSMS-KS ($\gamma = 0.15$), **H0** = HAC-KS ($\gamma = 0$), **H15** = HAC-KS ($\gamma = 0.15$).

T	(N, m)	S0	S15	R0	R15	H0	H15
1	(200,1000)	0.089	0.123	0.079	0.106	0.235	0.294
1	(200,2000)	0.072	0.105	0.052	0.072	0.153	0.198
1	(200,5000)	0.065	0.091	0.033	0.048	0.105	0.134
1	(500,1000)	0.090	0.122	0.080	0.102	0.237	0.297
1	(500,2000)	0.074	0.101	0.045	0.071	0.148	0.199
1	(500,5000)	0.058	0.083	0.027	0.039	0.094	0.122
2	(200,1000)	0.060	0.081	0.046	0.066	0.219	0.257
2	(200,2000)	0.056	0.073	0.023	0.034	0.146	0.173
2	(200,5000)	0.039	0.061	0.018	0.023	0.090	0.099
2	(500,1000)	0.063	0.087	0.043	0.070	0.217	0.264
2	(500,2000)	0.041	0.058	0.021	0.035	0.130	0.151
2	(500,5000)	0.035	0.052	0.010	0.018	0.082	0.097
5	(200,1000)	0.033	0.048	0.015	0.022	0.157	0.189
5	(200,2000)	0.028	0.040	0.008	0.014	0.119	0.145
5	(200,5000)	0.024	0.036	0.004	0.006	0.086	0.092
5	(500,1000)	0.028	0.046	0.013	0.023	0.164	0.202
5	(500,2000)	0.025	0.034	0.007	0.013	0.113	0.132
5	(500,5000)	0.025	0.037	0.003	0.006	0.081	0.091

5.2.2 Power and delay under H_1

Tables 4–8 report KS-type detection probabilities and delays under scenarios S1–S5, with HAC benchmarks in columns H0/H15. Tables 9–13 and Tables 14–18 report the corresponding results for the CvM-type monitors (left blocks: SSMS-CvM or RSMS-CvM; right blocks: HAC-CvM, for weights U/E/M/L).

Across all scenarios, early changes ($k^* = \lfloor 0.1mT \rfloor$) are detected with near-unit probability by all procedures. Differences are most pronounced for late changes ($k^* = \lfloor 0.8mT \rfloor$), where avoiding premature false alarms is crucial. This is precisely where SN is most beneficial: by keeping in-control signaling rates closer to nominal, SN procedures are less likely to stop before the change occurs and therefore retain high late-change detection probabilities under the sequential metric $\mathbb{P}(k^* < \mathcal{T}_m \leq mT)$. For KS-type monitoring, this effect is particularly clear: averaged over scenarios and all (T, N, m), R0 attains about 0.94 late-change detection probability versus about 0.91 for S0, while the HAC benchmark (H0) is lower (about 0.88), reflecting its tendency to trigger too early (see, e.g., Table 4, Panel B). Conditional delays decrease as m and N increase; among the SN variants, RSMS-KS with $\gamma = 0$ (R0) also tends to deliver smaller delays than SSMS-KS with $\gamma = 0$ (S0). For a fixed self-normalizer, $\gamma = 0$ typically yields slightly higher power than $\gamma = 0.15$.

For CvM-type monitoring, the weight choice dominates the power ranking for late changes: w_{Late} systematically improves power against late breaks (at the cost of weaker early-break sensitivity), whereas w_{Early} is tailored to early changes and can be substantially less powerful for late breaks.

Table 2: Null false-alarm probabilities for SSMS-CvM and HAC-CvM monitoring statistics ($\alpha = 0.05$, $q = 20$). Entries are $\mathbb{P}(\mathcal{T}_m \leq mT)$ based on 1,000 Monte Carlo replications per configuration and averaged over the three error designs. Column labels correspond to the four CvM weights in (21): **U** (w_{U}), **E** (w_{Early}), **M** (w_{Mid}), **L** (w_{Late}). Left block: SSMS-CvM; right block: HAC-CvM.

T	(N,m)	SSMS				HAC			
		U	E	M	L	U	E	M	L
1	(200,1000)	0.110	0.131	0.116	0.097	0.301	0.321	0.302	0.266
1	(200,2000)	0.091	0.122	0.102	0.077	0.202	0.244	0.207	0.176
1	(200,5000)	0.071	0.095	0.074	0.063	0.146	0.179	0.150	0.134
1	(500,1000)	0.104	0.144	0.112	0.089	0.296	0.343	0.299	0.260
1	(500,2000)	0.096	0.119	0.099	0.077	0.207	0.245	0.213	0.184
1	(500,5000)	0.074	0.095	0.079	0.061	0.129	0.166	0.135	0.113
2	(200,1000)	0.073	0.090	0.070	0.057	0.230	0.254	0.225	0.204
2	(200,2000)	0.059	0.084	0.060	0.050	0.163	0.193	0.162	0.146
2	(200,5000)	0.048	0.066	0.047	0.041	0.097	0.124	0.101	0.089
2	(500,1000)	0.075	0.098	0.074	0.064	0.236	0.268	0.232	0.208
2	(500,2000)	0.055	0.071	0.053	0.040	0.139	0.163	0.143	0.128
2	(500,5000)	0.043	0.061	0.044	0.035	0.095	0.117	0.096	0.085
5	(200,1000)	0.028	0.041	0.028	0.027	0.165	0.191	0.163	0.146
5	(200,2000)	0.027	0.036	0.027	0.023	0.125	0.148	0.125	0.109
5	(200,5000)	0.022	0.031	0.025	0.020	0.086	0.098	0.085	0.079
5	(500,1000)	0.027	0.034	0.027	0.022	0.165	0.192	0.166	0.146
5	(500,2000)	0.025	0.029	0.027	0.023	0.110	0.132	0.112	0.104
5	(500,5000)	0.022	0.031	0.026	0.020	0.083	0.093	0.080	0.077

Averaged across scenarios and configurations, SSMS-CvM with w_{Late} achieves strong late-change power (about 0.82), while w_{Early} is much weaker (about 0.43); RSMS-CvM provides modest power improvements for a fixed weight (e.g., about 0.85 for w_{Late} and about 0.46 for w_{Early}), but at the cost of more conservative size for longer horizons. Although HAC-CvM can appear more powerful for late breaks in some configurations, its severe over-rejection under the null implies that this comes with an unacceptably high false-alarm frequency, which undermines its practical usefulness as a monitoring statistic.

Overall, the simulations underscore the practical appeal of SN for sequential monitoring in dependent panel settings: relative to HAC-based studentization, SN monitoring delivers far more reliable false-alarm control (hence fewer premature signals) while maintaining strong detection performance across the instability scenarios. Within the SN class, RSMS is the preferred choice for KS-type monitoring when conservative size control and late-change performance are priorities, with $\gamma = 0$ as a reasonable default and $\gamma = 0.15$ useful as a sensitivity check. For CvM-type monitoring, SSMS combined with w_{Late} offers the best size–power compromise, with RSMS-CvM serving as a more conservative alternative.

Table 3: Null false-alarm probabilities for RSMS-CvM and HAC-CvM monitoring statistics ($\alpha = 0.05$, $q = 20$). Entries are $\mathbb{P}(\mathcal{T}_m \le mT)$ based on 1,000 Monte Carlo replications per configuration and averaged over the three error designs. Column labels correspond to the four CvM weights in (21): **U** (w_{U}), **E** (w_{Early}), **M** (w_{Mid}), **L** (w_{Late}). Left block: RSMS-CvM; right block: HAC-CvM.

T	(N,m)	RSMS				HAC			
		U	E	M	L	U	E	M	L
1	(200,1000)	0.122	0.156	0.126	0.098	0.301	0.321	0.302	0.266
1	(200,2000)	0.083	0.118	0.091	0.063	0.202	0.244	0.207	0.176
1	(200,5000)	0.051	0.081	0.057	0.042	0.146	0.179	0.150	0.134
1	(500,1000)	0.105	0.148	0.113	0.086	0.296	0.343	0.299	0.260
1	(500,2000)	0.080	0.125	0.088	0.057	0.207	0.245	0.213	0.184
1	(500,5000)	0.049	0.077	0.054	0.033	0.129	0.166	0.135	0.113
2	(200,1000)	0.058	0.092	0.059	0.046	0.230	0.254	0.225	0.204
2	(200,2000)	0.033	0.052	0.034	0.025	0.163	0.193	0.162	0.146
2	(200,5000)	0.024	0.039	0.026	0.018	0.097	0.124	0.101	0.089
2	(500,1000)	0.055	0.090	0.059	0.043	0.236	0.268	0.232	0.208
2	(500,2000)	0.033	0.054	0.034	0.024	0.139	0.163	0.143	0.128
2	(500,5000)	0.015	0.029	0.016	0.010	0.095	0.117	0.096	0.085
5	(200,1000)	0.012	0.025	0.014	0.010	0.165	0.191	0.163	0.146
5	(200,2000)	0.008	0.013	0.009	0.007	0.125	0.148	0.125	0.109
5	(200,5000)	0.005	0.008	0.005	0.005	0.086	0.098	0.085	0.079
5	(500,1000)	0.013	0.025	0.013	0.011	0.165	0.192	0.166	0.146
5	(500,2000)	0.010	0.016	0.010	0.008	0.110	0.132	0.112	0.104
5	(500,5000)	0.003	0.005	0.005	0.002	0.083	0.093	0.080	0.077

5.2.3 Graphical summary: power versus break magnitude

To provide a compact visual summary of how detection strength varies with the break magnitude, Figures 1–2 plot the sequential detection probability $\mathbb{P}\big(k^* < \mathcal{T}_m \le mT\big)$ as a function of b, averaging over scenarios S1–S5, the three error designs, and the (N, m, T) configurations reported in the tables. As expected, power increases with b in all cases. Across both the KS- and CvM-based panels, however, the figures also highlight the sequential cost of in-control size distortion: procedures that are prone to premature signals under H_0 (most notably the HAC benchmarks) may appear powerful for some values of b, but their inflated false-alarm propensity causes early stopping and can mechanically depress power for late breaks. In contrast, the self-normalized (SN) methods maintain a markedly better power–size trade-off, and the adjusted-range SN (AR–SN) variant is typically the most favorable overall, delivering strong detection probabilities while avoiding the size inflation that can confound comparisons based solely on raw power.

Scenario-level power–versus–b plots (by instability design) are reported in Appendix E.1, alongside the additional graphical summaries that complement the main simulation tables.

Table 4: KS-type monitoring under scenario **S1** ($\alpha = 0.05$, $q = 20$). Entries are $\mathbb{P}(k^* < \mathcal{T}_m \le mT)$ with the conditional average delay in parentheses, averaged over $b \in \{0.1, 0.2, 0.3, 0.5\}$ and the three error designs. Columns: S0, S15, R0, R15, H0, H15.

Panel A: Early change ($k^* = \lfloor 0.1mT \rfloor$)							
T	(N, m)	S0	S15	R0	R15	H0	H15
1	(200,1000)	0.998(11)	0.986(9)	1.000(10)	0.990(8)	0.997(9)	0.977(7)
2	(200,1000)	0.999(13)	0.990(11)	1.000(12)	0.990(10)	1.000(11)	0.974(8)
5	(200,1000)	0.999(18)	0.986(15)	1.000(16)	0.993(13)	0.999(14)	0.976(11)
1	(200,2000)	0.999(15)	0.991(12)	1.000(14)	0.995(11)	0.999(12)	0.984(10)
2	(200,2000)	0.997(18)	0.985(15)	0.999(16)	0.993(13)	0.998(15)	0.982(12)
5	(200,2000)	1.000(24)	0.989(21)	1.000(22)	0.995(19)	1.000(19)	0.983(16)
1	(200,5000)	0.999(24)	0.994(19)	1.000(22)	0.996(17)	0.999(20)	0.993(15)
2	(200,5000)	1.000(28)	0.989(23)	1.000(27)	0.995(22)	1.000(24)	0.994(19)
5	(200,5000)	1.000(39)	0.992(33)	1.000(36)	0.999(31)	1.000(32)	0.998(26)
1	(500,1000)	0.999(7)	0.983(6)	0.999(6)	0.989(5)	0.997(6)	0.972(5)
2	(500,1000)	0.999(9)	0.989(7)	1.000(8)	0.984(6)	1.000(7)	0.972(6)
5	(500,1000)	0.999(11)	0.984(10)	0.999(10)	0.990(9)	1.000(9)	0.976(8)
1	(500,2000)	0.998(10)	0.986(8)	1.000(9)	0.992(7)	0.999(8)	0.985(6)
2	(500,2000)	0.998(12)	0.985(10)	1.000(11)	0.991(9)	0.999(10)	0.985(8)
5	(500,2000)	1.000(16)	0.991(14)	1.000(15)	0.996(13)	1.000(13)	0.986(11)
1	(500,5000)	0.999(16)	0.992(12)	0.999(14)	0.996(11)	1.000(13)	0.994(10)
2	(500,5000)	0.999(18)	0.993(15)	1.000(17)	0.995(14)	1.000(16)	0.996(12)
5	(500,5000)	0.999(25)	0.990(21)	1.000(23)	0.997(20)	1.000(20)	0.996(17)
Panel B: Late change ($k^* = \lfloor 0.8mT \rfloor$)							
T	(N, m)	S0	S15	R0	R15	H0	H15
1	(200,1000)	0.937(14)	0.894(14)	0.944(12)	0.907(12)	0.837(10)	0.756(10)
2	(200,1000)	0.954(23)	0.930(24)	0.970(19)	0.946(19)	0.843(16)	0.789(16)
5	(200,1000)	0.968(63)	0.950(64)	0.987(48)	0.977(48)	0.868(35)	0.828(36)
1	(200,2000)	0.944(19)	0.904(19)	0.965(17)	0.940(17)	0.900(14)	0.842(14)
2	(200,2000)	0.962(32)	0.942(33)	0.986(28)	0.972(28)	0.899(23)	0.858(23)
5	(200,2000)	0.981(87)	0.965(88)	0.992(65)	0.986(65)	0.903(49)	0.871(50)
1	(200,5000)	0.958(30)	0.925(30)	0.979(27)	0.960(27)	0.942(22)	0.904(22)
2	(200,5000)	0.974(51)	0.948(52)	0.989(45)	0.982(45)	0.948(37)	0.931(36)
5	(200,5000)	0.980(133)	0.968(135)	0.997(99)	0.995(100)	0.934(78)	0.922(78)
1	(500,1000)	0.933(9)	0.895(9)	0.948(8)	0.917(8)	0.850(7)	0.764(7)
2	(500,1000)	0.959(15)	0.930(15)	0.973(12)	0.941(12)	0.842(10)	0.779(10)
5	(500,1000)	0.979(38)	0.959(39)	0.990(27)	0.978(27)	0.867(21)	0.823(21)
1	(500,2000)	0.947(12)	0.911(12)	0.973(11)	0.944(11)	0.909(9)	0.842(9)
2	(500,2000)	0.972(21)	0.951(21)	0.985(18)	0.970(18)	0.916(15)	0.882(15)
5	(500,2000)	0.981(53)	0.970(54)	0.994(39)	0.988(40)	0.914(31)	0.886(31)
1	(500,5000)	0.961(19)	0.929(19)	0.984(17)	0.967(17)	0.956(14)	0.913(14)
2	(500,5000)	0.977(32)	0.959(33)	0.993(29)	0.984(29)	0.953(24)	0.931(23)
5	(500,5000)	0.981(83)	0.968(84)	0.997(62)	0.994(62)	0.943(49)	0.928(49)

Table 5: KS-type monitoring under scenario **S2** ($\alpha = 0.05$, $q = 20$). Entries are $\mathbb{P}(k^* < \mathcal{T}_m \le mT)$ with the conditional average delay in parentheses, averaged over $b \in \{0.1, 0.2, 0.3, 0.5\}$ and the three error designs. Columns: S0, S15, R0, R15, H0, H15.

Panel A: Early change ($k^* = \lfloor 0.1mT \rfloor$)							
T	(N, m)	S0	S15	R0	R15	H0	H15
1	(200,1000)	0.998(28)	0.986(21)	1.000(23)	0.990(18)	0.997(20)	0.977(15)
2	(200,1000)	0.999(33)	0.990(26)	1.000(28)	0.990(22)	1.000(24)	0.974(19)
5	(200,1000)	0.999(47)	0.986(38)	1.000(39)	0.993(32)	0.999(32)	0.976(26)
1	(200,2000)	0.999(35)	0.991(27)	1.000(31)	0.995(24)	0.999(28)	0.984(21)
2	(200,2000)	0.997(42)	0.985(34)	0.999(38)	0.993(30)	0.998(34)	0.982(26)
5	(200,2000)	1.000(59)	0.989(50)	1.000(52)	0.995(43)	1.000(44)	0.983(36)
1	(200,5000)	0.999(53)	0.994(42)	1.000(48)	0.996(38)	0.999(43)	0.993(33)
2	(200,5000)	1.000(65)	0.989(53)	1.000(60)	0.995(48)	1.000(53)	0.994(42)
5	(200,5000)	1.000(87)	0.992(75)	1.000(80)	0.999(68)	1.000(70)	0.998(58)
1	(500,1000)	0.999(16)	0.983(13)	0.999(14)	0.989(11)	0.997(13)	0.972(10)
2	(500,1000)	0.999(19)	0.989(16)	1.000(17)	0.984(14)	1.000(15)	0.972(12)
5	(500,1000)	0.999(25)	0.984(22)	0.999(23)	0.990(19)	1.000(19)	0.976(16)
1	(500,2000)	0.998(22)	0.986(17)	1.000(20)	0.992(15)	0.999(18)	0.985(14)
2	(500,2000)	0.998(26)	0.985(21)	1.000(24)	0.991(19)	0.999(21)	0.985(17)
5	(500,2000)	1.000(35)	0.991(30)	1.000(32)	0.996(27)	1.000(28)	0.986(23)
1	(500,5000)	0.999(34)	0.992(27)	0.999(31)	0.996(24)	1.000(28)	0.994(22)
2	(500,5000)	0.999(41)	0.993(33)	1.000(38)	0.995(31)	1.000(34)	0.996(27)
5	(500,5000)	0.999(54)	0.990(46)	1.000(51)	0.997(43)	1.000(44)	0.996(37)
Panel B: Late change ($k^* = \lfloor 0.8mT \rfloor$)							
T	(N, m)	S0	S15	R0	R15	H0	H15
1	(200,1000)	0.880(44)	0.835(44)	0.911(39)	0.872(39)	0.824(30)	0.743(31)
2	(200,1000)	0.874(82)	0.848(83)	0.917(71)	0.891(72)	0.822(54)	0.767(55)
5	(200,1000)	0.861(215)	0.839(220)	0.904(182)	0.891(185)	0.837(133)	0.796(135)
1	(200,2000)	0.920(64)	0.880(65)	0.955(56)	0.928(56)	0.896(44)	0.838(44)
2	(200,2000)	0.932(115)	0.910(116)	0.966(99)	0.950(99)	0.893(74)	0.851(74)
5	(200,2000)	0.933(315)	0.915(323)	0.955(257)	0.946(261)	0.890(181)	0.858(185)
1	(200,5000)	0.956(90)	0.924(90)	0.979(78)	0.960(78)	0.942(62)	0.904(61)
2	(200,5000)	0.970(159)	0.944(161)	0.988(135)	0.981(135)	0.948(101)	0.931(101)
5	(200,5000)	0.974(445)	0.961(457)	0.994(351)	0.992(358)	0.933(238)	0.922(240)
1	(500,1000)	0.921(28)	0.882(29)	0.944(24)	0.913(24)	0.848(19)	0.763(19)
2	(500,1000)	0.941(51)	0.911(51)	0.964(41)	0.931(42)	0.840(31)	0.777(31)
5	(500,1000)	0.951(133)	0.930(136)	0.974(102)	0.961(103)	0.864(69)	0.820(71)
1	(500,2000)	0.946(38)	0.909(38)	0.973(31)	0.943(31)	0.909(25)	0.842(25)
2	(500,2000)	0.970(65)	0.949(66)	0.984(54)	0.969(54)	0.916(40)	0.882(40)
5	(500,2000)	0.977(173)	0.965(177)	0.992(130)	0.986(132)	0.913(88)	0.886(88)
1	(500,5000)	0.961(53)	0.929(53)	0.984(44)	0.967(43)	0.956(35)	0.913(35)
2	(500,5000)	0.977(87)	0.959(88)	0.993(71)	0.984(71)	0.953(56)	0.931(56)
5	(500,5000)	0.981(229)	0.968(234)	0.997(162)	0.994(164)	0.943(117)	0.928(118)

Table 6: KS-type monitoring under scenario **S3** ($\alpha = 0.05$, $q = 20$). Entries are $\mathbb{P}(k^* < \mathcal{T}_m \le mT)$ with the conditional average delay in parentheses, averaged over $b \in \{0.1, 0.2, 0.3, 0.5\}$ and the three error designs. Columns: S0, S15, R0, R15, H0, H15.

Panel A: Early change ($k^* = \lfloor 0.1mT \rfloor$)							
T	(N, m)	S0	S15	R0	R15	H0	H15
1	(200,1000)	0.998(116)	0.985(110)	1.000(111)	0.990(106)	0.997(108)	0.977(102)
2	(200,1000)	0.999(211)	0.990(203)	1.000(206)	0.990(198)	1.000(198)	0.974(190)
5	(200,1000)	0.987(511)	0.977(499)	0.991(492)	0.988(480)	0.998(471)	0.975(457)
1	(200,2000)	0.999(210)	0.991(201)	1.000(206)	0.995(198)	0.999(201)	0.984(192)
2	(200,2000)	0.997(392)	0.985(380)	0.999(386)	0.993(376)	0.998(376)	0.982(364)
5	(200,2000)	0.999(949)	0.989(931)	1.000(926)	0.995(910)	1.000(897)	0.983(876)
1	(200,5000)	0.999(483)	0.994(467)	1.000(478)	0.996(462)	0.999(470)	0.993(454)
2	(200,5000)	1.000(912)	0.989(889)	1.000(904)	0.995(883)	1.000(888)	0.994(867)
5	(200,5000)	1.000(2191)	0.992(2157)	1.000(2165)	0.999(2133)	1.000(2117)	0.998(2079)
1	(500,1000)	0.999(103)	0.983(99)	0.999(101)	0.989(97)	0.997(98)	0.972(93)
2	(500,1000)	0.999(192)	0.989(186)	1.000(188)	0.984(183)	1.000(184)	0.972(177)
5	(500,1000)	0.999(462)	0.984(453)	0.999(450)	0.990(442)	1.000(436)	0.976(425)
1	(500,2000)	0.998(193)	0.986(188)	1.000(191)	0.992(185)	0.999(187)	0.985(180)
2	(500,2000)	0.998(364)	0.985(357)	1.000(360)	0.991(351)	0.999(353)	0.985(344)
5	(500,2000)	1.000(878)	0.991(865)	1.000(863)	0.996(850)	1.000(842)	0.986(826)
1	(500,5000)	0.999(452)	0.992(438)	0.999(448)	0.996(436)	1.000(442)	0.994(428)
2	(500,5000)	0.999(859)	0.993(838)	1.000(853)	0.995(835)	1.000(840)	0.996(820)
5	(500,5000)	0.999(2061)	0.990(2034)	1.000(2044)	0.997(2019)	1.000(2005)	0.996(1975)
Panel B: Late change ($k^* = \lfloor 0.8mT \rfloor$)							
T	(N, m)	S0	S15	R0	R15	H0	H15
1	(200,1000)	0.800(57)	0.756(57)	0.845(53)	0.806(53)	0.788(46)	0.709(46)
2	(200,1000)	0.839(116)	0.812(117)	0.891(104)	0.865(104)	0.808(88)	0.752(89)
5	(200,1000)	0.741(275)	0.718(278)	0.787(258)	0.772(258)	0.772(220)	0.731(220)
1	(200,2000)	0.872(96)	0.832(97)	0.914(89)	0.887(89)	0.875(78)	0.817(78)
2	(200,2000)	0.915(186)	0.894(187)	0.956(168)	0.940(170)	0.888(144)	0.846(144)
5	(200,2000)	0.853(461)	0.831(462)	0.879(439)	0.869(437)	0.854(367)	0.822(370)
1	(200,5000)	0.942(181)	0.909(181)	0.971(170)	0.951(170)	0.940(156)	0.902(156)
2	(200,5000)	0.967(344)	0.941(346)	0.987(321)	0.980(322)	0.947(288)	0.930(288)
5	(200,5000)	0.944(891)	0.930(903)	0.964(841)	0.961(843)	0.923(737)	0.911(738)
1	(500,1000)	0.883(45)	0.843(45)	0.920(41)	0.888(41)	0.839(36)	0.754(36)
2	(500,1000)	0.926(86)	0.896(87)	0.956(78)	0.923(78)	0.837(68)	0.773(68)
5	(500,1000)	0.885(214)	0.862(216)	0.924(201)	0.909(202)	0.842(168)	0.797(169)
1	(500,2000)	0.932(73)	0.895(73)	0.967(67)	0.937(67)	0.907(61)	0.840(61)
2	(500,2000)	0.963(140)	0.942(140)	0.983(127)	0.968(128)	0.916(115)	0.882(115)
5	(500,2000)	0.945(355)	0.932(357)	0.966(329)	0.958(332)	0.906(286)	0.878(287)
1	(500,5000)	0.960(148)	0.929(148)	0.984(139)	0.967(139)	0.956(131)	0.913(131)
2	(500,5000)	0.977(278)	0.959(279)	0.993(265)	0.984(265)	0.953(250)	0.931(250)
5	(500,5000)	0.978(699)	0.964(703)	0.996(663)	0.993(666)	0.943(614)	0.928(616)

Table 7: KS-type monitoring under scenario **S4** ($\alpha = 0.05$, $q = 20$). Entries are $\mathbb{P}(k^* < \mathcal{T}_m \le mT)$ with the conditional average delay in parentheses, averaged over $b \in \{0.1, 0.2, 0.3, 0.5\}$ and the three error designs. Columns: S0, S15, R0, R15, H0, H15.

Panel A: Early change ($k^* = \lfloor 0.1mT \rfloor$)							
T	(N, m)	S0	S15	R0	R15	H0	H15
1	(200,1000)	0.992(75)	0.980(57)	0.997(63)	0.989(47)	0.997(52)	0.977(37)
2	(200,1000)	0.991(106)	0.983(80)	0.998(90)	0.989(66)	1.000(68)	0.974(49)
5	(200,1000)	0.974(180)	0.965(139)	0.983(162)	0.980(125)	0.996(111)	0.974(80)
1	(200,2000)	0.999(86)	0.990(65)	1.000(74)	0.995(55)	0.999(62)	0.984(45)
2	(200,2000)	0.996(115)	0.985(85)	0.999(99)	0.993(73)	0.998(77)	0.982(57)
5	(200,2000)	0.996(200)	0.986(155)	0.999(181)	0.994(132)	1.000(119)	0.983(88)
1	(200,5000)	0.999(116)	0.994(87)	1.000(99)	0.996(75)	0.999(87)	0.993(66)
2	(200,5000)	1.000(141)	0.989(111)	1.000(123)	0.995(97)	1.000(108)	0.994(85)
5	(200,5000)	1.000(194)	0.992(163)	1.000(177)	0.999(145)	1.000(146)	0.998(120)
1	(500,1000)	0.999(37)	0.983(28)	0.999(31)	0.989(23)	0.997(26)	0.972(20)
2	(500,1000)	0.999(46)	0.989(35)	1.000(38)	0.984(29)	1.000(32)	0.972(24)
5	(500,1000)	0.998(69)	0.983(56)	0.999(57)	0.990(45)	1.000(42)	0.976(34)
1	(500,2000)	0.998(46)	0.986(36)	1.000(39)	0.992(30)	0.999(35)	0.985(27)
2	(500,2000)	0.998(54)	0.985(43)	1.000(48)	0.991(38)	0.999(42)	0.985(33)
5	(500,2000)	1.000(78)	0.991(65)	1.000(69)	0.996(57)	1.000(56)	0.986(46)
1	(500,5000)	0.999(68)	0.992(53)	0.999(61)	0.996(47)	1.000(55)	0.994(43)
2	(500,5000)	0.999(83)	0.993(67)	1.000(76)	0.995(60)	1.000(67)	0.996(53)
5	(500,5000)	0.999(110)	0.990(94)	1.000(103)	0.997(87)	1.000(88)	0.996(74)
Panel B: Late change ($k^* = \lfloor 0.8mT \rfloor$)							
T	(N, m)	S0	S15	R0	R15	H0	H15
1	(200,1000)	0.704(72)	0.660(73)	0.758(70)	0.719(70)	0.736(57)	0.659(57)
2	(200,1000)	0.666(138)	0.640(139)	0.725(128)	0.697(128)	0.708(107)	0.654(108)
5	(200,1000)	0.619(357)	0.594(364)	0.667(336)	0.652(341)	0.696(259)	0.655(263)
1	(200,2000)	0.792(120)	0.752(122)	0.844(115)	0.815(115)	0.835(93)	0.779(93)
2	(200,2000)	0.776(223)	0.753(221)	0.819(206)	0.801(206)	0.812(164)	0.770(164)
5	(200,2000)	0.744(587)	0.720(589)	0.767(545)	0.754(549)	0.789(405)	0.756(411)
1	(200,5000)	0.907(199)	0.874(201)	0.941(188)	0.920(188)	0.926(148)	0.887(147)
2	(200,5000)	0.899(376)	0.871(379)	0.924(353)	0.915(355)	0.918(265)	0.901(264)
5	(200,5000)	0.879(1013)	0.864(1030)	0.905(924)	0.898(934)	0.890(663)	0.878(670)
1	(500,1000)	0.825(54)	0.785(54)	0.876(48)	0.844(48)	0.816(39)	0.731(39)
2	(500,1000)	0.823(102)	0.793(103)	0.868(92)	0.833(93)	0.795(71)	0.733(71)
5	(500,1000)	0.797(265)	0.772(269)	0.841(228)	0.824(233)	0.802(166)	0.756(169)
1	(500,2000)	0.900(81)	0.863(82)	0.942(71)	0.910(71)	0.896(56)	0.829(56)
2	(500,2000)	0.905(151)	0.883(152)	0.932(135)	0.916(136)	0.894(101)	0.859(101)
5	(500,2000)	0.885(395)	0.869(403)	0.916(343)	0.907(348)	0.882(241)	0.854(244)
1	(500,5000)	0.953(125)	0.921(126)	0.981(107)	0.965(107)	0.955(84)	0.912(83)
2	(500,5000)	0.962(225)	0.943(227)	0.984(194)	0.975(195)	0.951(146)	0.929(145)
5	(500,5000)	0.958(603)	0.944(618)	0.979(500)	0.974(509)	0.939(347)	0.923(350)

Table 8: KS-type monitoring under scenario **S5** ($\alpha = 0.05$, $q = 20$). Entries are $\mathbb{P}(k^* < \mathcal{T}_m \le mT)$ with the conditional average delay in parentheses, averaged over $b \in \{0.1, 0.2, 0.3, 0.5\}$ and the three error designs. Columns: S0, S15, R0, R15, H0, H15.

Panel A: Early change ($k^* = \lfloor 0.1mT \rfloor$)							
T	(N, m)	S0	S15	R0	R15	H0	H15
1	(200,1000)	0.998(451)	0.986(438)	1.000(445)	0.990(434)	0.997(430)	0.977(405)
2	(200,1000)	0.994(910)	0.984(893)	0.998(894)	0.988(879)	0.999(853)	0.974(822)
5	(200,1000)	0.899(2365)	0.882(2346)	0.915(2360)	0.908(2340)	0.969(2165)	0.947(2099)
1	(200,2000)	0.999(872)	0.991(851)	1.000(865)	0.995(848)	0.999(846)	0.984(815)
2	(200,2000)	0.997(1755)	0.985(1733)	0.999(1729)	0.993(1714)	0.998(1681)	0.982(1649)
5	(200,2000)	0.948(4501)	0.937(4468)	0.953(4502)	0.948(4486)	0.987(4253)	0.971(4160)
1	(200,5000)	0.999(2100)	0.994(2053)	1.000(2097)	0.996(2066)	0.999(2068)	0.993(2018)
2	(200,5000)	1.000(4217)	0.989(4153)	1.000(4157)	0.995(4133)	1.000(4094)	0.994(4045)
5	(200,5000)	0.992(10617)	0.984(10557)	0.990(10636)	0.989(10598)	0.999(10283)	0.998(10126)
1	(500,1000)	0.999(428)	0.983(417)	0.999(425)	0.989(415)	0.997(413)	0.972(391)
2	(500,1000)	0.999(862)	0.989(847)	1.000(846)	0.984(835)	1.000(819)	0.972(790)
5	(500,1000)	0.976(2213)	0.959(2194)	0.983(2188)	0.974(2175)	0.997(2055)	0.973(1993)
1	(500,2000)	0.998(834)	0.986(819)	1.000(834)	0.992(820)	0.999(818)	0.985(789)
2	(500,2000)	0.998(1683)	0.985(1668)	1.000(1658)	0.991(1641)	0.999(1626)	0.985(1600)
5	(500,2000)	0.996(4246)	0.987(4232)	0.997(4230)	0.993(4212)	1.000(4062)	0.986(3995)
1	(500,5000)	0.999(2030)	0.992(1987)	0.999(2033)	0.996(2008)	1.000(2012)	0.994(1962)
2	(500,5000)	0.999(4076)	0.993(4022)	1.000(4026)	0.995(4006)	1.000(3983)	0.996(3928)
5	(500,5000)	0.999(10144)	0.990(10101)	1.000(10152)	0.997(10131)	1.000(9926)	0.996(9822)
Panel B: Late change ($k^* = \lfloor 0.8mT \rfloor$)							
T	(N, m)	S0	S15	R0	R15	H0	H15
1	(200,1000)	0.882(127)	0.837(128)	0.921(123)	0.883(124)	0.828(116)	0.748(117)
2	(200,1000)	0.881(250)	0.854(251)	0.928(243)	0.903(244)	0.826(229)	0.771(231)
5	(200,1000)	0.780(644)	0.758(650)	0.827(635)	0.811(638)	0.797(592)	0.756(597)
1	(200,2000)	0.924(239)	0.883(241)	0.962(234)	0.936(235)	0.899(223)	0.841(224)
2	(200,2000)	0.937(472)	0.916(473)	0.974(462)	0.959(464)	0.896(440)	0.854(443)
5	(200,2000)	0.885(1213)	0.863(1221)	0.910(1205)	0.900(1209)	0.870(1128)	0.836(1133)
1	(200,5000)	0.954(556)	0.922(558)	0.979(547)	0.960(548)	0.942(527)	0.904(528)
2	(200,5000)	0.971(1094)	0.945(1099)	0.989(1079)	0.982(1081)	0.948(1038)	0.931(1040)
5	(200,5000)	0.959(2801)	0.946(2812)	0.978(2769)	0.975(2777)	0.930(2635)	0.918(2646)
1	(500,1000)	0.920(118)	0.880(118)	0.946(114)	0.915(114)	0.850(108)	0.764(109)
2	(500,1000)	0.944(229)	0.914(230)	0.968(224)	0.935(225)	0.840(213)	0.777(214)
5	(500,1000)	0.918(593)	0.896(598)	0.947(577)	0.932(580)	0.853(543)	0.808(547)
1	(500,2000)	0.944(222)	0.907(223)	0.973(217)	0.944(218)	0.909(209)	0.842(210)
2	(500,2000)	0.969(438)	0.948(440)	0.985(430)	0.970(432)	0.916(412)	0.882(414)
5	(500,2000)	0.959(1117)	0.947(1123)	0.979(1101)	0.971(1105)	0.910(1046)	0.883(1051)
1	(500,5000)	0.960(521)	0.929(523)	0.984(516)	0.967(517)	0.956(500)	0.913(502)
2	(500,5000)	0.977(1029)	0.959(1031)	0.993(1020)	0.984(1021)	0.953(988)	0.931(990)
5	(500,5000)	0.980(2595)	0.967(2603)	0.997(2571)	0.994(2577)	0.943(2472)	0.928(2481)

Table 9: SSMS-CvM monitoring under scenario **S1** ($\alpha = 0.05$, $q = 20$). Entries are $\mathbb{P}(k^* < \mathcal{T}_m \le mT)$ with the conditional average delay in parentheses, averaged over $b \in \{0.1, 0.2, 0.3, 0.5\}$ and the three error designs. Column labels correspond to the four CvM weights in (21). Left block: SSMS-CvM; right block: HAC-CvM.

Panel A: Early change ($k^* = \lfloor 0.1mT \rfloor$)

T	(N,m)	SSMS				HAC			
		U	E	M	L	U	E	M	L
1	(200,1000)	1.000(55)	1.000(40)	1.000(61)	1.000(90)	1.000(48)	1.000(35)	1.000(54)	1.000(80)
2	(200,1000)	1.000(88)	1.000(63)	1.000(102)	1.000(157)	1.000(76)	1.000(55)	1.000(89)	1.000(138)
5	(200,1000)	1.000(200)	1.000(133)	1.000(246)	1.000(479)	1.000(165)	1.000(113)	1.000(205)	1.000(389)
1	(200,2000)	1.000(88)	1.000(64)	1.000(99)	1.000(145)	1.000(77)	1.000(56)	1.000(88)	1.000(130)
2	(200,2000)	1.000(135)	1.000(98)	1.000(159)	1.000(241)	1.000(121)	1.000(88)	1.000(143)	1.000(218)
5	(200,2000)	1.000(279)	1.000(197)	1.000(345)	1.000(628)	1.000(244)	1.000(173)	1.000(306)	1.000(537)
1	(200,5000)	1.000(159)	1.000(116)	1.000(184)	1.000(269)	1.000(143)	1.000(105)	1.000(166)	1.000(244)
2	(200,5000)	1.000(241)	1.000(178)	1.000(288)	1.000(430)	1.000(223)	1.000(164)	1.000(266)	1.000(397)
5	(200,5000)	1.000(471)	1.000(344)	1.000(586)	1.000(942)	1.000(426)	1.000(312)	1.000(534)	1.000(860)
1	(500,1000)	1.000(40)	1.000(29)	1.000(45)	1.000(67)	1.000(35)	1.000(25)	1.000(40)	1.000(59)
2	(500,1000)	1.000(61)	1.000(45)	1.000(72)	1.000(108)	1.000(54)	1.000(40)	1.000(64)	1.000(96)
5	(500,1000)	1.000(125)	1.000(89)	1.000(154)	1.000(263)	1.000(106)	1.000(76)	1.000(133)	1.000(220)
1	(500,2000)	1.000(63)	1.000(46)	1.000(73)	1.000(107)	1.000(56)	1.000(41)	1.000(65)	1.000(96)
2	(500,2000)	1.000(96)	1.000(71)	1.000(115)	1.000(172)	1.000(86)	1.000(64)	1.000(103)	1.000(154)
5	(500,2000)	1.000(186)	1.000(136)	1.000(231)	1.000(369)	1.000(165)	1.000(121)	1.000(206)	1.000(330)
1	(500,5000)	1.000(116)	1.000(85)	1.000(136)	1.000(199)	1.000(104)	1.000(77)	1.000(124)	1.000(181)
2	(500,5000)	1.000(176)	1.000(130)	1.000(212)	1.000(312)	1.000(161)	1.000(119)	1.000(194)	1.000(286)
5	(500,5000)	1.000(329)	1.000(246)	1.000(409)	1.000(627)	1.000(297)	1.000(222)	1.000(370)	1.000(570)

Panel B: Late change ($k^* = \lfloor 0.8mT \rfloor$)

T	(N,m)	SSMS				HAC			
		U	E	M	L	U	E	M	L
1	(200,1000)	0.975(58)	0.791(70)	0.890(60)	0.995(56)	0.939(45)	0.717(55)	0.818(46)	0.987(45)
2	(200,1000)	0.977(120)	0.764(142)	0.885(123)	0.994(113)	0.963(92)	0.750(109)	0.869(92)	0.995(89)
5	(200,1000)	0.840(387)	0.553(382)	0.707(363)	0.906(363)	0.934(285)	0.656(303)	0.804(265)	0.973(275)
1	(200,2000)	0.983(95)	0.860(119)	0.930(100)	0.996(91)	0.965(77)	0.800(94)	0.887(78)	0.993(76)
2	(200,2000)	0.992(189)	0.860(237)	0.944(198)	1.000(179)	0.986(150)	0.831(185)	0.931(152)	0.999(147)
5	(200,2000)	0.929(618)	0.688(677)	0.820(613)	0.960(566)	0.968(461)	0.753(533)	0.888(454)	0.994(440)
1	(200,5000)	0.990(176)	0.924(216)	0.958(182)	0.999(169)	0.984(149)	0.874(174)	0.935(146)	0.999(147)
2	(200,5000)	0.994(340)	0.935(436)	0.973(358)	0.999(324)	0.992(287)	0.920(346)	0.965(285)	1.000(278)
5	(200,5000)	0.989(1074)	0.844(1372)	0.939(1125)	0.999(969)	0.993(824)	0.880(1051)	0.953(836)	1.000(772)
1	(500,1000)	0.974(43)	0.861(54)	0.926(45)	0.993(42)	0.934(33)	0.725(40)	0.833(33)	0.991(33)
2	(500,1000)	0.990(84)	0.875(107)	0.950(89)	0.998(80)	0.970(64)	0.787(78)	0.891(64)	0.995(64)
5	(500,1000)	0.951(278)	0.736(324)	0.872(279)	0.980(254)	0.980(192)	0.782(231)	0.897(191)	0.998(185)
1	(500,2000)	0.982(69)	0.903(86)	0.947(71)	0.997(67)	0.965(57)	0.819(67)	0.895(56)	0.995(56)
2	(500,2000)	0.992(134)	0.935(171)	0.978(140)	1.000(127)	0.987(109)	0.889(130)	0.947(108)	1.000(107)
5	(500,2000)	0.989(424)	0.855(545)	0.937(442)	0.998(382)	0.990(309)	0.869(391)	0.947(314)	0.999(293)
1	(500,5000)	0.990(129)	0.926(156)	0.963(131)	0.998(125)	0.987(110)	0.883(126)	0.944(107)	1.000(109)
2	(500,5000)	0.995(245)	0.958(303)	0.982(251)	1.000(235)	0.994(208)	0.919(242)	0.970(203)	1.000(203)
5	(500,5000)	0.999(718)	0.943(974)	0.990(760)	1.000(657)	0.997(548)	0.941(712)	0.977(549)	1.000(523)

Table 10: SSMS-CvM monitoring under scenario **S2** ($\alpha = 0.05$, $q = 20$). Entries are $\mathbb{P}(k^* < \mathcal{T}_m \leq mT)$ with the conditional average delay in parentheses, averaged over $b \in \{0.1, 0.2, 0.3, 0.5\}$ and the three error designs. Column labels correspond to the four CvM weights in (21). Left block: SSMS-CvM; right block: HAC-CvM.

T	(N,m)	SSMS				HAC			
		U	E	M	L	U	E	M	L
Panel A: Early change ($k^* = \lfloor 0.1mT \rfloor$)									
1	(200,1000)	1.000(119)	1.000(80)	1.000(124)	1.000(192)	1.000(99)	1.000(66)	1.000(104)	1.000(165)
2	(200,1000)	1.000(201)	1.000(130)	1.000(215)	1.000(353)	1.000(166)	1.000(108)	1.000(182)	1.000(304)
5	(200,1000)	1.000(537)	1.000(324)	1.000(582)	0.998(988)	1.000(423)	1.000(256)	1.000(481)	1.000(838)
1	(200,2000)	1.000(170)	1.000(116)	1.000(183)	1.000(288)	1.000(146)	1.000(100)	1.000(159)	1.000(254)
2	(200,2000)	1.000(279)	1.000(187)	1.000(313)	1.000(521)	1.000(243)	1.000(164)	1.000(276)	1.000(462)
5	(200,2000)	1.000(715)	1.000(442)	1.000(823)	1.000(1448)	1.000(599)	1.000(369)	1.000(711)	1.000(1276)
1	(200,5000)	1.000(291)	1.000(207)	1.000(324)	1.000(504)	1.000(255)	1.000(183)	1.000(287)	1.000(447)
2	(200,5000)	1.000(461)	1.000(326)	1.000(533)	1.000(861)	1.000(410)	1.000(293)	1.000(479)	1.000(772)
5	(200,5000)	1.000(1014)	1.000(672)	1.000(1241)	1.000(2200)	1.000(896)	1.000(601)	1.000(1116)	1.000(2001)
1	(500,1000)	1.000(78)	1.000(54)	1.000(84)	1.000(132)	1.000(65)	1.000(45)	1.000(72)	1.000(113)
2	(500,1000)	1.000(121)	1.000(83)	1.000(137)	1.000(225)	1.000(104)	1.000(72)	1.000(119)	1.000(195)
5	(500,1000)	1.000(290)	1.000(183)	1.000(342)	1.000(605)	1.000(238)	1.000(152)	1.000(289)	1.000(514)
1	(500,2000)	1.000(114)	1.000(81)	1.000(127)	1.000(197)	1.000(99)	1.000(72)	1.000(112)	1.000(173)
2	(500,2000)	1.000(178)	1.000(127)	1.000(207)	1.000(333)	1.000(159)	1.000(114)	1.000(186)	1.000(297)
5	(500,2000)	1.000(405)	1.000(269)	1.000(494)	1.000(872)	1.000(344)	1.000(233)	1.000(429)	1.000(764)
1	(500,5000)	1.000(205)	1.000(149)	1.000(233)	1.000(352)	1.000(183)	1.000(133)	1.000(210)	1.000(313)
2	(500,5000)	1.000(316)	1.000(231)	1.000(372)	1.000(574)	1.000(286)	1.000(209)	1.000(338)	1.000(516)
5	(500,5000)	1.000(629)	1.000(447)	1.000(781)	1.000(1332)	1.000(566)	1.000(404)	1.000(709)	1.000(1201)
Panel B: Late change ($k^* = \lfloor 0.8mT \rfloor$)									
T	(N,m)	SSMS				HAC			
		U	E	M	L	U	E	M	L
1	(200,1000)	0.714(110)	0.316(96)	0.471(91)	0.782(111)	0.823(91)	0.418(85)	0.580(80)	0.903(94)
2	(200,1000)	0.656(229)	0.266(188)	0.416(186)	0.728(233)	0.803(193)	0.404(171)	0.579(159)	0.875(195)
5	(200,1000)	0.565(651)	0.170(488)	0.310(538)	0.659(636)	0.760(520)	0.346(444)	0.531(429)	0.832(528)
1	(200,2000)	0.806(200)	0.434(184)	0.585(175)	0.867(198)	0.887(170)	0.519(165)	0.685(154)	0.943(169)
2	(200,2000)	0.770(413)	0.392(362)	0.556(350)	0.831(407)	0.878(349)	0.509(326)	0.688(300)	0.929(347)
5	(200,2000)	0.694(1175)	0.289(973)	0.463(999)	0.770(1133)	0.834(952)	0.457(867)	0.637(825)	0.900(940)
1	(200,5000)	0.926(402)	0.626(418)	0.760(386)	0.958(386)	0.961(343)	0.685(367)	0.828(328)	0.988(333)
2	(200,5000)	0.902(827)	0.585(839)	0.723(781)	0.942(788)	0.950(707)	0.677(726)	0.811(660)	0.979(676)
5	(200,5000)	0.852(2384)	0.498(2386)	0.667(2234)	0.915(2219)	0.935(1933)	0.626(1997)	0.771(1783)	0.966(1822)
1	(500,1000)	0.840(92)	0.488(86)	0.639(83)	0.896(90)	0.893(74)	0.532(75)	0.703(67)	0.965(73)
2	(500,1000)	0.823(190)	0.464(177)	0.616(166)	0.875(186)	0.910(150)	0.555(148)	0.722(133)	0.958(150)
5	(500,1000)	0.750(548)	0.362(496)	0.544(478)	0.831(524)	0.897(413)	0.539(403)	0.707(371)	0.945(408)
1	(500,2000)	0.918(158)	0.618(165)	0.754(150)	0.957(152)	0.947(129)	0.663(139)	0.807(123)	0.986(125)
2	(500,2000)	0.904(327)	0.595(324)	0.737(301)	0.945(311)	0.956(265)	0.684(277)	0.824(248)	0.984(255)
5	(500,2000)	0.858(939)	0.513(977)	0.671(876)	0.917(872)	0.944(715)	0.648(757)	0.792(672)	0.974(682)
1	(500,5000)	0.977(297)	0.770(350)	0.882(300)	0.993(282)	0.986(244)	0.811(291)	0.914(243)	0.999(236)
2	(500,5000)	0.973(596)	0.757(685)	0.876(603)	0.991(557)	0.992(487)	0.812(581)	0.924(484)	1.000(461)
5	(500,5000)	0.958(1735)	0.696(2023)	0.835(1753)	0.981(1566)	0.990(1323)	0.780(1581)	0.916(1333)	1.000(1229)

Table 11: SSMS-CvM monitoring under scenario **S3** ($\alpha = 0.05$, $q = 20$). Entries are $\mathbb{P}(k^* < \mathcal{T}_m \leq mT)$ with the conditional average delay in parentheses, averaged over $b \in \{0.1, 0.2, 0.3, 0.5\}$ and the three error designs. Column labels correspond to the four CvM weights in (21). Left block: SSMS-CvM; right block: HAC-CvM.

T	(N,m)	SSMS				HAC			
		U	E	M	L	U	E	M	L
Panel A: Early change ($k^* = \lfloor 0.1mT \rfloor$)									
1	(200,1000)	1.000(206)	0.999(172)	0.999(197)	0.999(255)	1.000(187)	1.000(158)	1.000(182)	1.000(230)
2	(200,1000)	1.000(404)	0.999(329)	0.999(386)	0.999(517)	1.000(366)	1.000(304)	1.000(356)	1.000(467)
5	(200,1000)	0.885(1554)	0.931(1049)	0.897(1386)	0.828(2136)	0.967(1296)	0.983(884)	0.971(1179)	0.941(1870)
1	(200,2000)	1.000(352)	1.000(304)	1.000(344)	1.000(427)	1.000(330)	1.000(287)	1.000(325)	1.000(397)
2	(200,2000)	1.000(678)	1.000(579)	1.000(664)	1.000(851)	1.000(636)	1.000(551)	1.000(629)	1.000(790)
5	(200,2000)	0.941(2434)	0.971(1715)	0.949(2214)	0.899(3557)	0.986(2057)	0.997(1523)	0.988(1931)	0.965(3178)
1	(200,5000)	1.000(750)	1.000(669)	1.000(745)	1.000(883)	1.000(720)	1.000(646)	1.000(718)	1.000(843)
2	(200,5000)	1.000(1422)	1.000(1272)	1.000(1420)	1.000(1699)	1.000(1372)	1.000(1233)	1.000(1373)	1.000(1629)
5	(200,5000)	0.991(4257)	0.999(3349)	0.994(4064)	0.968(6155)	1.000(3824)	1.000(3123)	1.000(3698)	0.994(5437)
1	(500,1000)	1.000(168)	1.000(147)	1.000(165)	1.000(202)	1.000(157)	1.000(138)	1.000(155)	1.000(186)
2	(500,1000)	1.000(318)	1.000(276)	1.000(314)	1.000(392)	1.000(299)	1.000(263)	1.000(297)	1.000(363)
5	(500,1000)	0.971(1020)	0.989(772)	0.976(956)	0.950(1503)	0.998(871)	1.000(678)	0.998(837)	0.989(1270)
1	(500,2000)	1.000(299)	1.000(267)	1.000(297)	1.000(352)	1.000(285)	1.000(256)	1.000(284)	1.000(333)
2	(500,2000)	1.000(565)	1.000(506)	1.000(564)	1.000(675)	1.000(542)	1.000(488)	1.000(543)	1.000(641)
5	(500,2000)	0.995(1670)	1.000(1329)	0.996(1598)	0.977(2358)	1.000(1449)	1.000(1228)	1.000(1425)	0.999(2039)
1	(500,5000)	1.000(662)	1.000(603)	1.000(662)	1.000(760)	1.000(640)	1.000(586)	1.000(642)	1.000(732)
2	(500,5000)	1.000(1250)	1.000(1148)	1.000(1257)	1.000(1441)	1.000(1216)	1.000(1119)	1.000(1223)	1.000(1394)
5	(500,5000)	1.000(3209)	1.000(2894)	1.000(3219)	0.999(4193)	1.000(3039)	1.000(2771)	1.000(3066)	1.000(3793)
Panel B: Late change ($k^* = \lfloor 0.8mT \rfloor$)									
T	(N,m)	SSMS				HAC			
		U	E	M	L	U	E	M	L
1	(200,1000)	0.603(116)	0.225(93)	0.359(92)	0.679(120)	0.757(99)	0.337(86)	0.498(82)	0.839(103)
2	(200,1000)	0.611(243)	0.217(192)	0.351(190)	0.687(247)	0.773(206)	0.359(177)	0.530(167)	0.850(211)
5	(200,1000)	0.397(674)	0.088(445)	0.188(499)	0.498(677)	0.641(565)	0.237(431)	0.399(433)	0.723(589)
1	(200,2000)	0.710(217)	0.327(183)	0.474(181)	0.774(218)	0.822(190)	0.430(172)	0.603(166)	0.887(191)
2	(200,2000)	0.742(441)	0.345(374)	0.509(374)	0.807(437)	0.862(377)	0.475(345)	0.658(324)	0.917(377)
5	(200,2000)	0.550(1243)	0.174(900)	0.314(953)	0.643(1237)	0.732(1065)	0.325(858)	0.505(860)	0.801(1078)
1	(200,5000)	0.859(458)	0.530(446)	0.671(429)	0.909(448)	0.927(404)	0.613(404)	0.760(371)	0.965(397)
2	(200,5000)	0.882(914)	0.544(899)	0.687(858)	0.925(879)	0.943(803)	0.651(806)	0.789(757)	0.973(771)
5	(200,5000)	0.729(2689)	0.343(2303)	0.526(2306)	0.807(2572)	0.844(2303)	0.498(2100)	0.670(2002)	0.909(2240)
1	(500,1000)	0.756(102)	0.383(88)	0.534(87)	0.823(101)	0.852(84)	0.460(79)	0.640(74)	0.932(84)
2	(500,1000)	0.783(209)	0.398(185)	0.556(180)	0.842(205)	0.892(170)	0.513(162)	0.687(149)	0.944(170)
5	(500,1000)	0.612(606)	0.222(467)	0.381(478)	0.695(586)	0.802(479)	0.409(413)	0.589(404)	0.864(485)
1	(500,2000)	0.856(182)	0.516(173)	0.666(165)	0.909(178)	0.919(153)	0.596(155)	0.747(142)	0.969(151)
2	(500,2000)	0.880(366)	0.546(356)	0.692(334)	0.924(351)	0.947(306)	0.655(311)	0.798(287)	0.979(297)
5	(500,2000)	0.732(1065)	0.354(980)	0.528(915)	0.810(1015)	0.868(872)	0.523(812)	0.695(772)	0.924(855)
1	(500,5000)	0.951(366)	0.689(395)	0.821(358)	0.976(352)	0.977(315)	0.751(350)	0.883(313)	0.997(307)
2	(500,5000)	0.965(716)	0.725(782)	0.846(713)	0.986(678)	0.989(617)	0.789(699)	0.913(619)	1.000(592)
5	(500,5000)	0.891(2102)	0.576(2139)	0.723(1969)	0.939(1958)	0.954(1772)	0.689(1870)	0.820(1683)	0.978(1680)

Table 12: SSMS-CvM monitoring under scenario **S4** ($\alpha = 0.05$, $q = 20$). Entries are $\mathbb{P}(k^* < \mathcal{T}_m \leq mT)$ with the conditional average delay in parentheses, averaged over $b \in \{0.1, 0.2, 0.3, 0.5\}$ and the three error designs. Column labels correspond to the four CvM weights in (21). Left block: SSMS-CvM; right block: HAC-CvM.

T	(N,m)	SSMS				HAC			
		U	E	M	L	U	E	M	L
Panel A: Early change ($k^* = \lfloor 0.1mT \rfloor$)									
1	(200,1000)	0.992(231)	0.991(157)	0.993(221)	0.992(325)	1.000(192)	0.999(126)	1.000(188)	0.999(286)
2	(200,1000)	0.991(434)	0.991(280)	0.991(422)	0.990(649)	1.000(358)	1.000(224)	0.999(356)	1.000(563)
5	(200,1000)	0.942(1253)	0.961(787)	0.952(1209)	0.921(1880)	0.988(1020)	0.995(620)	0.991(1014)	0.978(1647)
1	(200,2000)	1.000(333)	1.000(222)	1.000(331)	1.000(507)	1.000(285)	1.000(185)	1.000(289)	1.000(452)
2	(200,2000)	0.999(610)	0.999(385)	0.999(620)	0.999(1002)	1.000(522)	1.000(324)	1.000(542)	1.000(890)
5	(200,2000)	0.979(1796)	0.990(1100)	0.986(1805)	0.965(2943)	0.998(1500)	1.000(886)	0.999(1553)	0.994(2621)
1	(200,5000)	1.000(544)	1.000(366)	1.000(569)	1.000(893)	1.000(469)	1.000(314)	1.000(501)	1.000(804)
2	(200,5000)	1.000(932)	1.000(602)	1.000(1008)	1.000(1677)	1.000(812)	1.000(524)	1.000(895)	1.000(1519)
5	(200,5000)	1.000(2504)	1.000(1500)	1.000(2749)	0.998(4716)	1.000(2155)	1.000(1298)	1.000(2451)	1.000(4284)
1	(500,1000)	1.000(149)	1.000(99)	1.000(150)	1.000(230)	1.000(123)	1.000(81)	1.000(127)	1.000(199)
2	(500,1000)	1.000(255)	1.000(163)	1.000(265)	1.000(432)	1.000(213)	1.000(135)	1.000(227)	1.000(376)
5	(500,1000)	0.993(729)	0.997(439)	0.996(755)	0.985(1254)	1.000(581)	1.000(342)	1.000(628)	0.999(1068)
1	(500,2000)	1.000(213)	1.000(143)	1.000(223)	1.000(350)	1.000(181)	1.000(122)	1.000(194)	1.000(309)
2	(500,2000)	1.000(356)	1.000(231)	1.000(387)	1.000(646)	1.000(308)	1.000(201)	1.000(341)	1.000(577)
5	(500,2000)	1.000(984)	1.000(592)	1.000(1082)	0.999(1856)	1.000(806)	1.000(489)	1.000(924)	1.000(1627)
1	(500,5000)	1.000(358)	1.000(249)	1.000(391)	1.000(616)	1.000(311)	1.000(218)	1.000(345)	1.000(547)
2	(500,5000)	1.000(571)	1.000(392)	1.000(650)	1.000(1072)	1.000(503)	1.000(350)	1.000(581)	1.000(962)
5	(500,5000)	1.000(1356)	1.000(853)	1.000(1615)	1.000(2877)	1.000(1188)	1.000(753)	1.000(1451)	1.000(2599)
Panel B: Late change ($k^* = \lfloor 0.8mT \rfloor$)									
T	(N,m)	SSMS				HAC			
		U	E	M	L	U	E	M	L
1	(200,1000)	0.437(126)	0.112(96)	0.210(93)	0.518(135)	0.641(113)	0.215(87)	0.360(86)	0.732(121)
2	(200,1000)	0.351(263)	0.079(180)	0.152(184)	0.428(285)	0.578(238)	0.186(175)	0.329(171)	0.667(253)
5	(200,1000)	0.231(711)	0.033(417)	0.073(506)	0.325(742)	0.502(624)	0.132(422)	0.262(443)	0.588(668)
1	(200,2000)	0.548(246)	0.176(189)	0.294(189)	0.628(258)	0.703(225)	0.276(179)	0.439(183)	0.779(234)
2	(200,2000)	0.485(520)	0.135(371)	0.247(384)	0.568(541)	0.667(468)	0.246(344)	0.417(353)	0.736(486)
5	(200,2000)	0.367(1394)	0.063(882)	0.151(969)	0.469(1432)	0.593(1233)	0.183(857)	0.339(922)	0.680(1286)
1	(200,5000)	0.729(565)	0.335(480)	0.488(492)	0.792(561)	0.828(508)	0.438(445)	0.614(432)	0.885(509)
2	(200,5000)	0.664(1163)	0.269(927)	0.422(984)	0.734(1166)	0.773(1066)	0.390(873)	0.564(883)	0.837(1062)
5	(200,5000)	0.579(3246)	0.175(2429)	0.324(2604)	0.673(3191)	0.727(2844)	0.314(2250)	0.503(2311)	0.794(2827)
1	(500,1000)	0.612(119)	0.228(90)	0.361(94)	0.688(121)	0.762(101)	0.329(85)	0.512(82)	0.853(103)
2	(500,1000)	0.562(247)	0.184(181)	0.316(186)	0.635(253)	0.747(209)	0.321(168)	0.500(164)	0.814(217)
5	(500,1000)	0.449(697)	0.094(485)	0.213(495)	0.554(697)	0.695(565)	0.272(442)	0.442(446)	0.765(586)
1	(500,2000)	0.731(221)	0.335(185)	0.495(186)	0.797(219)	0.836(191)	0.449(171)	0.619(163)	0.903(191)
2	(500,2000)	0.675(465)	0.286(373)	0.441(374)	0.745(462)	0.806(402)	0.423(335)	0.599(336)	0.865(402)
5	(500,2000)	0.590(1268)	0.186(1047)	0.338(1020)	0.682(1254)	0.763(1063)	0.357(899)	0.547(896)	0.828(1068)
1	(500,5000)	0.870(466)	0.521(460)	0.672(425)	0.914(452)	0.934(404)	0.614(407)	0.766(372)	0.967(395)
2	(500,5000)	0.824(959)	0.478(889)	0.634(866)	0.882(930)	0.910(836)	0.588(826)	0.739(745)	0.949(811)
5	(500,5000)	0.762(2686)	0.375(2483)	0.561(2369)	0.839(2555)	0.877(2260)	0.531(2145)	0.702(2000)	0.933(2179)

Table 13: SSMS-CvM monitoring under scenario **S5** ($\alpha = 0.05$, $q = 20$). Entries are $\mathbb{P}(k^* < \mathcal{T}_m \leq mT)$ with the conditional average delay in parentheses, averaged over $b \in \{0.1, 0.2, 0.3, 0.5\}$ and the three error designs. Column labels correspond to the four CvM weights in (21). Left block: SSMS-CvM; right block: HAC-CvM.

Panel A: Early change ($k^* = \lfloor 0.1mT \rfloor$)									
T	(N,m)	SSMS				HAC			
		U	E	M	L	U	E	M	L
1	(200,1000)	0.997(562)	0.975(538)	0.991(542)	0.999(571)	1.000(538)	0.998(504)	1.000(518)	1.000(550)
2	(200,1000)	0.964(1165)	0.917(1110)	0.955(1117)	0.972(1182)	0.993(1109)	0.977(1039)	0.990(1061)	0.996(1134)
5	(200,1000)	0.694(3455)	0.577(3084)	0.670(3173)	0.735(3516)	0.859(3215)	0.789(2850)	0.840(2965)	0.887(3322)
1	(200,2000)	1.000(1070)	0.994(1033)	0.999(1037)	1.000(1086)	1.000(1036)	1.000(985)	1.000(1003)	1.000(1057)
2	(200,2000)	0.993(2195)	0.971(2117)	0.989(2118)	0.997(2227)	1.000(2118)	0.993(2018)	1.000(2041)	1.000(2160)
5	(200,2000)	0.767(6500)	0.684(5911)	0.753(6015)	0.805(6610)	0.904(6133)	0.829(5563)	0.889(5701)	0.928(6305)
1	(200,5000)	1.000(2505)	1.000(2429)	1.000(2441)	1.000(2543)	1.000(2460)	1.000(2372)	1.000(2396)	1.000(2502)
2	(200,5000)	1.000(5107)	0.998(4973)	1.000(4968)	1.000(5179)	1.000(4981)	1.000(4810)	1.000(4837)	1.000(5068)
5	(200,5000)	0.907(14728)	0.818(13796)	0.899(13805)	0.929(14923)	0.959(14044)	0.921(13188)	0.956(13217)	0.968(14363)
1	(500,1000)	1.000(521)	0.998(501)	1.000(506)	1.000(530)	1.000(504)	1.000(476)	1.000(489)	1.000(515)
2	(500,1000)	0.998(1067)	0.983(1031)	0.996(1033)	0.999(1083)	1.000(1023)	0.999(973)	1.000(989)	1.000(1045)
5	(500,1000)	0.860(3118)	0.755(2892)	0.834(2912)	0.897(3157)	0.962(2893)	0.914(2670)	0.952(2717)	0.969(2971)
1	(500,2000)	1.000(999)	1.000(966)	1.000(974)	1.000(1015)	1.000(977)	1.000(935)	1.000(951)	1.000(995)
2	(500,2000)	1.000(2034)	0.999(1977)	1.000(1979)	1.000(2063)	1.000(1975)	1.000(1902)	1.000(1919)	1.000(2011)
5	(500,2000)	0.923(5829)	0.842(5503)	0.914(5480)	0.942(5900)	0.976(5483)	0.947(5161)	0.971(5190)	0.986(5617)
1	(500,5000)	1.000(2375)	1.000(2310)	1.000(2324)	1.000(2408)	1.000(2340)	1.000(2268)	1.000(2290)	1.000(2377)
2	(500,5000)	1.000(4800)	1.000(4686)	1.000(4695)	1.000(4866)	1.000(4695)	1.000(4557)	1.000(4587)	1.000(4771)
5	(500,5000)	0.979(13073)	0.944(12590)	0.975(12500)	0.991(13249)	0.999(12609)	0.983(12116)	0.999(12112)	1.000(12857)
Panel B: Late change ($k^* = \lfloor 0.8mT \rfloor$)									
T	(N,m)	SSMS				HAC			
		U	E	M	L	U	E	M	L
1	(200,1000)	0.601(154)	0.099(120)	0.202(120)	0.686(159)	0.770(140)	0.210(117)	0.366(117)	0.857(146)
2	(200,1000)	0.542(312)	0.080(242)	0.166(244)	0.633(323)	0.734(288)	0.193(232)	0.347(229)	0.819(297)
5	(200,1000)	0.268(783)	0.022(457)	0.039(535)	0.375(817)	0.536(722)	0.093(499)	0.185(507)	0.634(769)
1	(200,2000)	0.715(309)	0.163(250)	0.297(256)	0.788(312)	0.839(289)	0.272(249)	0.453(257)	0.911(293)
2	(200,2000)	0.681(625)	0.140(494)	0.267(519)	0.758(631)	0.816(585)	0.252(478)	0.439(494)	0.882(593)
5	(200,2000)	0.416(1588)	0.036(1024)	0.082(1085)	0.534(1634)	0.629(1483)	0.115(1024)	0.243(1126)	0.722(1539)
1	(200,5000)	0.857(750)	0.318(701)	0.482(722)	0.911(743)	0.939(709)	0.442(670)	0.628(670)	0.975(705)
2	(200,5000)	0.832(1505)	0.282(1341)	0.447(1419)	0.892(1487)	0.918(1435)	0.411(1324)	0.597(1343)	0.959(1416)
5	(200,5000)	0.634(3940)	0.087(2921)	0.222(3272)	0.719(3930)	0.760(3725)	0.209(2942)	0.379(3123)	0.834(3723)
1	(500,1000)	0.756(153)	0.208(125)	0.352(133)	0.828(153)	0.862(138)	0.325(125)	0.521(124)	0.944(139)
2	(500,1000)	0.737(307)	0.185(249)	0.330(260)	0.808(308)	0.864(277)	0.326(245)	0.521(245)	0.925(282)
5	(500,1000)	0.497(818)	0.043(576)	0.126(619)	0.606(814)	0.727(721)	0.181(556)	0.339(584)	0.802(744)
1	(500,2000)	0.856(297)	0.320(272)	0.487(276)	0.913(294)	0.925(276)	0.444(263)	0.629(262)	0.974(275)
2	(500,2000)	0.829(605)	0.285(551)	0.457(558)	0.892(596)	0.925(562)	0.433(518)	0.617(527)	0.964(558)
5	(500,2000)	0.632(1572)	0.098(1352)	0.229(1286)	0.727(1570)	0.790(1451)	0.249(1210)	0.426(1264)	0.860(1461)
1	(500,5000)	0.947(701)	0.501(727)	0.668(705)	0.975(690)	0.981(661)	0.615(695)	0.774(669)	0.999(656)
2	(500,5000)	0.940(1408)	0.493(1427)	0.658(1428)	0.973(1378)	0.979(1329)	0.605(1396)	0.764(1334)	0.998(1309)
5	(500,5000)	0.801(3728)	0.254(3339)	0.446(3410)	0.890(3648)	0.908(3508)	0.395(3231)	0.598(3299)	0.952(3450)

Table 14: RSMS-CvM monitoring under scenario **S1** ($\alpha = 0.05$, $q = 20$). Entries are $\mathbb{P}(k^* < \mathcal{T}_m \leq mT)$ with the conditional average delay in parentheses, averaged over $b \in \{0.1, 0.2, 0.3, 0.5\}$ and the three error designs. Column labels correspond to the four CvM weights in (21). Left block: RSMS-CvM; right block: HAC-CvM.

T	(N,m)	RSMS				HAC			
		U	E	M	L	U	E	M	L
Panel A: Early change ($k^* = \lfloor 0.1mT \rfloor$)									
1	(200,1000)	1.000(52)	1.000(37)	1.000(58)	1.000(86)	1.000(48)	1.000(35)	1.000(54)	1.000(80)
2	(200,1000)	1.000(82)	1.000(59)	1.000(96)	1.000(149)	1.000(76)	1.000(55)	1.000(89)	1.000(138)
5	(200,1000)	1.000(187)	1.000(125)	1.000(231)	1.000(451)	1.000(165)	1.000(113)	1.000(205)	1.000(389)
1	(200,2000)	1.000(82)	1.000(60)	1.000(94)	1.000(138)	1.000(77)	1.000(56)	1.000(88)	1.000(130)
2	(200,2000)	1.000(129)	1.000(94)	1.000(153)	1.000(234)	1.000(121)	1.000(88)	1.000(143)	1.000(218)
5	(200,2000)	1.000(270)	1.000(189)	1.000(337)	1.000(621)	1.000(244)	1.000(173)	1.000(306)	1.000(537)
1	(200,5000)	1.000(152)	1.000(112)	1.000(177)	1.000(259)	1.000(143)	1.000(105)	1.000(166)	1.000(244)
2	(200,5000)	1.000(237)	1.000(175)	1.000(282)	1.000(423)	1.000(223)	1.000(164)	1.000(266)	1.000(397)
5	(200,5000)	1.000(462)	1.000(337)	1.000(578)	1.000(939)	1.000(426)	1.000(312)	1.000(534)	1.000(860)
1	(500,1000)	1.000(37)	1.000(27)	1.000(43)	1.000(62)	1.000(35)	1.000(25)	1.000(40)	1.000(59)
2	(500,1000)	1.000(58)	1.000(42)	1.000(68)	1.000(103)	1.000(54)	1.000(40)	1.000(64)	1.000(96)
5	(500,1000)	1.000(117)	1.000(84)	1.000(146)	1.000(249)	1.000(106)	1.000(76)	1.000(133)	1.000(220)
1	(500,2000)	1.000(59)	1.000(44)	1.000(69)	1.000(101)	1.000(56)	1.000(41)	1.000(65)	1.000(96)
2	(500,2000)	1.000(92)	1.000(68)	1.000(110)	1.000(165)	1.000(86)	1.000(64)	1.000(103)	1.000(154)
5	(500,2000)	1.000(180)	1.000(131)	1.000(225)	1.000(363)	1.000(165)	1.000(121)	1.000(206)	1.000(330)
1	(500,5000)	1.000(111)	1.000(82)	1.000(131)	1.000(192)	1.000(104)	1.000(77)	1.000(124)	1.000(181)
2	(500,5000)	1.000(171)	1.000(127)	1.000(206)	1.000(304)	1.000(161)	1.000(119)	1.000(194)	1.000(286)
5	(500,5000)	1.000(320)	1.000(239)	1.000(398)	1.000(616)	1.000(297)	1.000(222)	1.000(370)	1.000(570)
Panel B: Late change ($k^* = \lfloor 0.8mT \rfloor$)									
T	(N,m)	RSMS				HAC			
		U	E	M	L	U	E	M	L
1	(200,1000)	0.982(54)	0.809(66)	0.908(55)	0.998(52)	0.939(45)	0.717(55)	0.818(46)	0.987(45)
2	(200,1000)	0.991(111)	0.808(132)	0.917(115)	0.999(106)	0.963(92)	0.750(109)	0.869(92)	0.995(89)
5	(200,1000)	0.885(373)	0.611(379)	0.744(350)	0.933(346)	0.934(285)	0.656(303)	0.804(265)	0.973(275)
1	(200,2000)	0.986(90)	0.880(113)	0.953(93)	0.998(87)	0.965(77)	0.800(94)	0.887(78)	0.993(76)
2	(200,2000)	0.999(179)	0.910(227)	0.971(187)	1.000(170)	0.986(150)	0.831(185)	0.931(152)	0.999(147)
5	(200,2000)	0.942(596)	0.712(694)	0.849(599)	0.971(541)	0.968(461)	0.753(533)	0.888(454)	0.994(440)
1	(200,5000)	0.994(170)	0.943(209)	0.976(173)	1.000(164)	0.984(149)	0.874(174)	0.935(146)	0.999(147)
2	(200,5000)	0.999(331)	0.962(428)	0.993(343)	1.000(315)	0.992(287)	0.920(346)	0.965(285)	1.000(278)
5	(200,5000)	0.996(1038)	0.869(1382)	0.944(1086)	1.000(924)	0.993(824)	0.880(1051)	0.953(836)	1.000(772)
1	(500,1000)	0.978(40)	0.885(48)	0.941(40)	0.998(38)	0.934(33)	0.725(40)	0.833(33)	0.991(33)
2	(500,1000)	0.995(78)	0.905(98)	0.974(80)	1.000(75)	0.970(64)	0.787(78)	0.891(64)	0.995(64)
5	(500,1000)	0.972(252)	0.786(299)	0.914(257)	0.993(230)	0.980(192)	0.782(231)	0.897(191)	0.998(185)
1	(500,2000)	0.991(65)	0.911(80)	0.967(66)	0.999(64)	0.965(57)	0.819(67)	0.895(56)	0.995(56)
2	(500,2000)	0.996(128)	0.957(163)	0.986(131)	1.000(122)	0.987(109)	0.889(130)	0.947(108)	1.000(107)
5	(500,2000)	0.997(396)	0.887(515)	0.954(414)	1.000(355)	0.990(309)	0.869(391)	0.947(314)	0.999(293)
1	(500,5000)	0.994(125)	0.948(148)	0.980(125)	1.000(121)	0.987(110)	0.883(126)	0.944(107)	1.000(109)
2	(500,5000)	0.999(238)	0.981(291)	0.996(241)	0.999(228)	0.994(208)	0.919(242)	0.970(203)	1.000(203)
5	(500,5000)	1.000(670)	0.961(930)	1.000(707)	1.000(611)	0.997(548)	0.941(712)	0.977(549)	1.000(523)

Table 15: RSMS-CvM monitoring under scenario **S2** ($\alpha = 0.05$, $q = 20$). Entries are $\mathbb{P}(k^* < \mathcal{T}_m \leq mT)$ with the conditional average delay in parentheses, averaged over $b \in \{0.1, 0.2, 0.3, 0.5\}$ and the three error designs. Column labels correspond to the four CvM weights in (21). Left block: RSMS-CvM; right block: HAC-CvM.

T	(N,m)	RSMS				HAC			
		U	E	M	L	U	E	M	L
Panel A: Early change ($k^* = \lfloor 0.1mT \rfloor$)									
1	(200,1000)	1.000(110)	1.000(73)	1.000(115)	1.000(181)	1.000(99)	1.000(66)	1.000(104)	1.000(165)
2	(200,1000)	1.000(186)	1.000(120)	1.000(201)	1.000(336)	1.000(166)	1.000(108)	1.000(182)	1.000(304)
5	(200,1000)	1.000(509)	1.000(304)	1.000(558)	1.000(955)	1.000(423)	1.000(256)	1.000(481)	1.000(838)
1	(200,2000)	1.000(160)	1.000(110)	1.000(174)	1.000(277)	1.000(146)	1.000(100)	1.000(159)	1.000(254)
2	(200,2000)	1.000(268)	1.000(179)	1.000(301)	1.000(508)	1.000(243)	1.000(164)	1.000(276)	1.000(462)
5	(200,2000)	1.000(696)	1.000(427)	1.000(807)	1.000(1435)	1.000(599)	1.000(369)	1.000(711)	1.000(1276)
1	(200,5000)	1.000(275)	1.000(197)	1.000(309)	1.000(484)	1.000(255)	1.000(183)	1.000(287)	1.000(447)
2	(200,5000)	1.000(443)	1.000(315)	1.000(515)	1.000(842)	1.000(410)	1.000(293)	1.000(479)	1.000(772)
5	(200,5000)	1.000(1014)	1.000(666)	1.000(1250)	1.000(2234)	1.000(896)	1.000(601)	1.000(1116)	1.000(2001)
1	(500,1000)	1.000(71)	1.000(49)	1.000(78)	1.000(124)	1.000(65)	1.000(45)	1.000(72)	1.000(113)
2	(500,1000)	1.000(114)	1.000(78)	1.000(130)	1.000(215)	1.000(104)	1.000(72)	1.000(119)	1.000(195)
5	(500,1000)	1.000(275)	1.000(173)	1.000(328)	1.000(584)	1.000(238)	1.000(152)	1.000(289)	1.000(514)
1	(500,2000)	1.000(107)	1.000(77)	1.000(120)	1.000(187)	1.000(99)	1.000(72)	1.000(112)	1.000(173)
2	(500,2000)	1.000(172)	1.000(123)	1.000(201)	1.000(325)	1.000(159)	1.000(114)	1.000(186)	1.000(297)
5	(500,2000)	1.000(393)	1.000(260)	1.000(484)	1.000(859)	1.000(344)	1.000(233)	1.000(429)	1.000(764)
1	(500,5000)	1.000(195)	1.000(142)	1.000(223)	1.000(335)	1.000(183)	1.000(133)	1.000(210)	1.000(313)
2	(500,5000)	1.000(306)	1.000(224)	1.000(361)	1.000(557)	1.000(286)	1.000(209)	1.000(338)	1.000(516)
5	(500,5000)	1.000(623)	1.000(441)	1.000(778)	1.000(1339)	1.000(566)	1.000(404)	1.000(709)	1.000(1201)
Panel B: Late change ($k^* = \lfloor 0.8mT \rfloor$)									
T	(N,m)	RSMS				HAC			
		U	E	M	L	U	E	M	L
1	(200,1000)	0.767(107)	0.353(95)	0.521(89)	0.824(109)	0.823(91)	0.418(85)	0.580(80)	0.903(94)
2	(200,1000)	0.709(228)	0.314(177)	0.474(192)	0.771(230)	0.803(193)	0.404(171)	0.579(159)	0.875(195)
5	(200,1000)	0.612(654)	0.207(496)	0.359(528)	0.695(640)	0.760(520)	0.346(444)	0.531(429)	0.832(528)
1	(200,2000)	0.836(198)	0.467(183)	0.633(174)	0.893(195)	0.887(170)	0.519(165)	0.685(154)	0.943(169)
2	(200,2000)	0.794(417)	0.433(364)	0.599(367)	0.852(408)	0.878(349)	0.509(326)	0.688(300)	0.929(347)
5	(200,2000)	0.714(1176)	0.307(1021)	0.497(1021)	0.790(1129)	0.834(952)	0.457(867)	0.637(825)	0.900(940)
1	(200,5000)	0.940(400)	0.653(422)	0.785(383)	0.970(384)	0.961(343)	0.685(367)	0.828(328)	0.988(333)
2	(200,5000)	0.916(840)	0.605(868)	0.740(782)	0.947(792)	0.950(707)	0.677(726)	0.811(660)	0.979(676)
5	(200,5000)	0.866(2397)	0.513(2561)	0.680(2329)	0.927(2196)	0.935(1933)	0.626(1997)	0.771(1783)	0.966(1822)
1	(500,1000)	0.886(89)	0.558(83)	0.701(81)	0.933(87)	0.893(74)	0.532(75)	0.703(67)	0.965(73)
2	(500,1000)	0.861(185)	0.518(172)	0.678(164)	0.910(181)	0.910(150)	0.555(148)	0.722(133)	0.958(150)
5	(500,1000)	0.794(526)	0.432(486)	0.602(481)	0.872(500)	0.897(413)	0.539(403)	0.707(371)	0.945(408)
1	(500,2000)	0.946(151)	0.656(158)	0.807(144)	0.974(146)	0.947(129)	0.663(139)	0.807(123)	0.986(125)
2	(500,2000)	0.926(321)	0.629(328)	0.765(303)	0.957(303)	0.956(265)	0.684(277)	0.824(248)	0.984(255)
5	(500,2000)	0.887(913)	0.549(939)	0.702(867)	0.935(837)	0.944(715)	0.648(757)	0.792(672)	0.974(682)
1	(500,5000)	0.989(286)	0.810(339)	0.919(293)	0.999(271)	0.986(244)	0.811(291)	0.914(243)	0.999(236)
2	(500,5000)	0.984(583)	0.781(699)	0.908(598)	0.996(540)	0.992(487)	0.812(581)	0.924(484)	1.000(461)
5	(500,5000)	0.963(1668)	0.711(2083)	0.861(1759)	0.992(1491)	0.990(1323)	0.780(1581)	0.916(1333)	1.000(1229)

Table 16: RSMS-CvM monitoring under scenario **S3** ($\alpha = 0.05$, $q = 20$). Entries are $\mathbb{P}(k^* < \mathcal{T}_m \leq mT)$ with the conditional average delay in parentheses, averaged over $b \in \{0.1, 0.2, 0.3, 0.5\}$ and the three error designs. Column labels correspond to the four CvM weights in (21). Left block: RSMS-CvM; right block: HAC-CvM.

T	(N,m)	RSMS				HAC			
		U	E	M	L	U	E	M	L
Panel A: Early change ($k^* = \lfloor 0.1mT \rfloor$)									
1	(200,1000)	1.000(198)	1.000(166)	1.000(191)	1.000(245)	1.000(187)	1.000(158)	1.000(182)	1.000(230)
2	(200,1000)	1.000(392)	1.000(321)	1.000(375)	1.000(502)	1.000(366)	1.000(304)	1.000(356)	1.000(467)
5	(200,1000)	0.914(1520)	0.949(1010)	0.924(1359)	0.865(2108)	0.967(1296)	0.983(884)	0.971(1179)	0.941(1870)
1	(200,2000)	1.000(343)	1.000(298)	1.000(337)	1.000(416)	1.000(330)	1.000(287)	1.000(325)	1.000(397)
2	(200,2000)	1.000(668)	1.000(572)	1.000(655)	1.000(840)	1.000(636)	1.000(551)	1.000(629)	1.000(790)
5	(200,2000)	0.952(2383)	0.978(1679)	0.959(2172)	0.918(3545)	0.986(2057)	0.997(1523)	0.988(1931)	0.965(3178)
1	(200,5000)	1.000(741)	1.000(663)	1.000(737)	1.000(872)	1.000(720)	1.000(646)	1.000(718)	1.000(843)
2	(200,5000)	1.000(1413)	1.000(1264)	1.000(1410)	1.000(1692)	1.000(1372)	1.000(1233)	1.000(1373)	1.000(1629)
5	(200,5000)	0.996(4278)	1.000(3279)	0.997(4054)	0.971(6201)	1.000(3824)	1.000(3123)	1.000(3698)	0.994(5437)
1	(500,1000)	1.000(163)	1.000(143)	1.000(161)	1.000(195)	1.000(157)	1.000(138)	1.000(155)	1.000(186)
2	(500,1000)	1.000(311)	1.000(272)	1.000(308)	1.000(383)	1.000(299)	1.000(263)	1.000(297)	1.000(363)
5	(500,1000)	0.985(977)	0.996(739)	0.988(920)	0.968(1453)	0.998(871)	1.000(678)	0.998(837)	0.989(1270)
1	(500,2000)	1.000(294)	1.000(263)	1.000(292)	1.000(345)	1.000(285)	1.000(256)	1.000(284)	1.000(333)
2	(500,2000)	1.000(559)	1.000(501)	1.000(558)	1.000(667)	1.000(542)	1.000(488)	1.000(543)	1.000(641)
5	(500,2000)	0.999(1619)	1.000(1288)	0.999(1550)	0.987(2296)	1.000(1449)	1.000(1228)	1.000(1425)	0.999(2039)
1	(500,5000)	1.000(654)	1.000(598)	1.000(655)	1.000(751)	1.000(640)	1.000(586)	1.000(642)	1.000(732)
2	(500,5000)	1.000(1242)	1.000(1141)	1.000(1248)	1.000(1433)	1.000(1216)	1.000(1119)	1.000(1223)	1.000(1394)
5	(500,5000)	1.000(3144)	1.000(2844)	1.000(3160)	1.000(4161)	1.000(3039)	1.000(2771)	1.000(3066)	1.000(3793)
Panel B: Late change ($k^* = \lfloor 0.8mT \rfloor$)									
T	(N,m)	RSMS				HAC			
		U	E	M	L	U	E	M	L
1	(200,1000)	0.665(114)	0.260(94)	0.415(90)	0.730(119)	0.757(99)	0.337(86)	0.498(82)	0.839(103)
2	(200,1000)	0.671(242)	0.263(182)	0.414(200)	0.738(245)	0.773(206)	0.359(177)	0.530(167)	0.850(211)
5	(200,1000)	0.444(694)	0.098(463)	0.218(531)	0.540(710)	0.641(565)	0.237(431)	0.399(433)	0.723(589)
1	(200,2000)	0.745(216)	0.354(184)	0.520(180)	0.805(216)	0.822(190)	0.430(172)	0.603(166)	0.887(191)
2	(200,2000)	0.772(443)	0.390(386)	0.551(383)	0.830(434)	0.862(377)	0.475(345)	0.658(324)	0.917(377)
5	(200,2000)	0.572(1280)	0.182(994)	0.327(1040)	0.664(1277)	0.732(1065)	0.325(858)	0.505(860)	0.801(1078)
1	(200,5000)	0.879(458)	0.557(444)	0.703(425)	0.925(447)	0.927(404)	0.613(404)	0.760(371)	0.965(397)
2	(200,5000)	0.904(926)	0.567(919)	0.714(860)	0.940(881)	0.943(803)	0.651(806)	0.789(757)	0.973(771)
5	(200,5000)	0.732(2770)	0.350(2666)	0.535(2547)	0.813(2627)	0.844(2303)	0.498(2100)	0.670(2002)	0.909(2240)
1	(500,1000)	0.808(99)	0.455(86)	0.604(86)	0.872(98)	0.852(84)	0.460(79)	0.640(74)	0.932(84)
2	(500,1000)	0.828(202)	0.460(182)	0.624(176)	0.885(200)	0.892(170)	0.513(162)	0.687(149)	0.944(170)
5	(500,1000)	0.665(600)	0.273(476)	0.439(497)	0.741(582)	0.802(479)	0.409(413)	0.589(404)	0.864(485)
1	(500,2000)	0.896(176)	0.563(168)	0.721(160)	0.936(172)	0.919(153)	0.596(155)	0.747(142)	0.969(151)
2	(500,2000)	0.910(357)	0.591(358)	0.733(337)	0.945(340)	0.947(306)	0.655(311)	0.798(287)	0.979(297)
5	(500,2000)	0.752(1073)	0.389(973)	0.564(958)	0.836(1018)	0.868(872)	0.523(812)	0.695(772)	0.924(855)
1	(500,5000)	0.966(356)	0.731(385)	0.860(353)	0.988(341)	0.977(315)	0.751(350)	0.883(313)	0.997(307)
2	(500,5000)	0.978(702)	0.753(800)	0.885(718)	0.994(661)	0.989(617)	0.789(699)	0.913(619)	1.000(592)
5	(500,5000)	0.910(2150)	0.591(2262)	0.728(2057)	0.947(1962)	0.954(1772)	0.689(1870)	0.820(1683)	0.978(1680)

Table 17: RSMS-CvM monitoring under scenario **S4** ($\alpha = 0.05$, $q = 20$). Entries are $\mathbb{P}(k^* < \mathcal{T}_m \leq mT)$ with the conditional average delay in parentheses, averaged over $b \in \{0.1, 0.2, 0.3, 0.5\}$ and the three error designs. Column labels correspond to the four CvM weights in (21). Left block: RSMS-CvM; right block: HAC-CvM.

		RSMS				HAC			
T	(N,m)	U	E	M	L	U	E	M	L
Panel A: Early change ($k^* = \lfloor 0.1mT \rfloor$)									
1	(200,1000)	0.997(216)	0.997(144)	0.998(208)	0.997(312)	1.000(192)	0.999(126)	1.000(188)	0.999(286)
2	(200,1000)	0.998(407)	0.997(260)	0.998(399)	0.998(620)	1.000(358)	1.000(224)	0.999(356)	1.000(563)
5	(200,1000)	0.959(1218)	0.972(754)	0.966(1175)	0.943(1855)	0.988(1020)	0.995(620)	0.991(1014)	0.978(1647)
1	(200,2000)	1.000(318)	1.000(209)	1.000(318)	1.000(493)	1.000(285)	1.000(185)	1.000(289)	1.000(452)
2	(200,2000)	1.000(590)	1.000(370)	1.000(601)	1.000(978)	1.000(522)	1.000(324)	1.000(542)	1.000(890)
5	(200,2000)	0.988(1776)	0.994(1078)	0.992(1783)	0.977(2947)	0.998(1500)	1.000(886)	0.999(1553)	0.994(2621)
1	(200,5000)	1.000(518)	1.000(345)	1.000(546)	1.000(872)	1.000(469)	1.000(314)	1.000(501)	1.000(804)
2	(200,5000)	1.000(907)	1.000(581)	1.000(984)	1.000(1662)	1.000(812)	1.000(524)	1.000(895)	1.000(1519)
5	(200,5000)	1.000(2548)	1.000(1510)	1.000(2797)	1.000(4798)	1.000(2155)	1.000(1298)	1.000(2451)	1.000(4284)
1	(500,1000)	1.000(137)	1.000(91)	1.000(140)	1.000(218)	1.000(123)	1.000(81)	1.000(127)	1.000(199)
2	(500,1000)	1.000(241)	1.000(152)	1.000(252)	1.000(415)	1.000(213)	1.000(135)	1.000(227)	1.000(376)
5	(500,1000)	0.999(694)	0.999(412)	0.999(723)	0.994(1218)	1.000(581)	1.000(342)	1.000(628)	0.999(1068)
1	(500,2000)	1.000(199)	1.000(133)	1.000(211)	1.000(336)	1.000(181)	1.000(122)	1.000(194)	1.000(309)
2	(500,2000)	1.000(345)	1.000(223)	1.000(376)	1.000(636)	1.000(308)	1.000(201)	1.000(341)	1.000(577)
5	(500,2000)	1.000(961)	1.000(576)	1.000(1064)	1.000(1829)	1.000(806)	1.000(489)	1.000(924)	1.000(1627)
1	(500,5000)	1.000(336)	1.000(235)	1.000(371)	1.000(591)	1.000(311)	1.000(218)	1.000(345)	1.000(547)
2	(500,5000)	1.000(550)	1.000(379)	1.000(630)	1.000(1053)	1.000(503)	1.000(350)	1.000(581)	1.000(962)
5	(500,5000)	1.000(1363)	1.000(848)	1.000(1626)	1.000(2916)	1.000(1188)	1.000(753)	1.000(1451)	1.000(2599)
Panel B: Late change ($k^* = \lfloor 0.8mT \rfloor$)									
		RSMS				HAC			
T	(N,m)	U	E	M	L	U	E	M	L
1	(200,1000)	0.499(127)	0.135(95)	0.249(90)	0.570(137)	0.641(113)	0.215(87)	0.360(86)	0.732(121)
2	(200,1000)	0.403(271)	0.096(164)	0.183(200)	0.480(290)	0.578(238)	0.186(175)	0.329(171)	0.667(253)
5	(200,1000)	0.266(750)	0.034(471)	0.081(507)	0.359(798)	0.502(624)	0.132(422)	0.262(443)	0.588(668)
1	(200,2000)	0.583(253)	0.189(183)	0.329(190)	0.659(262)	0.703(225)	0.276(179)	0.439(183)	0.779(234)
2	(200,2000)	0.507(537)	0.146(372)	0.268(410)	0.587(559)	0.667(468)	0.246(344)	0.417(353)	0.736(486)
5	(200,2000)	0.384(1447)	0.054(946)	0.162(1016)	0.496(1480)	0.593(1233)	0.183(857)	0.339(922)	0.680(1286)
1	(200,5000)	0.742(575)	0.339(474)	0.511(483)	0.801(570)	0.828(508)	0.438(445)	0.614(432)	0.885(509)
2	(200,5000)	0.671(1201)	0.266(997)	0.435(980)	0.735(1207)	0.773(1066)	0.390(873)	0.564(883)	0.837(1062)
5	(200,5000)	0.582(3387)	0.177(2883)	0.318(2913)	0.676(3294)	0.727(2844)	0.314(2250)	0.503(2311)	0.794(2827)
1	(500,1000)	0.677(118)	0.286(88)	0.427(96)	0.745(120)	0.762(101)	0.329(85)	0.512(82)	0.853(103)
2	(500,1000)	0.612(249)	0.220(182)	0.367(192)	0.680(255)	0.747(209)	0.321(168)	0.500(164)	0.814(217)
5	(500,1000)	0.505(694)	0.127(510)	0.257(550)	0.600(696)	0.695(565)	0.272(442)	0.442(446)	0.765(586)
1	(500,2000)	0.771(218)	0.375(182)	0.553(182)	0.830(218)	0.836(191)	0.449(171)	0.619(163)	0.903(191)
2	(500,2000)	0.698(466)	0.306(378)	0.471(389)	0.764(464)	0.806(402)	0.423(335)	0.599(336)	0.865(402)
5	(500,2000)	0.617(1301)	0.208(1020)	0.365(1090)	0.702(1260)	0.763(1063)	0.357(899)	0.547(896)	0.828(1068)
1	(500,5000)	0.890(463)	0.560(445)	0.705(422)	0.935(450)	0.934(404)	0.614(407)	0.766(372)	0.967(395)
2	(500,5000)	0.838(981)	0.502(937)	0.658(889)	0.899(936)	0.910(836)	0.588(826)	0.739(745)	0.949(811)
5	(500,5000)	0.761(2755)	0.387(2775)	0.571(2493)	0.857(2584)	0.877(2260)	0.531(2145)	0.702(2000)	0.933(2179)

Table 18: RSMS-CvM monitoring under scenario **S5** ($\alpha = 0.05$, $q = 20$). Entries are $\mathbb{P}(k^* < \mathcal{T}_m \leq mT)$ with the conditional average delay in parentheses, averaged over $b \in \{0.1, 0.2, 0.3, 0.5\}$ and the three error designs. Column labels correspond to the four CvM weights in (21). Left block: RSMS-CvM; right block: HAC-CvM.

T	(N,m)	RSMS				HAC			
		U	E	M	L	U	E	M	L
Panel A: Early change ($k^* = \lfloor 0.1mT \rfloor$)									
1	(200,1000)	0.999(555)	0.984(531)	0.996(535)	1.000(565)	1.000(538)	0.998(504)	1.000(518)	1.000(550)
2	(200,1000)	0.975(1151)	0.939(1100)	0.967(1101)	0.985(1171)	0.993(1109)	0.977(1039)	0.990(1061)	0.996(1134)
5	(200,1000)	0.723(3458)	0.616(3116)	0.704(3189)	0.763(3508)	0.859(3215)	0.789(2850)	0.840(2965)	0.887(3322)
1	(200,2000)	1.000(1060)	0.999(1024)	1.000(1027)	1.000(1078)	1.000(1036)	1.000(985)	1.000(1003)	1.000(1057)
2	(200,2000)	0.996(2184)	0.973(2108)	0.994(2103)	0.999(2217)	1.000(2118)	0.993(2018)	1.000(2041)	1.000(2160)
5	(200,2000)	0.782(6532)	0.696(5978)	0.764(6058)	0.831(6631)	0.904(6133)	0.829(5563)	0.889(5701)	0.928(6305)
1	(200,5000)	1.000(2501)	1.000(2429)	1.000(2437)	1.000(2538)	1.000(2460)	1.000(2372)	1.000(2396)	1.000(2502)
2	(200,5000)	1.000(5081)	0.999(4950)	1.000(4932)	1.000(5157)	1.000(4981)	1.000(4810)	1.000(4837)	1.000(5068)
5	(200,5000)	0.913(14850)	0.815(14013)	0.908(13935)	0.932(15014)	0.959(14044)	0.921(13188)	0.956(13217)	0.968(14363)
1	(500,1000)	1.000(516)	1.000(496)	1.000(501)	1.000(525)	1.000(504)	1.000(476)	1.000(489)	1.000(515)
2	(500,1000)	1.000(1052)	0.991(1017)	0.999(1017)	1.000(1070)	1.000(1023)	0.999(973)	1.000(989)	1.000(1045)
5	(500,1000)	0.896(3082)	0.791(2870)	0.875(2887)	0.925(3125)	0.962(2893)	0.914(2670)	0.952(2717)	0.969(2971)
1	(500,2000)	1.000(993)	1.000(962)	1.000(968)	1.000(1009)	1.000(977)	1.000(935)	1.000(951)	1.000(995)
2	(500,2000)	1.000(2017)	1.000(1961)	1.000(1959)	1.000(2048)	1.000(1975)	1.000(1902)	1.000(1919)	1.000(2011)
5	(500,2000)	0.934(5804)	0.866(5524)	0.928(5465)	0.950(5873)	0.976(5483)	0.947(5161)	0.971(5190)	0.986(5617)
1	(500,5000)	1.000(2369)	1.000(2308)	1.000(2319)	1.000(2403)	1.000(2340)	1.000(2268)	1.000(2290)	1.000(2377)
2	(500,5000)	1.000(4767)	1.000(4653)	1.000(4655)	1.000(4836)	1.000(4695)	1.000(4557)	1.000(4587)	1.000(4771)
5	(500,5000)	0.986(13113)	0.944(12667)	0.982(12543)	0.997(13279)	0.999(12609)	0.983(12116)	0.999(12112)	1.000(12857)
Panel B: Late change ($k^* = \lfloor 0.8mT \rfloor$)									
T	(N,m)	RSMS				HAC			
		U	E	M	L	U	E	M	L
1	(200,1000)	0.681(154)	0.128(122)	0.253(120)	0.756(159)	0.770(140)	0.210(117)	0.366(117)	0.857(146)
2	(200,1000)	0.605(316)	0.099(219)	0.196(260)	0.687(324)	0.734(288)	0.193(232)	0.347(229)	0.819(297)
5	(200,1000)	0.302(823)	0.019(518)	0.036(573)	0.421(867)	0.536(722)	0.093(499)	0.185(507)	0.634(769)
1	(200,2000)	0.765(311)	0.190(257)	0.341(261)	0.835(313)	0.839(289)	0.272(249)	0.453(257)	0.911(293)
2	(200,2000)	0.709(636)	0.153(509)	0.286(552)	0.781(640)	0.816(585)	0.252(478)	0.439(494)	0.882(593)
5	(200,2000)	0.435(1652)	0.019(1063)	0.072(1187)	0.552(1688)	0.629(1483)	0.115(1024)	0.243(1126)	0.722(1539)
1	(200,5000)	0.900(756)	0.340(680)	0.527(709)	0.942(745)	0.939(709)	0.442(670)	0.628(670)	0.975(705)
2	(200,5000)	0.851(1525)	0.283(1415)	0.475(1413)	0.917(1499)	0.918(1435)	0.411(1324)	0.597(1343)	0.959(1416)
5	(200,5000)	0.632(4055)	0.069(3419)	0.207(3663)	0.716(4019)	0.760(3725)	0.209(2942)	0.379(3123)	0.834(3723)
1	(500,1000)	0.825(152)	0.282(127)	0.435(137)	0.892(151)	0.862(138)	0.325(125)	0.521(124)	0.944(139)
2	(500,1000)	0.787(308)	0.231(261)	0.393(271)	0.854(307)	0.864(277)	0.326(245)	0.521(245)	0.925(282)
5	(500,1000)	0.548(816)	0.054(619)	0.153(651)	0.655(823)	0.727(721)	0.181(556)	0.339(584)	0.802(744)
1	(500,2000)	0.905(295)	0.375(270)	0.565(275)	0.950(293)	0.925(276)	0.444(263)	0.629(262)	0.974(275)
2	(500,2000)	0.863(603)	0.312(554)	0.498(581)	0.921(593)	0.925(562)	0.433(518)	0.617(527)	0.964(558)
5	(500,2000)	0.659(1615)	0.099(1254)	0.238(1383)	0.739(1584)	0.790(1451)	0.249(1210)	0.426(1264)	0.860(1461)
1	(500,5000)	0.972(700)	0.560(718)	0.716(710)	0.994(687)	0.981(661)	0.615(695)	0.774(669)	0.999(656)
2	(500,5000)	0.956(1412)	0.518(1465)	0.687(1451)	0.982(1375)	0.979(1329)	0.605(1396)	0.764(1334)	0.998(1309)
5	(500,5000)	0.805(3824)	0.238(3500)	0.444(3606)	0.901(3691)	0.908(3508)	0.395(3231)	0.598(3299)	0.952(3450)

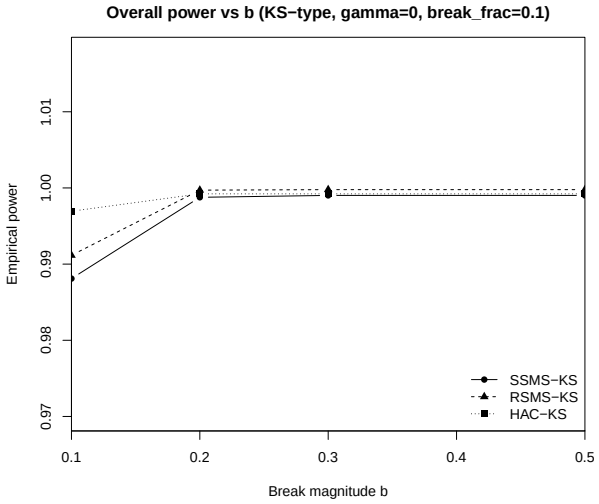

(a) Early change ($k^*/(mT) = 0.1$), $\gamma = 0$.

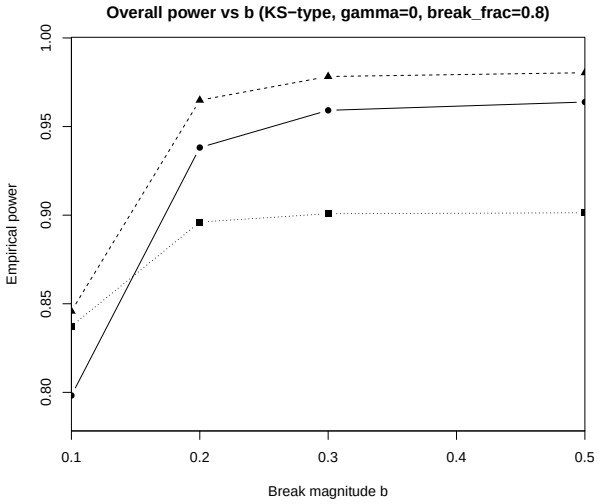

(b) Late change ($k^*/(mT) = 0.8$), $\gamma = 0$.

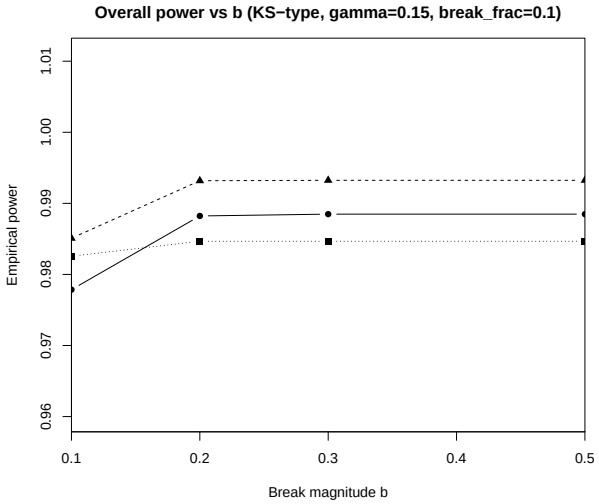

(c) Early change ($k^*/(mT) = 0.1$), $\gamma = 0.15$.

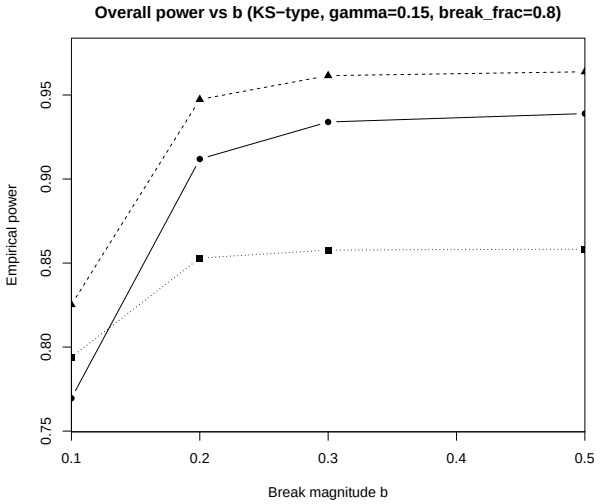

(d) Late change ($k^*/(mT) = 0.8$), $\gamma = 0.15$.

Figure 1: Overall power versus break magnitude for KS-type monitoring (SSMS/RSMS versus HAC). Each panel plots the Monte Carlo estimate of $\mathbb{P}(k^* < \mathcal{T}_m \leq mT)$ against b and is averaged over scenarios S1–S5, the three error designs, and the reported (N, m, T) configurations.

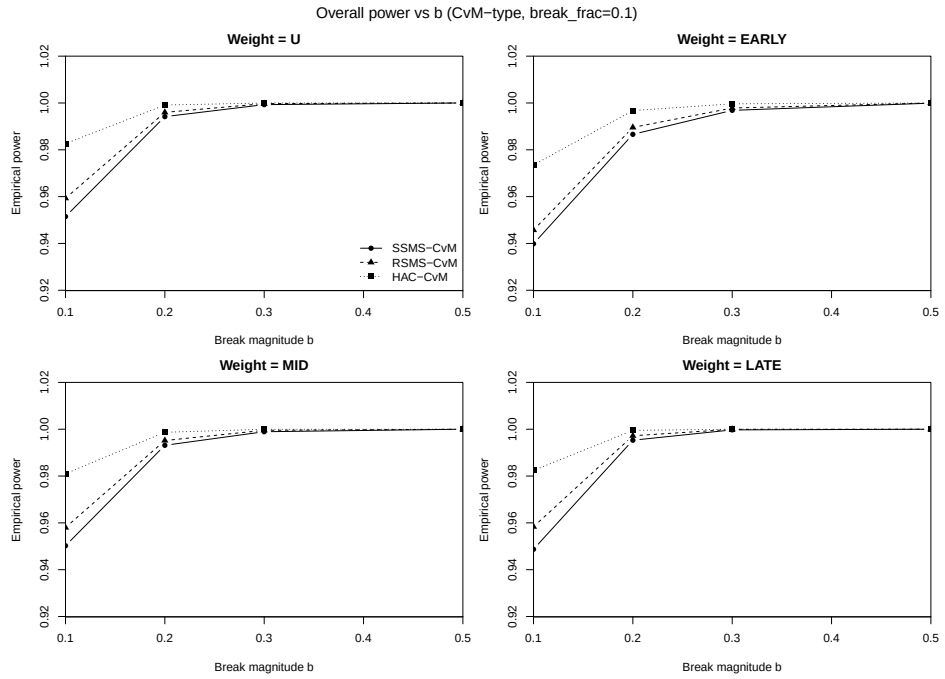

(a) Early change ($k^*/(mT) = 0.1$).

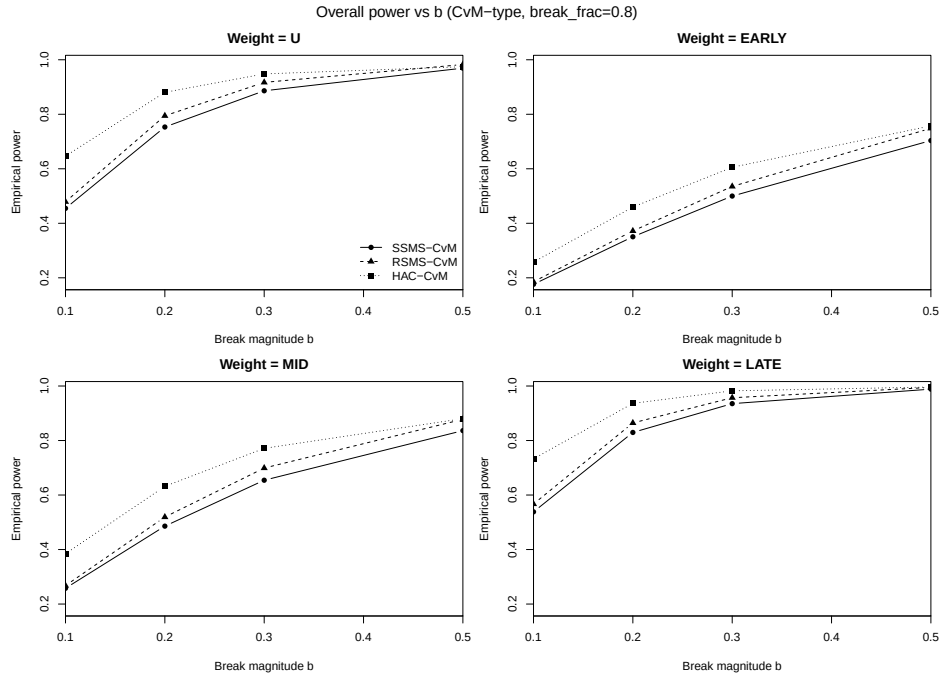

(b) Late change ($k^*/(mT) = 0.8$).

Figure 2: Overall power versus break magnitude for CvM-type monitoring. Each panel reports $\mathbb{P}(k^* < \mathcal{T}_m \leq mT)$ as a function of b, averaged over scenarios S1–S5, the three error designs, and the reported (N, m, T) configurations, and shows the four CvM weights (U/E/M/L) in separate subpanels.

6 Empirical illustration

We illustrate our online monitoring procedure in Algorithm 1 using the quarterly FHFA House Price Index (HPI) for U.S. metropolitan statistical areas (MSAs) and metropolitan divisions. The panel is high-dimensional (hundreds of local housing markets observed over a long span), and a low-dimensional factor structure—interpretable as a national housing cycle plus regional components—is a natural benchmark. Our goal is to monitor, in real time, whether the loading space governing metro comovement remains stable, or whether metro exposures to the common housing factors shift in an economically relevant way.

We also consider an empirical example based on the monthly Federal Reserve Economic Data–Macroeconomic Database (FRED–MD) U.S. macroeconomic panel, using the vintage downloaded in January 2026. That application follows the same DFT-score monitoring steps and documents alarms around the onset of the Great Financial Crisis. Due to page constraints, it is relegated to Appendix G.

6.1 Data source and preprocessing

We use the publicly available "All-Transactions" quarterly HPI for "Metropolitan Statistical Areas and Divisions (Not Seasonally Adjusted)" released by FHFA.[2] Let H_{it} denote the HPI level for metro $i = 1, \dots, N$ in quarter t. We work with quarterly log growth rates

$$X_{it} = 100\,\Delta \log H_{it} = 100\big(\log H_{it} - \log H_{i,t-1}\big), \tag{25}$$

so that X_{it} is approximately a quarterly percentage change. We then implement the standard "training normalization" used throughout the paper: in the Phase-I training window we compute each series' mean and standard deviation and standardize X_{it} using these training moments; in Phase II we apply the same normalization to incoming observations to avoid any look-ahead.

Because the theory is stated for a balanced panel, we keep metros with complete observations over 1995Q1–2025Q4. This yields a balanced panel with $N = 405$ metros and $n = 124$ quarters in levels (hence $n - 1$ growth observations after differencing). Figure 3 plots the cross-sectional average growth rate and highlights the major housing-cycle episodes visible in the data: the mid-2000s boom, the sharp contraction around the Great Financial Crisis, the post-2012 recovery, and the pandemic-era housing surge.

[2] FHFA HPI download page: `https://www.fhfa.gov/data/hpi/datasets` (Quarterly data → All-Transactions → "Metropolitan Statistical Areas and Divisions"). A direct CSV link (at the time of download) is `https://www.fhfa.gov/hpi/download/quarterly_datasets/hpi_at_metro.csv`.

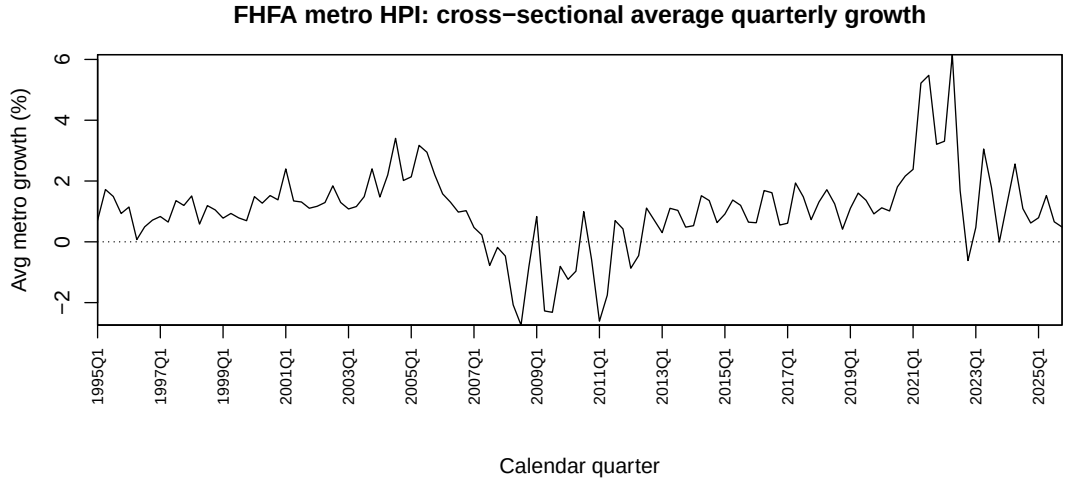

Figure 3: FHFA metro HPI panel: cross-sectional average quarterly growth $N^{-1}\sum_{i=1}^{N} X_{it}$ for the balanced sample (1995Q1–2025Q4).

6.2 Training/monitor split and DFT score construction

Let $X_t = (X_{1t}, \ldots, X_{Nt})'$ denote the balanced growth panel. We use a clean Phase-I training sample and monitor the subsequent stream in Phase II as in Algorithm 1. Our baseline split is

$$\text{Training (Phase I): 1995Q1–2004Q4 } (m = 40), \qquad \text{Monitoring (Phase II): 2005Q1–2025Q4 } (n-m = 84),$$

so the effective monitoring horizon is $T = (n-m)/m \approx 2.10$. The training window ends before the mid-2000s boom and therefore serves as an "in-control" calibration period, while the monitoring window spans the boom/bust and later regime changes.

In Phase I we estimate the baseline loading space $\widehat{\Lambda}_0$ by PCA and select the factor dimension using a training-sample information criterion; for this panel the selected dimension is $\widehat{K} = 3$. We then freeze $\widehat{\Lambda}_0$ and, for each incoming X_t in Phase II, compute projected factors and residuals $(\widetilde{F}_t, \widetilde{\varepsilon}_t)$ via (5). Following Section 2.3, we construct the complex DFT score curve $\eta_t(u)$ in (6).

To obtain a finite-dimensional score vector we use the frequency-grid construction and evaluate the score curve at the first J Fourier frequencies $\{u_1, \ldots, u_J\}$. We vectorize real and imaginary parts as

$$\psi_t = \Big(\Re\{\eta_t(u_1)\}', \Im\{\eta_t(u_1)\}', \ldots, \Re\{\eta_t(u_J)\}', \Im\{\eta_t(u_J)\}'\Big)' \in \mathbb{R}^q, \qquad q = 2\widehat{K}J.$$

We take $J = 5$, so that $q = 2 \times 3 \times 5 = 30$. This choice keeps the score dimension moderate while retaining multiple frequency components that can capture changes in both low- and higher-frequency comovement.

6.3 Monitoring statistics and calibration

We feed the score stream $\{\psi_t\}$ into three sequential monitoring families:

1. **SSMS:** the self-normalized monitor in (10) (KS) and (17) (CvM);
2. **RSMS:** the adjusted-range self-normalized monitor in (16) (KS) and (19) (CvM), using the training-window prewhitening step;
3. **HAC benchmark:** a conventional LRV/HAC standardization computed from Phase-I scores, recorded as a baseline comparator.

For the HAC benchmark we use the Bartlett (Newey–West) kernel $\mathcal{K}(x) = \max\{0, 1 - |x|\}$ and set the truncation lag to $h = \lfloor m^{1/3} \rfloor$ based on the Phase-I training size m (with ridge $\varepsilon = 10^{-10} I_q$ in the inversion). In the FHFA application $m = 40$, so $h = 3$.

For KS-type monitoring we report results for both the classical boundary $\gamma = 0$ and the mildly increasing boundary $\gamma = 0.10$, using significance level $\alpha = 5\%$. For CvM-type monitoring we report the uniform weight w_{U} and three alternative weight functions that emphasize early-, middle-, and late-horizon deviations (Section 3.3). Because the statistics have markedly different scales across SSMS/RSMS/HAC, we report a small set of representative monitoring paths in Appendix F.2; additional combinations of weights and the HAC benchmark yield visually similar trajectories and are omitted for brevity.

Note that tabulated asymptotic critical values in Appendix C cover $q \leq 20$. The FHFA design uses $q = 30$, so we simulate the required critical values by Monte Carlo from the pivotal Brownian-motion limits in Theorems 1–4 (SSMS/RSMS) and Theorems A.1–A.2 (HAC benchmark), using the empirical horizon $T = 2.10$ and 10,000 replications (for KS-type monitoring, separately for $\gamma = 0$ and $\gamma = 0.10$). Each monitoring-path figure overlays the corresponding critical value as a dashed horizontal line; the numerical thresholds are summarized in Appendix F.1.

6.4 Empirical findings

Table 19 reports the first alarm time for each monitoring rule. All KS-type monitors (SSMS/RSMS/HAC) signal an immediate departure at the start of Phase II (2005Q1) for both $\gamma = 0$ and $\gamma = 0.10$. CvM-type monitoring also alarms very early for RSMS and HAC (often in 2005Q1–2005Q2), while SSMS–CvM is more sensitive to the weight choice: the uniform and early weights alarm in 2005Q2, whereas the mid and late weights delay detection to 2005Q4 and 2006Q1, respectively. Selected monitoring paths (with critical values overlaid) are reported in Appendix F.2.

The mid-2000s coincide with the acceleration of the U.S. housing boom and a rapid expansion of mortgage credit. From a metro-level perspective, this is a natural period for a change in the loading space: local markets differed sharply in their exposure to credit conditions, construction supply constraints, and local labor-market fundamentals. An online procedure that treats 1995Q1–2004Q4 as the baseline therefore has good reason to flag the onset of instability around 2005. The fact that all KS-type monitors alarm immediately in 2005Q1 suggests that metro exposures to the common

Table 19: First detection times for the FHFA metro HPI panel ($\alpha = 0.05$, $q = 30$). "Stop k" is the monitoring index (quarters into Phase II) at which the statistic first crosses its critical value. For KS-type monitoring we report both $\gamma = 0$ and $\gamma = 0.10$.

Method	Statistic	Weight	γ	Stop k	First alarm (quarter)
SSMS	KS	–	0.00	1	2005Q1
RSMS	KS	–	0.00	1	2005Q1
HAC	KS	–	0.00	1	2005Q1
SSMS	KS	–	0.10	1	2005Q1
RSMS	KS	–	0.10	1	2005Q1
HAC	KS	–	0.10	1	2005Q1
SSMS	CvM	U	0	2	2005Q2
RSMS	CvM	U	0	1	2005Q1
HAC	CvM	U	0	1	2005Q1
SSMS	CvM	Early	0	2	2005Q2
RSMS	CvM	Early	0	1	2005Q1
HAC	CvM	Early	0	1	2005Q1
SSMS	CvM	Mid	0	4	2005Q4
RSMS	CvM	Mid	0	2	2005Q2
HAC	CvM	Mid	0	2	2005Q2
SSMS	CvM	Late	0	5	2006Q1
RSMS	CvM	Late	0	2	2005Q2
HAC	CvM	Late	0	2	2005Q2

housing factors begin to drift right at the onset of the boom, rather than only at the subsequent bust.

Differences across CvM weights are also informative. When the weight emphasizes early portions of the monitoring horizon, CvM alarms essentially at the same time as KS. When the weight emphasizes later portions, SSMS–CvM delays detection, consistent with a change that is already present early in Phase II but continues to evolve in subsequent quarters, so late-horizon weights require more accumulated evidence before crossing their thresholds.

To interpret the alarm, we compare factor loadings before and after the detected break. Let $\widehat{\Lambda}_{\text{pre}}$ be the PCA loading matrix estimated on the Phase-I training window (1995Q1–2004Q4). Starting from the earliest alarm quarter (2005Q1), we re-estimate a post-alarm loading matrix $\widehat{\Lambda}_{\text{post}}$ on a window of equal length $m = 40$ quarters (2005Q1–2014Q4), align the two loading spaces by an orthogonal Procrustes rotation, and compute metro-level loading changes.

First, the principal angles between the column spaces of $\widehat{\Lambda}_{\text{pre}}$ and $\widehat{\Lambda}_{\text{post}}$ are sizeable (about 26.9°, 56.6°, and 60.6° for $K = 3$), indicating a non-trivial rotation of the loading space after 2005Q1. Second, Figure 4 shows that loading changes are heterogeneous across metros: most metros exhibit moderate shifts, while a subset shows very large changes. The metros with the largest changes include several Great Lakes/Rust Belt areas (e.g., the Detroit region, Flint, Grand Rapids, Toledo, Akron/Cleveland), alongside rapidly growing boom markets (e.g., Phoenix and Atlanta) and some smaller markets that behaved very differently from the national cycle (e.g., Bend, OR). These patterns are consistent with a shift in how housing fundamentals and credit conditions propagate

across local markets as the boom period begins.

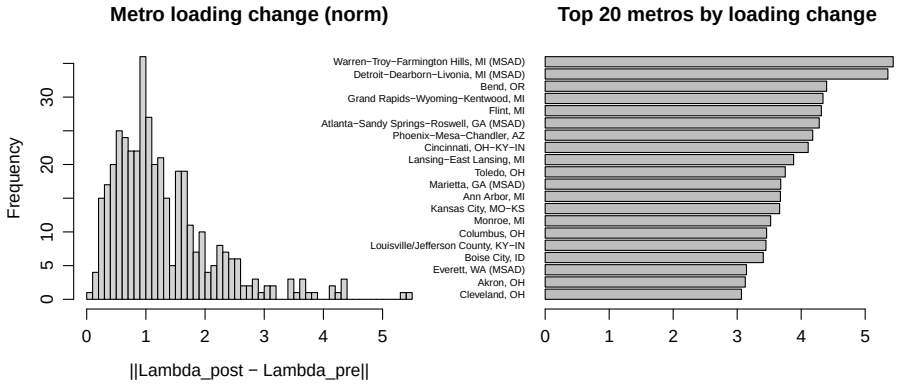

Figure 4: Loading-space diagnostics around the first alarm. Left: distribution of metro-level loading-change norms $\|\widehat{\lambda}_{i,\mathrm{post}} - \widehat{\lambda}_{i,\mathrm{pre}}\|$ (after aligning loading spaces). Right: top 20 metros by loading-change norm. The post window is 2005Q1–2014Q4 (length $m = 40$).

7 Conclusion

This paper develops an online sequential monitoring framework for detecting loading-space instability in high-dimensional approximate factor models using DFT-based spectral scores. After estimating a baseline loading space on a clean Phase-I window, we track a stream of frequency-domain score objects that summarize deviations from factor-model stability and reduce them to a fixed-dimensional real score vector for monitoring.

To deliver tuning-lean sequential inference, we propose two self-normalized monitoring families: SSMS, the sequential monitoring statistic based on Shao's (2010) quadratic SN, and RSMS, the sequential monitoring statistic based on adjusted-range-based SN (with an optional training-window prewhitening step for cross-coordinate dependence). For each family we develop both KS-type stopping rules (based on running maxima) and CvM-type stopping rules (based on weighted integrals), derive pivotal null limits, and provide a practical Monte Carlo calibration method based on simulating the limiting Brownian-motion functionals.

Our simulation results underscore the practical value of SN in sequential environments. The overall power–versus–b plots in Section 5 visualize how detection strength increases with the break magnitude and how improved size control translates into stronger late-break sequential power, while Appendix E.1 provides the corresponding scenario-level views. Relative to HAC studentization, which can exhibit substantial size distortion and therefore frequent premature signals, the self-normalized procedures deliver markedly more stable false-alarm control across horizons and dependence designs. Among KS-type monitors, RSMS tends to provide stronger late-break detection power with shorter delays, while for CvM-type monitoring the weight choice is central and a late-emphasis weight offers a favorable size–power compromise under the null and late-change alternatives. To reflect the practical reality that Phase-I screening may miss small instabilities, Appendix E.2 further reports a

targeted robustness experiment with mild training-window contamination: in this borderline regime, adjusted-range RSMS remains closer to the clean-training benchmark and retains higher post-break detection, whereas quadratic SN and HAC can suffer more premature stopping and a corresponding loss of late-break power. The empirical illustration using the FHFA metro house price index panel further shows how the proposed procedures can serve as an operational model-maintenance tool: the monitoring rules detect an early alarm around the onset of the mid-2000s housing boom and the post-alarm diagnostics reveal heterogeneous metro-level shifts in factor exposures.

Several extensions are of independent interest—including multiple-change settings with principled restart rules and monitoring broader forms of factor-model instability—but are beyond the scope of the present paper. We nevertheless provide a brief theoretical discussion of the open-end benchmark $T = \infty$ in Appendix B.

Acknowledgements

The research is supported by National Natural Science Foundation of China (NSFC) grants No. 71988101 and No. 72173120.

References

Andrews, D. W. K. (1991). Heteroskedasticity and autocorrelation consistent covariance matrix estimation. *Econometrica 59*(3), 817–858.

Andrews, D. W. K. and J. C. Monahan (1992). An improved heteroskedasticity and autocorrelation consistent covariance matrix estimator. *Econometrica 60*(4), 953–966.

Bai, J. (2003). Inferential theory for factor models of large dimensions. *Econometrica 71*(1), 135–171.

Bai, J. and X. Han (2016). Structural changes in high dimensional factor models. *Frontiers of Economics in China 11*(1), 9–39.

Bai, J. and S. Ng (2002). Determining the number of factors in approximate factor models. *Econometrica 70*(1), 191–221.

Brillinger, D. R. (1969). Asymptotic properties of spectral estimates of second order. *Biometrika 56*(2), 375–390.

Durbin, J. (1969). Tests for serial correlation in regression analysis based on the periodogram of least-squares residuals. *Biometrika 56*(1), 1–15.

Fu, Z. and Y. Hong (2019). A model-free consistent test for structural change in regression possibly with endogeneity. *Journal of Econometrics 211*(1), 206–242.

Fu, Z., Y. Hong, and X. Wang (2023). Testing for structural changes in large dimensional factor models via discrete Fourier transform. *Journal of Econometrics 233*(1), 302–331.

Hong, Y. (1996). Consistent testing for serial correlation of unknown form. *Econometrica 64*(4), 837–864.

Hong, Y. (1999). Hypothesis testing in time series via the empirical characteristic function: A generalized spectral density approach. *Journal of the American Statistical Association 94*(448), 1201–1220.

Hong, Y. (2000). Generalized spectral tests for serial dependence. *Journal of the Royal Statistical Society Series B: Statistical Methodology 62*(3), 557–574.

Hong, Y. and T.-H. Lee (2003). Diagnostic checking for the adequacy of nonlinear time series models. *Econometric Theory 19*(6), 1065–1121.

Hong, Y. and Y.-J. Lee (2005). Generalized spectral tests for conditional mean models in time series with conditional heteroscedasticity of unknown form. *The Review of Economic Studies 72*(2), 499–541.

Hong, Y., Z. Lin, O. Linton, W. Newey, and J. Sun (2025). Confidence interval estimation and hypothesis testing using the adjusted-range-based self-normalization approach. Working paper.

Hong, Y., O. Linton, B. McCabe, J. Sun, and S. Wang (2024). Kolmogorov–Smirnov type testing for structural breaks: A new adjusted-range based self-normalization approach. *Journal of Econometrics 238*(2), 105603.

Kiefer, N. M. and T. J. Vogelsang (2005). A new asymptotic theory for heteroskedasticity-autocorrelation robust tests. *Econometric Theory 21*(6), 1130–1164.

Mandelbrot, B. B. (1972). Statistical methodology for nonperiodic cycles: from the covariance to R/S analysis. In *Annals of Economic and Social Measurement*, Volume 1, pp. 259–290. National Bureau of Economic Research.

Mandelbrot, B. B. (1975). Limit theorems on the self-normalized range for weakly and strongly dependent processes. *Zeitschrift für Wahrscheinlichkeitstheorie und Verwandte Gebiete 31*(4), 271–285.

Müller, U. K. (2007). A theory of robust long-run variance estimation. *Journal of Econometrics 141*(2), 1331–1352.

Newey, W. K. and K. D. West (1987). A simple, positive semi-definite, heteroskedasticity and autocorrelation consistent covariance matrix. *Econometrica 55*(3), 703–708.

Shao, X. (2010). A self-normalized approach to confidence interval construction in time series. *Journal of the Royal Statistical Society Series B: Statistical Methodology 72*(3), 343–366.

Shao, X. (2015). Self-normalization for time series: A review of recent developments. *Journal of the American Statistical Association 110*(512), 1797–1817.

Shao, X. and X. Zhang (2010). Testing for change points in time series. *Journal of the American Statistical Association 105*(491), 1228–1240.

Stock, J. and M. Watson (2009). Forecasting in dynamic factor models subject to structural instability. In J. Castle and N. Shephard (Eds.), *Methodology and Practice of Econometrics, a Festschrift in Honour of Professor David F. Hendry*, pp. 1–57. Oxford: Oxford University Press.

Stock, J. H. and M. W. Watson (2002a). Forecasting using principal components from a large number of predictors. *Journal of the American statistical association 97*(460), 1167–1179.

Stock, J. H. and M. W. Watson (2002b). Macroeconomic forecasting using diffusion indexes. *Journal of Business & Economic Statistics 20*(2), 147–162.

Student (1908). The probable error of a mean. *Biometrika 6*(1), 1–25.

Sun, J., Y. Hong, Z. Lin, and W. Xu (2025). Structural stability of functional data — a new adjusted-range-based self-normalization approach. *Economics Letters 253*, 112350.

Sun, J., Y. Hong, O. Linton, and X. Zhao (2022). Adjusted-range self-normalized confidence interval construction for censored dependent data. *Economics Letters 220*, 110873.

Sun, J., M. Zhu, and O. Linton (2025). Adjusted-range-based self-normalized autocorrelation tests. *Economics Letters 251*, 112315.

Zhu, M., Y. Hong, J. Sun, and O. Linton (2025). Sequential change-point detection in time series: An adjusted-range-based self-normalization approach. Manuscript, revise and resubmit at Journal of Business & Economic Statistics.

Appendix

A HAC-based inference

All KS- and CvM-type monitoring statistics developed so far are self-normalized and therefore avoid estimating a long-run covariance matrix. For completeness, and to provide a baseline for comparison in simulations, this appendix records the conventional HAC approach that standardizes by a training-window long-run covariance estimator. Throughout the paper we focus on finite (closed-end) monitoring horizons $T < \infty$; the formal open-end case $T \to \infty$ is discussed separately in Appendix B. We restrict that discussion to theoretical remarks because monitoring indefinitely is typically unrealistic in practice.

A.1 Training-window HAC long-run covariance estimator

Recall the centered scores $\phi_t = \psi_t - \bar{\psi}_m$ and the monitoring partial sum $S_m(k) = \sum_{t=m+1}^{m+k} \phi_t$. Let Σ denote the long-run covariance matrix from Assumption 6. Fix an even kernel $\mathcal{K}(\cdot)$ with $\mathcal{K}(0) = 1$ and a bandwidth (truncation lag) $h = h_m \in \mathbb{N}$. Define the training-window HAC long-run covariance estimator

$$\widehat{\Sigma}_{m,h} \equiv \widehat{\Gamma}_0 + \sum_{\ell=1}^{h} \mathcal{K}\Big(\frac{\ell}{h}\Big) \big(\widehat{\Gamma}_\ell + \widehat{\Gamma}_\ell^\top\big), \qquad \widehat{\Gamma}_\ell \equiv \frac{1}{m} \sum_{t=\ell+1}^{m} \phi_t \phi_{t-\ell}^\top. \tag{A.1}$$

In practice, one may invert $\widehat{\Sigma}_{m,h}$ using a small ridge correction $\widehat{\Sigma}_{m,h} + \varepsilon I_q$ with $\varepsilon > 0$.

Assumption A.1 (HAC consistency)**.** *With a bandwidth sequence $h = h_m$, the estimator in* (A.1) *satisfies $\widehat{\Sigma}_{m,h} \xrightarrow{p} \Sigma$ and $\mathbb{P}(\det \widehat{\Sigma}_{m,h} > 0) \to 1$.*

A.2 KS-type HAC monitor

For $\gamma \in [0, 1/2)$ define the HAC-normalized KS-type statistic

$$\mathcal{M}_m^{\mathrm{H}}(k) = \frac{S_m(k)^\top \widehat{\Sigma}_{m,h}^{-1} S_m(k)}{m\,\big(1 + \frac{k}{m}\big)^2 \Big(\frac{k}{k+m}\Big)^{2\gamma}}, \qquad k = 1, \ldots, mT, \tag{A.2}$$

and the associated stopping time

$$\mathcal{T}_m^{\mathrm{H}} = \inf\Big\{1 \le k \le mT : \ \mathcal{M}_m^{\mathrm{H}}(k) > c_{\alpha,\mathrm{KS}}^{\mathrm{H}}(T, q, \gamma)\Big\}, \tag{A.3}$$

with the convention $\inf \emptyset = mT + 1$.

Lemma A.1 (CUSUM bridge limit)**.** *Under Assumption 6,*

$$\Big\{\frac{1}{\sqrt{m}} S_m(\lfloor ms \rfloor)\Big\}_{s \in [0,T]} \ \Rightarrow \ \Big\{\Sigma^{1/2} U_q(s)\Big\}_{s \in [0,T]} \quad \text{in } D([0,T], \mathbb{R}^q),$$

where $U_q(s) = B_q(1+s) - (1+s)B_q(1)$ and B_q is a standard q-dimensional Brownian motion.

Proof. Write, for $k = \lfloor ms \rfloor$,

$$\frac{1}{\sqrt{m}} S_m(k) = \frac{1}{\sqrt{m}} \sum_{t=m+1}^{m+k} (\psi_t - \mu) - \frac{k}{\sqrt{m}} (\bar{\psi}_m - \mu).$$

With $G_m(r) \equiv m^{-1/2} \sum_{t=1}^{\lfloor mr \rfloor} (\psi_t - \mu)$ as in Assumption 6, the first term equals $G_m(1+s) - G_m(1) + o_p(1)$ and the second term equals $(k/m)G_m(1) = sG_m(1) + o_p(1)$, uniformly in $s \in [0,T]$. Hence

$$\frac{1}{\sqrt{m}} S_m(\lfloor ms \rfloor) = G_m(1+s) - (1+s)G_m(1) + o_p(1),$$

uniformly on $[0,T]$. By Assumption 6 and the continuous mapping theorem, $G_m(\cdot) \Rightarrow \Sigma^{1/2} B_q(\cdot)$ in $D([0, 1+T], \mathbb{R}^q)$, which implies the stated limit with $U_q(s) = B_q(1+s) - (1+s)B_q(1)$. □

Theorem A.1 (HAC KS-type null limit)**.** *Suppose Assumptions 5, 6, 7 and A.1 hold. Then, for any fixed $\gamma \in [0, 1/2)$,*

$$\sup_{1 \le k \le mT} \mathcal{M}_m^{\mathrm{H}}(k) \xrightarrow{d} \sup_{0 < s \le T} \frac{\|U_q(s)\|^2}{(1+s)^2 \left(\frac{s}{1+s}\right)^{2\gamma}}.$$

In particular, the limiting null distribution is pivotal (depends only on T, q, and γ), so $c_{\alpha,\mathrm{KS}}^{\mathrm{H}}(T,q,\gamma)$ can be simulated using standard Brownian motion paths.

Proof. By Lemma A.1, for $s \in [0,T]$, $m^{-1/2} S_m(\lfloor ms \rfloor) \Rightarrow \Sigma^{1/2} U_q(s)$ in $D([0,T], \mathbb{R}^q)$. Assumption A.1 implies $\widehat{\Sigma}_{m,h}^{-1} \xrightarrow{p} \Sigma^{-1}$ and $\mathbb{P}(\det \widehat{\Sigma}_{m,h} > 0) \to 1$, so the quadratic form satisfies, in $D([0,T], \mathbb{R})$,

$$\frac{1}{m} S_m(\lfloor ms \rfloor)^\top \widehat{\Sigma}_{m,h}^{-1} S_m(\lfloor ms \rfloor) \xrightarrow{d} U_q(s)^\top U_q(s) = \|U_q(s)\|^2,$$

by another application of the continuous mapping theorem. Dividing by the deterministic boundary factor $(1+s)^2 \left(\frac{s}{1+s}\right)^{2\gamma}$ and taking the supremum over $s \in (0,T]$ yields the stated limit. □

A.3 CvM-type HAC monitor

Fix a nonnegative weight function $w(\cdot)$ on $[0,T]$ such as the four choices in (21), and (as in Section 4.2) set $\gamma = 0$ in the underlying KS-type statistic. Define the integrated (CvM-type) HAC monitor

$$\mathcal{I}_m^{\mathrm{H}}(k) \equiv \frac{1}{m} \sum_{j=1}^{k} w\left(\frac{j}{m}\right) \mathcal{M}_m^{\mathrm{H}}(j), \qquad k = 1, \ldots, mT, \tag{A.4}$$

and the stopping time $\mathcal{T}_{m,\mathrm{CvM}}^{\mathrm{H}} = \inf\{1 \le k \le mT : \mathcal{I}_m^{\mathrm{H}}(k) > c_{\alpha,\mathrm{CvM}}^{\mathrm{H}}(T,q,w)\}$.

Theorem A.2 (HAC CvM-type null limit)**.** *Under the assumptions of Theorem A.1 and for any bounded Riemann-integrable weight $w(\cdot)$ on $[0,T]$,*

$$\mathcal{I}_m^{\mathrm{H}}(\lfloor ms \rfloor) \xrightarrow{d} \int_0^s w(u) \frac{\|U_q(u)\|^2}{(1+u)^2}\, du, \qquad s \in [0,T].$$

Consequently,

$$\sup_{1 \le k \le mT} \mathcal{I}_m^{\mathrm{H}}(k) \xrightarrow{d} \sup_{0 \le s \le T} \int_0^s w(u) \frac{\|U_q(u)\|^2}{(1+u)^2}\, du = \int_0^T w(u) \frac{\|U_q(u)\|^2}{(1+u)^2}\, du,$$

where the last equality uses $w(u) \ge 0$.

Proof. Theorem A.1 (with $\gamma = 0$) implies $\mathcal{M}_m^{\mathrm{H}}(\lfloor ms \rfloor) \xrightarrow{d} \|U_q(s)\|^2/(1+s)^2$ in $D([0,T],\mathbb{R})$. Since the limit is a.s. continuous and $w(\cdot)$ is bounded and Riemann-integrable, standard Riemann-sum arguments yield, for each fixed s,

$$\mathcal{I}_m^{\mathrm{H}}(\lfloor ms \rfloor) = \frac{1}{m} \sum_{j=1}^{\lfloor ms \rfloor} w\left(\frac{j}{m}\right) \mathcal{M}_m^{\mathrm{H}}(j) \xrightarrow{d} \int_0^s w(u) \frac{\|U_q(u)\|^2}{(1+u)^2}\, du.$$

Because the integrand is nonnegative, the process $s \mapsto \int_0^s w(u) \|U_q(u)\|^2/(1+u)^2\, du$ is nondecreasing, so the supremum over $s \in [0,T]$ is attained at $s = T$. □

A.4 Consistency and local power

Define the HAC stopping times $\mathcal{T}_m^{\mathrm{H}}$ and $\mathcal{T}_{m,\mathrm{CvM}}^{\mathrm{H}}$ as above. Under the fixed alternative in Assumption 10 (a post-change mean shift $\Delta \neq 0$), both HAC monitoring statistics are consistent.

Proposition A.1 (Consistency under fixed alternatives)**.** *Suppose Assumptions 5, 6, 7, A.1 and 10 hold, and $\Delta \neq 0$ in (22). Then for any $\gamma \in [0, 1/2)$ and any fixed horizon $T > 0$,*

$$\mathbb{P}(\mathcal{T}_m^{\mathrm{H}} \le mT \mid H_1) \to 1, \qquad \mathbb{P}(\mathcal{T}_{m,\mathrm{CvM}}^{\mathrm{H}} \le mT \mid H_1) \to 1.$$

Proof. Let $k^\star = \lfloor ms^\star \rfloor$ denote the change point and fix any $s \in (s^\star, T]$, with $k = \lfloor ms \rfloor$. Using $S_m(k) = \sum_{t=m+1}^{m+k} (\psi_t - \mu) - k(\bar{\psi}_m - \mu)$ and adding/subtracting $\mathbb{E}\psi_t$, we can write

$$S_m(k) = \sum_{t=m+1}^{m+k} (\psi_t - \mathbb{E}\psi_t) - k(\bar{\psi}_m - \mu) + \sum_{t=m+1}^{m+k} (\mathbb{E}\psi_t - \mu).$$

By Assumption 10, $\sum_{t=m+1}^{m+k} (\mathbb{E}\psi_t - \mu) = (k - k^\star)\Delta + o(m)$, whereas the first two terms are $O_p(\sqrt{m})$. Therefore,

$$\frac{1}{m} S_m(\lfloor ms \rfloor) = (s - s^\star)\Delta + o_p(1).$$

Assumption A.1 implies $\widehat{\Sigma}_{m,h}^{-1} \xrightarrow{p} \Sigma^{-1}$, so by the continuous mapping theorem,

$$\Big(\frac{S_m(\lfloor ms \rfloor)}{m}\Big)^\top \widehat{\Sigma}_{m,h}^{-1} \Big(\frac{S_m(\lfloor ms \rfloor)}{m}\Big) \xrightarrow{p} (s - s^\star)^2 \, \Delta^\top \Sigma^{-1} \Delta > 0.$$

Hence,

$$\frac{1}{m} S_m(\lfloor ms \rfloor)^\top \widehat{\Sigma}_{m,h}^{-1} S_m(\lfloor ms \rfloor) = m \Big(\frac{S_m(\lfloor ms \rfloor)}{m}\Big)^\top \widehat{\Sigma}_{m,h}^{-1} \Big(\frac{S_m(\lfloor ms \rfloor)}{m}\Big) \xrightarrow{p} +\infty.$$

For fixed $s > s^\star$ and any $\gamma \in [0, 1/2)$, the remaining boundary terms in (A.2) converge to finite positive constants, so $\mathcal{M}_m^{\mathrm{H}}(\lfloor ms \rfloor) \to \infty$ in probability. Therefore $\mathbb{P}(\sup_{1 \le k \le mT} \mathcal{M}_m^{\mathrm{H}}(k) > c) \to 1$ for any fixed c, which implies $\mathbb{P}(\mathcal{T}_m^{\mathrm{H}} \le mT) \to 1$.

For the CvM-type monitor, $\mathcal{I}_m^{\mathrm{H}}(k)$ is a nondecreasing sum of nonnegative terms (since $w \ge 0$ and $\mathcal{M}_m^{\mathrm{H}}(j) \ge 0$). Fix any $s_1 \in (s^\star, T)$ and set $k_1 = \lfloor ms_1 \rfloor$. The argument above extends to show that $\mathcal{M}_m^{\mathrm{H}}(\lfloor ms \rfloor)/m \xrightarrow{p} c(s)$ uniformly for $s \in [s_1, T]$, where $c(s) > 0$ on $[s_1, T]$ because $s - s^\star$ is bounded away from zero there. In particular, there exists a constant $c_1 > 0$ such that

$$\mathbb{P}\Big(\inf_{k_1 \le k \le mT} \mathcal{M}_m^{\mathrm{H}}(k) \ge c_1 m \Big) \to 1.$$

Therefore, on this event,

$$\mathcal{I}_m^{\mathrm{H}}(mT) \ge \frac{1}{m} \sum_{j=k_1}^{mT} w(j/m) \, \mathcal{M}_m^{\mathrm{H}}(j) \ge c_1 \sum_{j=k_1}^{mT} w(j/m).$$

Since $w(\cdot)$ is nonnegative and not identically zero on $(s^\star, T]$, we have $\int_{s_1}^T w(u)\, du > 0$ for some choice of $s_1 > s^\star$, and the Riemann sum satisfies $\sum_{j=k_1}^{mT} w(j/m) \sim m \int_{s_1}^T w(u)\, du \to \infty$. Hence $\mathcal{I}_m^{\mathrm{H}}(mT) \to \infty$ in probability and thus $\mathbb{P}(\mathcal{T}_{m,\mathrm{CvM}}^{\mathrm{H}} \le mT) \to 1$. □

Under local alternatives (Definition 1), the HAC monitoring statistics converge to drifted Brownian functionals.

Theorem A.3 (Local power: HAC KS and CvM)**.** *Suppose Assumptions 5, 6, 7, A.1 and the local alternative $\Delta_m = \delta/\sqrt{m}$ in Definition 1 hold. Then, for any fixed $\gamma \in [0, 1/2)$,*

$$\sup_{1 \le k \le mT} \mathcal{M}_m^{\mathrm{H}}(k) \xrightarrow{d} \sup_{0 < s \le T} \frac{\big\| U_q(s) + (s - s^*)_+ \, \Sigma^{-1/2} \delta \big\|^2}{(1+s)^2 \left(\frac{s}{1+s}\right)^{2\gamma}},$$

and, for the CvM-type statistic with weight $w(\cdot)$,

$$\mathcal{I}_m^{\mathrm{H}}(\lfloor ms \rfloor) \xrightarrow{d} \int_0^s w(u) \frac{\big\| U_q(u) + (u - s^*)_+ \, \Sigma^{-1/2} \delta \big\|^2}{(1+u)^2} \, du, \qquad s \in [0, T].$$

Proof. The proof follows the same steps as Lemma A.1 and Theorem A.1. Under the local alternative,

the mean component contributes an additional drift: for $k = \lfloor ms \rfloor$,

$$\frac{1}{\sqrt{m}} \sum_{t=m+1}^{m+k} (\mathbb{E}\psi_t - \mu) = \frac{1}{\sqrt{m}} \sum_{t=m+k^*+1}^{m+k} \Delta_m + o_p(1) = \frac{k-k^*}{m}\,\delta + o_p(1) \to (s-s^*)_+\,\delta.$$

Hence $m^{-1/2} S_m(\lfloor ms \rfloor) \Rightarrow \Sigma^{1/2} U_q(s) + (s-s^*)_+ \delta$ in $D([0,T], \mathbb{R}^q)$. Premultiplying by $\widehat{\Sigma}_{m,h}^{-1/2}$ (or equivalently using the quadratic form with $\widehat{\Sigma}_{m,h}^{-1}$) and applying Assumption A.1 yields the stated drifted limits after scaling by the deterministic boundary factors. The CvM statement follows by the same Riemann-sum argument as in Theorem A.2. □

In applications, one selects a kernel $\mathcal{K}$ and bandwidth h in (A.1) to compute $\widehat{\Sigma}_{m,h}$ from the training window. In our numerical work (Sections 5 and 6) we use the Bartlett (Newey–West) kernel $\mathcal{K}(x) = \max\{0, 1-|x|\}$ and set the truncation lag to $h = \lfloor m^{1/3} \rfloor$ (with ridge $\varepsilon = 10^{-10} I_q$ in the matrix inversion for numerical stability). For KS-type monitoring we report results for $\gamma = 0$ and $\gamma = 0.15$; for CvM-type monitoring we consider the four weights in (21). The null critical values $c^{\mathrm{H}}_{\alpha,\mathrm{KS}}(T, q, \gamma)$ and $c^{\mathrm{H}}_{\alpha,\mathrm{CvM}}(T, q, w)$ are obtained by simulating the pivotal Brownian limits in Theorems A.1–A.2.

B Open-end monitoring and the limit $T \to \infty$

The main text and simulation design adopt closed-end monitoring: a finite horizon $T < \infty$ is fixed in advance (e.g. $T \le 10$ in Section 5). This reflects typical empirical practice, where online monitoring systems are run over finite operational periods and then restarted or re-estimated. Nevertheless, it is sometimes useful to understand what happens as the horizon grows. This appendix records the formal open-end limits obtained by letting $T \to \infty$ in the Brownian-motion functionals that appear in Theorems 1–4 and Theorems A.1–A.2. We restrict ourselves to theoretical remarks, because monitoring with $T = \infty$ is generally unrealistic in practice.

B.1 A useful tail property of the bridge process

Recall the Gaussian bridge process

$$U_q(s) = B_q(1+s) - (1+s) B_q(1), \qquad s \ge 0,$$

where B_q is a standard q-dimensional Brownian motion. A key observation is that, componentwise,

$$\frac{U_q(s)}{1+s} = \frac{B_q(1+s)}{1+s} - B_q(1) \xrightarrow[s\to\infty]{\text{a.s.}} -B_q(1), \tag{B.1}$$

because $B_q(t)/t \to 0$ a.s. as $t \to \infty$. Consequently, for any fixed positive definite matrix A, the quadratic form $U_q(s)^\top A\, U_q(s)/(1+s)^2$ has an a.s. finite limit as $s \to \infty$. Since $s \mapsto U_q(s)$ is continuous, the resulting scaled quadratic forms are a.s. bounded on $[0, \infty)$.

B.2 KS-type monitors (SSMS, RSMS, HAC) as $T \to \infty$

Consider the KS-type stopping rules based on SSMS (10), RSMS (16), and HAC (A.2). For each procedure and any fixed boundary exponent $\gamma \in [0, 1/2)$ (in particular, $\gamma \in \{0, 0.10\}$), the finite-horizon null limits extend to

$$\sup_{1\le k\le mT} \mathcal{M}_m^{\mathrm{S}}(k) \xrightarrow{d} \sup_{0<s<\infty} \frac{U_q(s)^\top V^{-1} U_q(s)}{(1+s)^2 \left(\frac{s}{1+s}\right)^{2\gamma}},$$

$$\sup_{1\le k\le mT} \widetilde{\mathcal{M}}_m^{\mathrm{R}}(k) \xrightarrow{d} \sup_{0<s<\infty} \frac{U_q(s)^\top R^{-2} U_q(s)}{(1+s)^2 \left(\frac{s}{1+s}\right)^{2\gamma}},$$

$$\sup_{1\le k\le mT} \mathcal{M}_m^{\mathrm{H}}(k) \xrightarrow{d} \sup_{0<s<\infty} \frac{\|U_q(s)\|^2}{(1+s)^2 \left(\frac{s}{1+s}\right)^{2\gamma}},$$

where $V = \int_0^1 B_q^0(r) B_q^0(r)^\top dr$ and $R = \mathrm{diag}(R_1, \ldots, R_q)$ are as in Theorems 1–2. The suprema over $(0, \infty)$ are well-defined because: (i) (B.1) implies that each scaled quadratic form has an a.s. finite limit as $s \to \infty$, and (ii) the early-time behavior is also controlled since $U_q(s) = O_p(s^{1/2})$ as $s \downarrow 0$ while $\gamma < 1/2$ ensures $s^{1-2\gamma} \to 0$.

Thus, one may define open-end KS critical values as quantiles of the corresponding infinite-horizon Brownian functionals, e.g. $c^{\mathrm{S}}_{\alpha,\mathrm{KS}}(\infty, q, \gamma)$ for SSMS, $c^{\mathrm{R}}_{\alpha,\mathrm{KS}}(\infty, q, \gamma)$ for RSMS, and $c^{\mathrm{H}}_{\alpha,\mathrm{KS}}(\infty, q, \gamma)$ for HAC. As T increases, the finite-horizon suprema are monotone in T, and their distributions converge to these open-end limits.

B.3 CvM-type monitors (SSMS, RSMS, HAC) as $T \to \infty$

Now consider the CvM / integral-type statistics (17), (19) and (A.4), which (for nonnegative w) accumulate nonnegative evidence over monitoring time. For a fixed finite horizon $T < \infty$ and any bounded Riemann-integrable weight $w(\cdot)$, the null limits in Theorems 3, 4 and A.2 are finite.

For $T = \infty$, however, the tail behavior (B.1) implies that the integrands

$$\frac{U_q(s)^\top V^{-1} U_q(s)}{(1+s)^2}, \qquad \frac{U_q(s)^\top R^{-2} U_q(s)}{(1+s)^2}, \qquad \frac{\|U_q(s)\|^2}{(1+s)^2}$$

typically converge to nondegenerate *nonzero* random limits as $s \to \infty$. Therefore, the unweighted choice $w \equiv 1$ leads to divergence of the open-end CvM integral under H_0 and hence eventual false alarms with probability one.

A sufficient condition for a *finite* open-end CvM limit is that $w(\cdot)$ is nonnegative and integrable on $[0, \infty)$:

$$w(s) \ge 0, \qquad \int_0^\infty w(s)\, ds < \infty. \tag{B.2}$$

Under (B.2), the corresponding open-end null limits become the finite random variables

$$\int_0^\infty w(u)\,\frac{U_q(u)^\top V^{-1}U_q(u)}{(1+u)^2}\,du, \qquad \int_0^\infty w(u)\,\frac{U_q(u)^\top R^{-2}U_q(u)}{(1+u)^2}\,du, \qquad \int_0^\infty w(u)\,\frac{\|U_q(u)\|^2}{(1+u)^2}\,du,$$

for SSMS, RSMS and HAC, respectively. Because these CvM limits are nondecreasing in the upper integration limit, their suprema over $s \in [0,\infty)$ are attained at $s=\infty$. In practice, open-end CvM calibration can therefore proceed by simulating the above infinite-horizon weighted integrals.

Typical choices satisfying (B.2) include polynomially decaying weights $w(s)=(1+s)^{-\eta}$ with $\eta>1$ and exponentially decaying weights $w(s)=e^{-\eta s}$ with $\eta>0$. These weights discount very late monitoring times, preventing the CvM accumulation from diverging under H_0.

Remark 3 (Why we do not pursue $T=\infty$ empirically)**.** *Although the open-end limits above provide useful large-T benchmarks, $T=\infty$ is rarely a realistic operational design: monitoring is typically conducted over finite horizons, with periodic restarts, re-training, or model revision after an alarm (or after a fixed time). Accordingly, we focus on finite-T procedures and report only closed-end critical values in Appendix C.*

C Simulated critical values

This appendix reports the simulated asymptotic critical values used to calibrate the sequential monitoring statistics in the simulation study and the empirical illustration. All entries are obtained by Monte Carlo simulation of the relevant pivotal Brownian-motion limits—Section 4.3 for the SSMS/RSMS limits and Appendix A for the HAC benchmark—using 10,000 replications and a fine equispaced grid for the required Riemann approximations. For each horizon $T \in \{1,2,5,10\}$ and each score dimension $q \in \{1,\dots,20\}$, we report the $(1-\alpha)$ quantiles for $\alpha \in \{0.05, 0.10\}$.

C.1 KS-type monitoring (SSMS and RSMS)

Tables C.1 and C.2 report KS-type critical values for the SSMS- and RSMS-based monitors, respectively. Within each table, Panel A corresponds to the default boundary exponent $\gamma=0$, and Panel B corresponds to $\gamma=0.15$ (a sensitivity check). Columns are grouped by the monitoring horizon T, and within each T block we report the critical values for $\alpha=0.05$ and $\alpha=0.10$.

C.2 CvM-type monitoring (weight-dependent critical values)

For CvM-type monitoring we set $\gamma=0$ and the decision boundary depends on the weight function $w(\cdot)$. Although the CvM limits in Theorems 3–4 are pivotal, their distributions (and hence quantiles) vary with w. Accordingly, we tabulate separate critical values for each weight in (21). Tables C.3 and C.4 report the uniform-weight case $w_{\mathrm{U}}(s)\equiv 1$. Tables C.5–C.10 report the corresponding critical values for the non-constant weights w_{Late}, w_{Early}, and w_{Mid}.

Table C.1: Critical values for SSMS (KS) for two boundary exponents $\gamma \in \{0, 0.15\}$

Panel A: $\gamma = 0$								
	$T = 1$		$T = 2$		$T = 5$		$T = 10$	
q	0.05	0.1	0.05	0.1	0.05	0.1	0.05	0.1
1	32.7258	22.1591	45.8954	30.7701	53.7975	37.2349	62.0154	42.4631
2	66.6268	48.5072	92.9504	67.4811	110.5803	82.7167	123.7205	91.4123
3	108.9289	83.4714	147.4078	110.9598	186.7649	142.1685	206.8708	154.6299
4	159.2089	124.6814	206.3431	163.4394	270.1868	211.2319	306.5439	232.1413
5	218.5677	170.3210	280.5398	222.7883	354.8600	285.8250	406.7011	321.1939
6	279.1300	225.4792	362.5287	294.1692	464.3820	372.5477	515.4844	414.5120
7	348.2288	284.5871	447.7015	369.7363	570.9342	463.5198	636.8051	522.3679
8	420.9176	347.0096	538.7612	450.8265	701.0175	574.2443	777.0256	641.8620
9	496.6725	416.5989	645.2948	540.3669	829.8143	689.1502	924.5440	766.9828
10	583.7221	485.5654	766.5619	631.8476	969.2089	810.8890	1085.0200	907.4008
11	675.2754	571.0045	884.8694	738.5715	1121.8956	937.6697	1245.2027	1050.3861
12	779.7793	654.4629	1017.7936	856.1294	1274.2362	1078.9284	1422.4930	1203.5314
13	878.3596	737.8942	1143.9864	963.5850	1454.9605	1232.7635	1605.7082	1356.9447
14	988.0208	840.2613	1297.5476	1098.1133	1624.5173	1387.6936	1805.6441	1543.3200
15	1096.6955	936.8429	1447.8596	1231.8370	1791.0398	1547.4138	2017.1735	1720.4177
16	1217.8114	1042.0533	1597.1241	1376.6456	1972.2509	1713.4438	2224.7402	1907.5704
17	1336.0690	1147.5856	1759.5165	1514.7511	2176.2866	1898.1928	2436.5802	2108.5895
18	1442.3506	1251.0695	1919.1384	1657.2091	2395.9977	2084.8728	2676.5581	2306.6925
19	1573.5624	1364.7193	2082.6119	1827.4256	2604.4808	2275.3752	2953.3159	2532.3285
20	1722.2450	1489.3294	2257.8051	1985.5430	2854.0616	2486.3050	3174.9608	2768.2551
Panel B: $\gamma = 0.15$								
	$T = 1$		$T = 2$		$T = 5$		$T = 10$	
q	0.05	0.1	0.05	0.1	0.05	0.1	0.05	0.1
1	43.5841	30.2456	55.5930	39.1039	61.6436	43.3043	68.9495	47.9834
2	88.7728	65.1229	112.1324	81.9121	125.0469	95.0829	135.8995	102.4043
3	141.6571	110.4683	176.2494	134.8827	209.2979	160.2459	224.5483	171.1760
4	209.5982	164.0076	246.8474	196.8125	303.3772	237.6468	330.9420	255.2317
5	281.7272	223.8936	336.5669	265.5484	396.8837	321.9688	441.2219	349.2220
6	359.9652	293.9266	427.7711	350.1683	511.7752	415.0403	553.7712	449.1153
7	446.5727	369.6907	531.3681	441.0598	629.1840	514.5814	686.1611	564.0993
8	541.1048	448.1467	635.3852	533.0248	761.9476	639.3377	836.4094	689.3037
9	642.8357	533.7764	755.5265	636.4059	912.9737	762.0676	984.8651	825.3698
10	746.6774	624.8431	889.4109	744.4037	1057.0473	892.2286	1155.6050	973.0264
11	856.3417	728.5583	1029.9591	868.3347	1229.2113	1031.1771	1323.4056	1118.5053
12	988.1140	835.8018	1190.9568	1002.1216	1388.5032	1189.8009	1518.0035	1281.0668
13	1118.1032	942.7088	1335.0339	1128.3005	1584.7649	1347.2848	1705.0010	1450.8972
14	1252.7743	1070.1810	1504.5684	1285.0523	1760.1069	1518.4718	1909.6508	1643.1319
15	1401.4749	1195.6958	1678.5316	1436.7028	1946.1422	1689.9500	2135.5080	1833.9026
16	1538.3146	1319.8536	1849.2122	1603.8337	2143.4371	1864.1697	2350.8525	2030.4109
17	1695.9224	1457.5775	2050.7858	1768.2288	2371.5968	2070.5134	2581.1045	2234.1087
18	1822.7312	1593.5277	2242.4366	1929.2357	2592.6166	2269.1692	2819.3590	2443.1353
19	1986.9062	1732.7958	2412.4993	2130.8871	2813.3855	2481.9569	3099.2448	2687.4153
20	2170.1974	1886.4717	2616.6118	2310.6794	3071.1611	2699.8316	3344.7842	2928.6039

Table C.2: Critical values for RSMS (KS) for two boundary exponents $\gamma \in \{0, 0.15\}$

Panel A: $\gamma = 0$								
	$T = 1$		$T = 2$		$T = 5$		$T = 10$	
q	0.05	0.1	0.05	0.1	0.05	0.1	0.05	0.1
1	1.9925	1.4779	2.7805	2.0364	3.4008	2.5140	3.9650	2.9021
2	2.9129	2.2511	3.9855	3.0592	5.0714	3.9059	5.7179	4.4587
3	3.7502	2.9756	4.9983	3.9664	6.5091	5.1060	7.2974	5.8273
4	4.4390	3.5944	5.9156	4.8165	7.7120	6.2329	8.7542	7.0542
5	5.0786	4.1386	6.7578	5.5983	8.7734	7.2300	9.9806	8.2231
6	5.7526	4.7723	7.5603	6.3511	9.8112	8.2057	11.1807	9.3078
7	6.3758	5.3547	8.4551	7.0613	10.9096	9.1727	12.4074	10.3624
8	6.8447	5.8931	9.2540	7.7929	11.9914	10.1802	13.4861	11.4235
9	7.4205	6.4505	10.0158	8.5582	12.8860	11.0627	14.3981	12.4135
10	7.9795	6.9178	10.7189	9.2273	13.8436	11.9737	15.5739	13.4290
11	8.5250	7.4576	11.4776	9.9515	14.7765	12.8092	16.6391	14.3638
12	9.0589	7.9430	12.1643	10.6196	15.6114	13.5481	17.7923	15.2893
13	9.6137	8.4171	12.8262	11.2836	16.5029	14.4192	18.6639	16.2490
14	10.1218	8.8741	13.5981	11.9542	17.3871	15.3556	19.6791	17.1850
15	10.5794	9.3834	14.3192	12.5823	18.3327	16.1104	20.7248	18.1018
16	11.1055	9.8665	14.9398	13.2272	19.1599	16.9399	21.8882	19.0927
17	11.6167	10.3158	15.5310	13.9064	20.0423	17.7710	22.7999	19.9960
18	12.1745	10.7560	16.1989	14.4890	21.0763	18.6091	23.6421	20.9990
19	12.5471	11.2381	16.8383	15.0926	21.9153	19.3823	24.5531	21.7902
20	13.0754	11.7099	17.5383	15.7200	22.7343	20.1502	25.4671	22.6626
Panel B: $\gamma = 0.15$								
	$T = 1$		$T = 2$		$T = 5$		$T = 10$	
q	0.05	0.1	0.05	0.1	0.05	0.1	0.05	0.1
1	2.6593	1.9825	3.3489	2.4900	3.8334	2.8929	4.3807	3.2778
2	3.8380	2.9610	4.7465	3.7082	5.6880	4.3973	6.2052	4.9145
3	4.8515	3.8925	5.9118	4.7388	7.1855	5.7329	7.9311	6.3360
4	5.7120	4.6520	7.0002	5.7190	8.4974	6.9349	9.4343	7.5914
5	6.5023	5.3475	7.9875	6.6084	9.5766	8.0247	10.6953	8.8668
6	7.3596	6.1343	8.8768	7.4314	10.7012	9.0331	11.9496	9.9843
7	8.0913	6.8186	9.8922	8.3033	11.9326	10.0793	13.1752	11.0827
8	8.7777	7.4948	10.8158	9.0978	13.1099	11.1370	14.2441	12.1845
9	9.4313	8.2234	11.6311	9.9832	14.0492	12.0399	15.3010	13.1607
10	10.1244	8.7830	12.4273	10.7989	15.0227	13.0084	16.4930	14.1973
11	10.8155	9.4469	13.2727	11.5456	15.9702	13.9211	17.5638	15.1910
12	11.4910	10.0538	14.0875	12.3536	16.9734	14.7466	18.7424	16.1569
13	12.1005	10.6292	14.7881	13.0727	17.8675	15.6778	19.6320	17.1933
14	12.7452	11.2461	15.6708	13.8504	18.7978	16.6261	20.7782	18.1762
15	13.3815	11.8531	16.4460	14.5889	19.8403	17.4422	21.8479	19.1202
16	13.9686	12.4132	17.2197	15.3256	20.7587	18.3312	23.0227	20.1130
17	14.6265	13.0117	17.9081	16.0324	21.5706	19.2548	23.9830	21.0443
18	15.2566	13.5738	18.6692	16.7313	22.6260	20.0448	24.7984	22.0255
19	15.7061	14.1094	19.3750	17.4136	23.5368	20.8889	25.8522	22.9387
20	16.4097	14.7132	20.2335	18.0853	24.4177	21.7397	26.7636	23.8333

Table C.3: Critical values for SSMS (CvM) with weight $w(s) \equiv 1$

	$T=1$		$T=2$		$T=5$		$T=10$	
q	0.05	0.1	0.05	0.1	0.05	0.1	0.05	0.1
1	12.4831	7.9667	39.0419	24.9028	130.7605	86.4907	340.4839	216.8629
2	27.8427	19.4439	85.6971	59.0860	303.1414	213.6119	737.3930	517.8093
3	47.9836	35.3542	143.0395	106.9866	534.8422	385.6275	1293.8032	938.6998
4	71.8261	55.2497	206.9816	160.0788	794.2037	602.6968	1949.4938	1458.2328
5	99.4274	77.8702	286.6123	223.0352	1079.3082	837.4491	2702.1933	2062.1315
6	132.1883	103.9565	383.4618	301.1943	1408.8691	1120.0598	3473.6331	2751.0903
7	166.7455	134.5215	476.7068	390.0942	1756.6218	1412.2169	4391.1470	3499.7412
8	204.0344	166.5416	582.9529	478.1437	2188.4395	1776.6201	5339.7633	4376.8240
9	244.0054	202.4356	708.2127	585.8998	2633.8031	2157.3586	6461.5896	5264.4689
10	286.5843	241.1741	837.9230	694.4213	3119.9578	2569.7499	7645.6092	6335.8622
11	333.7254	283.2525	993.6640	817.2316	3599.8977	3007.2056	8895.2734	7382.5099
12	387.5293	326.3135	1133.4439	958.9579	4139.3917	3479.5096	10143.8546	8539.4626
13	440.0944	371.7023	1289.0720	1099.4870	4740.8271	4004.9131	11576.0696	9738.0569
14	497.6703	425.6982	1474.3745	1248.4386	5307.3721	4523.0921	13112.5502	11059.7465
15	557.2715	478.4514	1645.1896	1412.6605	5912.6562	5101.5135	14616.7280	12491.1475
16	618.4450	535.1778	1835.4763	1577.2417	6581.9386	5651.1664	16271.4021	13897.9046
17	683.9055	591.5175	2028.2237	1758.8164	7326.2074	6270.2800	17897.7936	15443.3610
18	747.1973	653.2766	2231.6431	1931.3025	8041.4725	6918.3581	19629.0903	16889.3650
19	822.0322	717.0759	2431.1349	2126.7561	8775.1902	7628.4827	21598.5747	18695.4074
20	905.4688	782.5649	2659.8507	2314.5874	9536.9259	8385.8904	23542.7040	20426.9562

Table C.4: Critical values for RSMS (CvM) with weight $w(s) \equiv 1$

	$T=1$		$T=2$		$T=5$		$T=10$	
q	0.05	0.1	0.05	0.1	0.05	0.1	0.05	0.1
1	0.8081	0.5558	2.5303	1.7084	8.9547	6.0965	23.2067	15.7661
2	1.3113	0.9762	3.8894	2.9216	14.6385	10.8397	36.3015	27.1709
3	1.7367	1.3634	5.1054	4.0637	19.8677	15.1662	48.6004	37.3293
4	2.1128	1.7100	6.2361	5.0566	23.8226	19.2654	59.8905	47.0338
5	2.4985	2.0259	7.3407	6.0151	27.8574	22.8364	69.8668	56.8827
6	2.8535	2.3745	8.4773	6.9211	31.4830	26.2678	79.3757	64.9150
7	3.1833	2.6968	9.5087	7.8888	35.6874	29.9305	88.7204	73.3050
8	3.5072	2.9971	10.5392	8.8256	39.2932	33.3851	98.1332	82.5124
9	3.8576	3.3125	11.5225	9.8364	42.7428	36.6949	105.9106	90.1600
10	4.1537	3.6003	12.3260	10.7163	46.2610	39.9692	114.7735	98.2679
11	4.4643	3.8916	13.3236	11.6009	49.5511	42.8818	123.6573	105.7360
12	4.7957	4.1696	14.3021	12.4994	52.7121	46.2800	131.9580	113.7843
13	5.0842	4.4832	15.1060	13.3343	56.0446	49.3454	139.3321	121.1828
14	5.3863	4.7522	16.0928	14.1921	59.1841	52.5848	148.5164	129.5599
15	5.6774	5.0552	16.9740	15.0753	62.7730	55.4852	156.1917	136.3403
16	5.9897	5.3525	17.8708	15.8410	66.4328	58.5409	165.0739	144.0632
17	6.2727	5.6100	18.8057	16.6553	69.3122	61.4981	172.6589	151.7058
18	6.5443	5.8977	19.6237	17.5126	72.8319	64.4390	180.2972	159.3538
19	6.8089	6.1491	20.4797	18.3616	75.7253	67.5470	187.7837	166.3586
20	7.1217	6.4240	21.3497	19.1284	79.1625	70.7520	195.4551	173.5832

Table C.5: Critical values for SSMS (CvM) with weight $w_{\text{Late}}(s) = 2(s/T)$

	$T=1$		$T=2$		$T=5$		$T=10$	
q	0.05	0.1	0.05	0.1	0.05	0.1	0.05	0.1
1	16.7624	10.5264	47.1603	29.2238	162.6064	102.9721	379.9984	236.8898
2	37.7179	25.8995	111.0339	76.9651	378.9229	262.6918	863.1241	589.7701
3	61.8906	45.9542	182.0999	134.6215	627.7233	460.8225	1444.7471	1053.5945
4	93.1054	71.4290	273.5108	203.3745	941.6815	705.1424	2124.5159	1614.4767
5	129.7962	101.3461	377.8880	287.8358	1280.2775	998.0065	2958.9680	2259.6539
6	170.4401	133.0569	500.5483	390.6937	1686.8990	1319.4484	3907.6708	3066.8455
7	214.2197	171.7646	633.4989	500.2893	2141.9485	1698.6784	4924.5500	3893.1734
8	261.7935	213.6155	770.6654	620.5385	2599.3233	2099.5267	5979.1245	4828.6288
9	315.2031	259.2465	909.6151	762.8859	3147.9590	2541.8056	7131.0180	5932.7840
10	372.8723	309.4581	1086.6130	894.2628	3690.1211	3034.5499	8472.3476	7062.3619
11	435.2090	362.9171	1251.0566	1048.2201	4311.5305	3560.3835	9873.7373	8313.5675
12	510.4827	423.4641	1440.2239	1217.5370	4910.8490	4127.2592	11457.9682	9605.0564
13	579.0214	484.8691	1637.2582	1388.5352	5686.0981	4745.1549	12838.5356	11003.9561
14	653.1007	553.5567	1843.9302	1581.7804	6382.4615	5374.4930	14575.2159	12397.8473
15	727.5114	623.4033	2078.0267	1777.2936	7225.2892	6112.5390	16290.6486	13860.8413
16	812.9299	695.6921	2309.6221	1978.8339	7976.2549	6800.2213	18052.6631	15455.2197
17	895.3913	765.0064	2577.8667	2217.0210	8816.6314	7555.6038	20091.7446	17248.9712
18	981.0841	843.7270	2825.7451	2431.7586	9755.8644	8359.1092	22200.5561	19102.7747
19	1081.1034	930.9899	3101.5492	2697.1976	10568.6420	9162.2442	24036.9638	20942.1083
20	1182.9425	1024.1844	3379.0382	2950.5492	11550.4644	10076.0011	26313.0956	23058.4514

Table C.6: Critical values for RSMS (CvM) with weight $w_{\text{Late}}(s) = 2(s/T)$

	$T=1$		$T=2$		$T=5$		$T=10$	
q	0.05	0.1	0.05	0.1	0.05	0.1	0.05	0.1
1	1.0873	0.7400	3.1574	2.1382	11.0666	7.4634	25.9003	16.9939
2	1.7564	1.2851	5.0528	3.6873	17.6220	13.0722	42.2701	30.3646
3	2.3160	1.7877	6.7304	5.1308	23.1657	18.0172	54.6094	42.1560
4	2.7820	2.2259	8.1483	6.5087	28.6259	22.5798	67.2635	52.4245
5	3.2457	2.6676	9.5079	7.7329	33.3687	27.0018	78.4190	63.6517
6	3.6891	3.0463	10.8180	8.9499	38.2835	31.4263	88.8228	72.9646
7	4.1413	3.4728	12.1557	10.0607	43.1302	35.3158	99.3482	83.0344
8	4.5756	3.8340	13.4307	11.2408	46.9925	38.9675	108.8796	91.9618
9	4.9381	4.2318	14.6427	12.3433	50.9589	43.1234	119.4133	100.9090
10	5.3796	4.6127	15.7990	13.4761	55.1542	46.6075	128.8882	109.9683
11	5.8164	5.0051	16.9280	14.6031	59.0478	50.3171	138.6849	119.3844
12	6.2090	5.3933	18.0170	15.6861	62.5778	54.1256	148.5791	128.7446
13	6.5909	5.7756	19.2806	16.7677	66.5670	57.6518	156.9494	137.5501
14	6.9538	6.1384	20.3435	17.8196	70.4922	61.0609	165.2996	146.1319
15	7.3279	6.5144	21.4981	18.8840	73.7703	64.8618	175.4537	153.7093
16	7.6942	6.8256	22.5916	19.7880	77.3875	68.3433	185.4441	161.4116
17	8.0654	7.2006	23.8494	20.7812	81.2248	71.6474	194.7714	170.3180
18	8.4329	7.5541	24.7658	21.8511	84.9913	75.1335	202.6990	178.0267
19	8.8313	7.9000	25.9576	22.9123	88.6435	78.8867	209.9624	187.1377
20	9.1740	8.2414	26.8903	23.8621	91.9591	82.6143	218.2454	195.6769

Table C.7: Critical values for SSMS (CvM) with weight $w_{\text{Early}}(s) = 2(1 - s/T)$

	$T = 1$		$T = 2$		$T = 5$		$T = 10$	
q	0.05	0.1	0.05	0.1	0.05	0.1	0.05	0.1
1	9.0950	5.9191	29.0180	18.3502	113.6748	72.8328	282.5729	180.3731
2	21.4713	14.9148	65.2704	46.5371	257.4094	183.2295	650.8602	450.2588
3	36.3876	26.4401	109.0674	82.4716	437.5676	324.0056	1094.5161	797.5620
4	53.0312	41.0504	163.5864	126.4203	653.3512	486.0588	1619.2687	1236.5079
5	72.5599	57.3228	224.4361	177.0562	894.2361	687.7702	2244.2809	1764.3554
6	95.3859	76.3238	296.6965	235.2714	1155.6881	932.0927	2903.5588	2333.9922
7	118.0530	96.2719	374.7852	301.5520	1474.9264	1185.3147	3644.6173	2935.5426
8	146.1653	119.7432	462.2332	378.4760	1828.1964	1476.5341	4465.7232	3629.6988
9	174.4131	144.8227	559.2147	457.4010	2217.7457	1786.7947	5434.1097	4465.2696
10	206.2346	173.5963	658.2418	546.5077	2587.7276	2145.5619	6503.4766	5349.9454
11	243.9754	204.5334	768.0736	641.3195	3038.4537	2530.0450	7567.5657	6317.0530
12	277.5633	234.5213	880.5661	743.4073	3524.8373	2934.4164	8706.7888	7269.3093
13	317.7942	270.4111	1005.8156	855.0863	3961.1554	3354.8364	9965.1850	8368.6425
14	362.1444	306.9867	1131.6891	967.4510	4470.4029	3821.5772	11093.2042	9522.1421
15	404.5097	345.8796	1273.7543	1093.1827	5006.5685	4315.2347	12536.2504	10776.3563
16	448.5090	390.1764	1416.3380	1218.9903	5556.1656	4805.4590	14078.4378	12073.6402
17	500.9080	434.3542	1565.3470	1368.6507	6106.6946	5300.7370	15546.1437	13369.7946
18	550.4289	481.5475	1734.5148	1511.3277	6744.7796	5878.7850	17034.6419	14783.1075
19	605.6575	529.4866	1898.3270	1668.2665	7395.5703	6412.0112	18669.2159	16208.7066
20	661.7640	579.6477	2074.5855	1819.2968	8064.5705	7025.6656	20290.5012	17686.4998

Table C.8: Critical values for RSMS (CvM) with weight $w_{\text{Early}}(s) = 2(1 - s/T)$

	$T = 1$		$T = 2$		$T = 5$		$T = 10$	
q	0.05	0.1	0.05	0.1	0.05	0.1	0.05	0.1
1	0.5827	0.3973	1.8836	1.3007	7.5413	5.0278	19.6063	13.2722
2	0.9497	0.7127	3.0246	2.2871	12.4023	9.1062	31.2198	23.3030
3	1.2632	0.9825	4.0189	3.1437	16.2528	12.6658	40.9111	32.0481
4	1.5537	1.2346	4.9146	3.9834	19.5421	15.9302	50.3153	39.8448
5	1.8172	1.5087	5.7189	4.7699	22.7376	18.9433	59.2172	47.9492
6	2.0711	1.7412	6.5459	5.4651	25.9146	21.7340	67.0036	55.7926
7	2.3186	1.9755	7.3583	6.1793	28.8792	24.3486	74.9470	62.8964
8	2.5750	2.2054	8.0918	6.8877	32.2761	27.3314	82.6438	70.0932
9	2.8055	2.4298	8.8213	7.5481	34.9452	30.2659	90.7473	77.6706
10	3.0221	2.6275	9.5483	8.2178	38.4682	33.0326	97.7954	84.3950
11	3.2190	2.8342	10.2964	8.9089	40.9914	35.6863	104.3357	91.2007
12	3.4656	3.0407	10.9864	9.6087	43.9309	38.4884	112.2912	97.8292
13	3.7134	3.2564	11.7104	10.2317	46.4940	40.9878	119.0618	104.3057
14	3.9328	3.4749	12.4952	10.9240	49.3182	43.6076	125.6317	110.6260
15	4.1497	3.6944	13.1454	11.6421	52.1311	46.1533	133.2982	117.3418
16	4.3804	3.8972	13.8466	12.2571	54.6373	48.6129	140.4765	124.1660
17	4.5801	4.1017	14.4375	12.8754	57.2148	50.9947	147.7718	130.9617
18	4.7974	4.3080	15.1701	13.5356	59.9949	53.4341	155.3140	137.4754
19	5.0137	4.5067	15.8273	14.1427	62.8375	56.1984	161.7731	144.0950
20	5.2553	4.7068	16.5687	14.7379	65.8050	58.8241	168.2702	150.6724

Table C.9: Critical values for SSMS (CvM) with weight $w_{\text{Mid}}(s) = 6(s/T)(1 - s/T)$

	$T = 1$		$T = 2$		$T = 5$		$T = 10$	
q	0.05	0.1	0.05	0.1	0.05	0.1	0.05	0.1
1	13.3904	8.3678	38.9630	24.7687	142.8892	92.4457	348.9241	216.4948
2	30.4463	21.3589	93.3758	64.0977	331.0299	229.9523	804.2676	565.1167
3	51.5312	37.6332	155.5556	114.5357	560.1339	416.1393	1346.9477	993.0969
4	74.7573	57.8904	227.7021	172.1801	857.6693	643.0259	2064.8974	1526.9235
5	104.9749	80.3081	314.3586	240.2733	1176.3540	905.2231	2736.4150	2147.4678
6	135.7643	108.7998	409.3054	322.4743	1504.1481	1193.0201	3564.3147	2833.7363
7	171.6189	138.8041	516.2393	415.2779	1892.2831	1525.1021	4507.0043	3591.0535
8	211.3019	172.4250	630.9660	516.3200	2352.0931	1905.8722	5556.8407	4479.0523
9	252.4316	209.9445	777.0658	628.1236	2833.1431	2313.3296	6726.2495	5442.1354
10	300.2512	250.8029	921.4753	755.0257	3297.3123	2722.9182	7941.6180	6492.9517
11	347.2469	296.8392	1069.8981	888.8666	3866.2020	3223.7435	9167.8317	7614.7917
12	402.6937	342.2144	1226.0141	1032.9627	4414.7003	3781.9147	10540.7750	8875.1940
13	464.9189	392.6965	1395.8749	1190.6420	5033.2846	4274.9799	12193.2383	10273.3351
14	522.9445	449.4446	1563.5085	1340.3499	5689.0909	4868.3352	13612.2859	11641.3920
15	584.5674	504.3551	1763.5528	1512.7627	6402.5921	5441.8472	15253.6208	13058.4269
16	655.5350	561.5667	1953.6058	1680.1109	7153.3893	6077.9435	16929.9814	14542.5622
17	717.7366	627.9770	2175.1713	1864.6983	7883.3049	6763.1312	18639.6662	16091.3724
18	791.1041	690.2347	2382.9068	2062.1185	8715.4914	7502.6814	20586.1570	17731.4509
19	863.5943	754.9393	2611.9399	2276.9289	9504.4596	8249.2332	22682.0092	19736.0845
20	947.1258	829.8703	2863.4022	2490.4515	10429.7763	9046.2420	24564.5745	21429.5060

Table C.10: Critical values for RSMS (CvM) with weight $w_{\text{Mid}}(s) = 6(s/T)(1 - s/T)$

	$T = 1$		$T = 2$		$T = 5$		$T = 10$	
q	0.05	0.1	0.05	0.1	0.05	0.1	0.05	0.1
1	0.8550	0.5913	2.5538	1.7486	9.7265	6.5418	23.9134	16.1154
2	1.4242	1.0297	4.3435	3.1693	15.6764	11.7765	38.9004	28.8813
3	1.8324	1.4517	5.6371	4.3668	20.7707	16.1491	51.5516	39.8241
4	2.2757	1.8135	6.8139	5.4970	25.4189	20.2150	62.2314	49.7610
5	2.6417	2.1701	7.9559	6.5266	30.2213	24.1295	72.7535	58.9408
6	3.0167	2.5101	9.0187	7.5568	34.3105	27.9651	81.8130	68.0089
7	3.3617	2.8322	10.1005	8.5138	38.2337	31.5672	92.3416	76.1182
8	3.7157	3.1673	11.0802	9.4826	42.2302	35.3670	101.4118	85.5648
9	4.0389	3.4965	12.2301	10.4718	46.1830	38.8623	110.5265	93.9293
10	4.3570	3.7880	13.2306	11.4851	49.4950	42.2566	119.9994	103.1656
11	4.6546	4.0824	14.1785	12.3595	53.1843	45.4864	128.2704	110.9167
12	5.0140	4.3973	15.2290	13.2202	56.4235	48.8367	136.9247	118.0578
13	5.3266	4.6814	16.2347	14.1585	60.2928	52.0944	146.3057	127.0494
14	5.6423	4.9860	17.2609	15.1132	64.0448	55.7450	154.7642	135.3204
15	5.9633	5.2434	18.1102	16.0460	67.3935	59.0044	164.1971	143.2964
16	6.2356	5.5339	19.0769	16.9401	70.7955	61.9279	172.6235	151.3639
17	6.5644	5.8402	20.0206	17.8455	74.2418	65.2322	180.5433	159.7446
18	6.8608	6.1026	20.9678	18.6309	77.5601	68.6469	188.0300	166.9751
19	7.1609	6.3881	21.9381	19.4953	81.0636	71.8970	195.9663	174.6103
20	7.4703	6.6695	22.8626	20.3897	84.2645	75.2771	203.5381	181.7112

C.3 HAC monitoring statistics

Tables C.11–C.15 report Monte Carlo critical values at the 5% and 10% levels for the HAC-based KS and CvM monitoring statistics under the null hypothesis, across horizons $T \in \{1, 2, 5, 10\}$ and monitoring lengths $q = 1, \ldots, 20$; they are used to calibrate the rejection boundaries of the HAC monitoring statistics in the size and power comparisons.

D Proofs for Section 4

Throughout the appendix, all weak convergence statements are in the Skorokhod space $D(\cdot)$ equipped with the usual J_1 topology. Because all limiting Gaussian processes appearing below have continuous sample paths, J_1 convergence implies uniform convergence on compact sets along a Skorokhod representation; we repeatedly use this fact to justify continuous-mapping arguments.

D.1 Auxiliary weak limits

Recall $\phi_t = \psi_t - \bar{\psi}_m$ and $S_m(k) = \sum_{t=m+1}^{m+k} \phi_t$. Let

$$G_m(r) \equiv \frac{1}{\sqrt{m}} \sum_{t=1}^{\lfloor mr \rfloor} (\psi_t - \mu), \qquad r \in [0, 1+T],$$

so Assumption 6 states $G_m(\cdot) \Rightarrow \Sigma^{1/2} B_q(\cdot)$ in $D([0, 1+T], \mathbb{R}^q)$.

Lemma D.1 (Training-bridge process and D_m)**.** *Under Assumption 6,*

(i) the training bridge partial-sum process

$$H_m(r) \equiv \frac{1}{\sqrt{m}} \sum_{t=1}^{\lfloor mr \rfloor} \phi_t, \qquad r \in [0, 1],$$

satisfies $H_m(\cdot) \Rightarrow \Sigma^{1/2} B_q^0(\cdot)$ in $D([0,1], \mathbb{R}^q)$, where $B_q^0(r) = B_q(r) - r B_q(1)$;

(ii) the quadratic self-normalizer satisfies

$$D_m = \frac{1}{m^2} \sum_{t=1}^{m} \Big(\sum_{j=1}^{t} \phi_j \Big) \Big(\sum_{j=1}^{t} \phi_j \Big)^\top \xrightarrow{d} \Sigma^{1/2} V \Sigma^{1/2}, \qquad V = \int_0^1 B_q^0(r) B_q^0(r)^\top dr;$$

(iii) in particular, $\mathbb{P}(\det D_m > 0) \to 1$ and $D_m^{-1} \xrightarrow{d} \Sigma^{-1/2} V^{-1} \Sigma^{-1/2}$.

Table C.11: Critical values for HAC (KS) for two boundary exponents $\gamma \in \{0, 0.15\}$

Panel A: $\gamma = 0$								
	$T = 1$		$T = 2$		$T = 5$		$T = 10$	
q	0.05	0.1	0.05	0.1	0.05	0.1	0.05	0.1
1	2.4713	1.9058	3.3506	2.5777	4.1281	3.1779	4.7551	3.6068
2	3.5571	2.8361	4.7790	3.8548	6.0085	4.8843	6.6921	5.4050
3	4.4816	3.7357	5.9168	4.9272	7.6351	6.2955	8.3873	6.9746
4	5.3241	4.4936	7.1059	5.9473	9.0354	7.6338	10.0197	8.3952
5	6.1984	5.2170	8.0883	6.9231	10.3508	8.8394	11.4496	9.7797
6	6.9293	5.9773	9.1450	7.8111	11.6327	10.0447	12.8584	11.1103
7	7.7560	6.6664	10.2500	8.7933	12.9168	11.1981	14.3544	12.3347
8	8.4727	7.3484	11.1796	9.6927	14.1702	12.3236	15.6745	13.6835
9	9.1680	8.0282	12.1083	10.6830	15.2416	13.4326	16.9896	14.8983
10	9.8832	8.7049	13.0045	11.5602	16.2949	14.5465	18.2448	16.0962
11	10.5907	9.3835	13.9690	12.4553	17.4654	15.6115	19.4915	17.3003
12	11.2575	10.0157	14.9215	13.2872	18.5344	16.6472	20.5743	18.5570
13	11.8942	10.6501	15.7262	14.1560	19.7888	17.6775	21.9053	19.6960
14	12.5442	11.2753	16.7189	14.9033	20.9366	18.8054	23.0826	20.7882
15	13.1966	11.9205	17.5872	15.7676	21.9766	19.7951	24.4177	21.9370
16	13.8731	12.5168	18.3533	16.5807	23.1074	20.8065	25.5814	23.0813
17	14.4310	13.1443	19.2665	17.4316	24.1722	21.9279	26.7243	24.1976
18	15.0962	13.7778	20.1528	18.2340	25.4031	22.8966	27.7326	25.3204
19	15.7025	14.3349	21.0546	19.0491	26.4593	23.8933	28.8452	26.3523
20	16.4353	14.9263	21.8501	19.8742	27.4740	24.9387	29.9739	27.3837
Panel B: $\gamma = 0.15$								
	$T = 1$		$T = 2$		$T = 5$		$T = 10$	
q	0.05	0.1	0.05	0.1	0.05	0.1	0.05	0.1
1	3.2117	2.5292	3.9966	3.1454	4.6802	3.6129	5.1890	3.9990
2	4.6011	3.7386	5.6785	4.5738	6.6474	5.4657	7.1968	5.8883
3	5.7860	4.8183	6.9680	5.8678	8.3494	6.9435	9.0128	7.5011
4	6.8158	5.7362	8.2889	7.0094	9.8442	8.3691	10.6770	8.9757
5	7.8959	6.6842	9.4116	8.1074	11.2464	9.6757	12.1684	10.4288
6	8.8303	7.6083	10.6885	9.1649	12.7247	11.0048	13.6407	11.7778
7	9.8426	8.4871	11.9092	10.2608	14.0076	12.2027	15.1370	13.1013
8	10.6732	9.2726	12.9355	11.2764	15.2769	13.3809	16.5133	14.5204
9	11.5558	10.1771	14.0298	12.3966	16.5005	14.5913	17.9920	15.6749
10	12.4349	11.0133	15.0069	13.3988	17.6495	15.7567	19.1755	16.9920
11	13.3082	11.8273	16.0876	14.4507	18.7940	16.8973	20.5090	18.2083
12	14.1108	12.6368	17.1716	15.3908	19.9653	17.9742	21.6052	19.5281
13	14.9179	13.4275	18.0806	16.3015	21.2630	19.0772	22.8900	20.7531
14	15.7155	14.2146	19.1933	17.1915	22.5507	20.2998	24.1240	21.8929
15	16.5774	14.9614	20.2027	18.1783	23.6387	21.3715	25.5932	23.0427
16	17.3497	15.6886	21.1600	19.0793	24.7986	22.4299	26.7989	24.1853
17	18.0783	16.4590	22.1101	20.0642	25.9966	23.5482	27.8565	25.2920
18	18.9039	17.2651	23.0867	21.0044	27.2183	24.6288	29.0233	26.4857
19	19.6341	17.9560	24.1597	21.8910	28.3003	25.7154	30.1888	27.5285
20	20.4917	18.6875	25.0255	22.7964	29.3998	26.8126	31.2638	28.6336

Table C.12: Critical values for HAC (CvM) with $w(s) \equiv 1$

	$T=1$		$T=2$		$T=5$		$T=10$	
q	0.05	0.1	0.05	0.1	0.05	0.1	0.05	0.1
1	1.0541	0.7413	3.1105	2.2476	11.2151	8.1582	29.1254	20.5650
2	1.6112	1.2692	4.8614	3.7961	17.9828	14.0967	44.8368	34.1988
3	2.1599	1.7455	6.3079	5.1893	23.7983	19.1767	57.4246	47.0633
4	2.6300	2.1766	7.7279	6.4576	28.8886	24.0234	70.2736	58.0650
5	3.1159	2.5944	8.9744	7.6361	33.5293	28.5335	82.0688	69.1328
6	3.5384	3.0530	10.3439	8.8272	38.3777	32.8596	93.2848	79.1095
7	3.9834	3.4281	11.7720	10.0665	43.2114	37.0611	105.1645	89.9917
8	4.3798	3.8408	12.9000	11.2526	47.6850	41.2338	116.4416	100.5454
9	4.7864	4.2088	14.2023	12.4635	51.7784	45.6465	126.7681	110.3136
10	5.2260	4.6098	15.2705	13.6779	55.8857	49.4161	136.7569	120.3509
11	5.5932	5.0000	16.6009	14.8078	59.7303	53.6331	147.0252	129.3937
12	6.0022	5.3650	17.7410	15.8955	64.1379	57.3951	157.2153	139.8985
13	6.3663	5.7565	18.8273	16.9615	68.5411	61.4310	166.4214	150.0398
14	6.7510	6.1291	20.0848	18.0086	72.9287	65.4497	175.9403	159.1141
15	7.1395	6.5104	21.2410	19.1063	76.7726	69.4470	186.8867	167.6688
16	7.5535	6.8694	22.4084	20.1682	80.9702	73.1965	196.4221	176.5970
17	7.9484	7.2124	23.5158	21.2332	84.6226	76.9886	205.3142	185.6261
18	8.3393	7.5824	24.6125	22.3459	88.9156	80.9831	214.4613	194.2498
19	8.7001	7.9455	25.7263	23.3814	92.7093	84.7647	223.5046	202.9607
20	9.0609	8.3345	26.9441	24.3780	97.0351	88.4034	231.6495	212.0151

Table C.13: Critical values for HAC (CvM) with $w_{\text{Early}}(s) = 2(1 - s/T)$

	$T=1$		$T=2$		$T=5$		$T=10$	
q	0.05	0.1	0.05	0.1	0.05	0.1	0.05	0.1
1	0.7386	0.5388	2.3360	1.6991	9.3387	6.6683	24.9546	17.8824
2	1.1564	0.9315	3.6600	2.8786	14.7800	11.6240	38.8304	29.8584
3	1.5620	1.2613	4.8113	3.9804	19.5405	15.8191	50.3018	40.9423
4	1.8924	1.5878	5.8938	4.9571	23.6585	19.7754	61.0345	50.8249
5	2.2544	1.8876	6.9432	5.9027	27.7491	23.6192	71.8125	60.1557
6	2.5578	2.2122	7.8672	6.7979	31.7281	27.2401	81.7362	69.3844
7	2.8820	2.5071	8.9327	7.7449	35.6089	30.7953	91.2592	78.5550
8	3.1808	2.7849	9.9222	8.6594	39.3478	34.2397	101.0729	88.4066
9	3.4781	3.0729	10.9232	9.6070	42.8248	37.7283	110.9216	96.3982
10	3.7886	3.3466	11.7864	10.5050	46.3273	41.2829	118.9795	105.2476
11	4.0458	3.6255	12.7742	11.4143	49.7074	44.4188	128.7640	113.2061
12	4.3823	3.9094	13.6996	12.2474	53.1117	47.5726	137.2949	122.6212
13	4.6740	4.1955	14.5662	13.0791	57.0383	51.1265	145.4557	131.1691
14	4.9256	4.4804	15.4600	13.8994	60.2779	54.3747	153.4811	139.3561
15	5.2092	4.7405	16.3846	14.7131	63.7364	57.8380	162.7421	146.9676
16	5.4984	5.0059	17.3261	15.5737	67.2744	61.1133	171.1982	154.6376
17	5.7898	5.2704	18.1970	16.4465	70.5598	64.2868	179.2604	162.9712
18	6.0629	5.5448	19.0357	17.2461	73.8107	67.5710	187.0565	170.5896
19	6.3465	5.8013	19.9301	18.0634	76.8951	70.6094	195.7402	177.5313
20	6.5994	6.0663	20.7070	18.8812	80.4655	73.7503	203.6779	185.7295

Table C.14: Critical values for HAC (CvM) with $w_{\text{Mid}}(s) = 6(s/T)(1 - s/T)$

	$T = 1$		$T = 2$		$T = 5$		$T = 10$	
q	0.05	0.1	0.05	0.1	0.05	0.1	0.05	0.1
1	1.0971	0.7746	3.3068	2.3673	12.1168	8.7029	30.9495	21.9965
2	1.6751	1.3384	5.1196	4.0254	19.1898	15.0424	47.7910	36.3502
3	2.2508	1.8165	6.6581	5.4628	25.3177	20.3571	61.3621	49.7143
4	2.7360	2.2721	8.1834	6.8017	30.6792	25.5067	74.7383	61.7547
5	3.2646	2.7114	9.5413	8.0320	35.7364	30.3967	87.0933	73.2250
6	3.6978	3.1631	10.9119	9.3050	40.9901	34.8226	99.3461	83.8660
7	4.1565	3.5885	12.3240	10.6383	46.0248	39.3388	111.2194	95.1919
8	4.5990	3.9861	13.6950	11.8849	50.6263	43.8657	123.1751	106.6393
9	5.0076	4.3880	15.0091	13.1524	54.9984	48.4746	134.4803	116.8846
10	5.4390	4.7959	16.1792	14.3920	59.5920	52.6037	145.2354	127.2465
11	5.8033	5.2002	17.5461	15.5920	63.6519	56.8134	156.1692	137.4063
12	6.2508	5.5768	18.7543	16.7590	68.0864	60.9398	166.4717	147.8920
13	6.6501	6.0023	19.8868	17.8673	72.7263	65.2224	176.3358	158.5416
14	7.0741	6.3677	21.1479	19.0265	77.5303	69.3753	186.6901	168.1493
15	7.4759	6.7679	22.4009	20.1038	81.5291	73.6674	197.8090	177.1890
16	7.8865	7.1352	23.6075	21.2943	85.7587	77.7713	207.9812	186.6501
17	8.2836	7.5150	24.8228	22.4078	89.8457	81.6108	217.4524	195.9734
18	8.6780	7.8919	25.9838	23.5048	94.3147	85.8642	226.5309	205.0962
19	9.0589	8.2588	27.1308	24.6126	98.3597	89.7356	236.4274	214.5445
20	9.4201	8.6699	28.3571	25.7138	102.9361	93.3736	245.0451	223.6880

Table C.15: Critical values for HAC (CvM) with $w_{\text{Late}}(s) = 2(s/T)$

	$T = 1$		$T = 2$		$T = 5$		$T = 10$	
q	0.05	0.1	0.05	0.1	0.05	0.1	0.05	0.1
1	1.3624	0.9643	3.9474	2.8470	13.4268	9.6518	33.7042	23.5504
2	2.0974	1.6474	6.2063	4.7271	21.4629	16.6329	51.2967	38.9570
3	2.8102	2.2519	7.8916	6.4721	28.2343	22.7592	65.8682	53.1681
4	3.3884	2.8298	9.6851	7.9694	34.3604	28.2910	79.7848	66.0726
5	4.0219	3.3627	11.2452	9.5143	39.9116	33.7173	92.4996	78.3906
6	4.5773	3.9062	12.9776	10.9700	45.6708	38.6171	106.0711	89.5819
7	5.1697	4.4195	14.6240	12.4719	51.2384	43.7803	119.6536	101.4302
8	5.6738	4.9339	16.1653	13.9125	56.4160	48.7415	131.9568	113.5097
9	6.2004	5.4053	17.6909	15.4960	61.1437	53.6187	143.5287	125.1852
10	6.7148	5.9198	19.0755	16.9512	65.9890	58.1953	155.4333	136.1067
11	7.2094	6.4065	20.5816	18.3743	70.8002	62.8680	167.3386	146.3693
12	7.7610	6.8868	22.0494	19.6841	75.8736	67.4544	177.7775	158.2284
13	8.2148	7.3978	23.4085	21.0034	80.9881	72.0206	188.5686	169.3326
14	8.6948	7.8737	24.9298	22.2805	85.9124	76.9906	200.2890	179.5796
15	9.1606	8.3195	26.3518	23.6252	90.4195	81.4518	211.3392	188.9791
16	9.7260	8.7596	27.7603	24.9770	95.1348	85.9087	222.0494	199.6690
17	10.1888	9.2277	29.2137	26.3143	99.9836	90.2899	231.8644	209.9503
18	10.7086	9.7135	30.4064	27.6862	105.1577	94.9505	242.1198	219.4804
19	11.1324	10.1707	31.8860	28.9203	109.4908	99.0380	252.4597	229.2760
20	11.5975	10.6386	33.2423	30.2514	114.5696	103.8403	262.0914	239.2422

Proof. Write $\phi_t = (\psi_t - \mu) - (\bar{\psi}_m - \mu)$ and note that $\sqrt{m}(\bar{\psi}_m - \mu) = G_m(1) + o_p(1)$. For $r \in [0,1]$,

$$\begin{aligned} H_m(r) &= \frac{1}{\sqrt{m}} \sum_{t=1}^{\lfloor mr \rfloor} (\psi_t - \mu) - \frac{\lfloor mr \rfloor}{m} \cdot \frac{1}{\sqrt{m}} \sum_{t=1}^{m} (\psi_t - \mu) \\ &= G_m(r) - \frac{\lfloor mr \rfloor}{m} G_m(1). \end{aligned} \tag{D.1}$$

Since $\sup_{r\in[0,1]} \left| \lfloor mr \rfloor / m - r \right| \le 1/m$ and $\sup_{r\in[0,1]} \|G_m(r)\| = O_p(1)$ (tightness under the FCLT),

$$\sup_{r\in[0,1]} \left\| G_m(r) - \frac{\lfloor mr \rfloor}{m} G_m(1) - \big(G_m(r) - r G_m(1)\big) \right\| \le \frac{1}{m} \|G_m(1)\| = o_p(1).$$

Therefore,

$$H_m(r) = G_m(r) - r G_m(1) + o_p(1) \quad \text{uniformly on } [0,1].$$

By Assumption 6 and the continuous mapping theorem applied to the map $x(\cdot) \mapsto x(\cdot) - (\cdot)\, x(1)$ (continuous at continuous limits),

$$\{G_m(r) - r G_m(1)\}_{r\in[0,1]} \;\Rightarrow\; \{\Sigma^{1/2}(B_q(r) - r B_q(1))\}_{r\in[0,1]} = \{\Sigma^{1/2} B_q^0(r)\}_{r\in[0,1]}.$$

Combining with the uniform $o_p(1)$ remainder yields (i).

Let $S_t^{\mathrm{tr}} = \sum_{j=1}^{t} \phi_j$. Then for $r \in ((t-1)/m,\ t/m]$ we have $\lceil mr \rceil = t$ and $m^{-1/2} S^{\mathrm{tr}}_{\lceil mr \rceil} = m^{-1/2} S_t^{\mathrm{tr}}$. Hence,

$$\begin{aligned} D_m &= \frac{1}{m^2} \sum_{t=1}^{m} S_t^{\mathrm{tr}} (S_t^{\mathrm{tr}})^\top = \frac{1}{m} \sum_{t=1}^{m} \Big(\frac{S_t^{\mathrm{tr}}}{\sqrt{m}}\Big)\Big(\frac{S_t^{\mathrm{tr}}}{\sqrt{m}}\Big)^\top \\ &= \int_0^1 \Big(\frac{S^{\mathrm{tr}}_{\lceil mr \rceil}}{\sqrt{m}}\Big)\Big(\frac{S^{\mathrm{tr}}_{\lceil mr \rceil}}{\sqrt{m}}\Big)^\top dr. \end{aligned} \tag{D.2}$$

Moreover,

$$\sup_{r\in[0,1]} \left\| \frac{S^{\mathrm{tr}}_{\lceil mr \rceil}}{\sqrt{m}} - H_m(r) \right\| \le \frac{1}{\sqrt{m}} \max_{1\le t\le m} \|\phi_t\| = o_p(1),$$

where the last step follows from $\max_{t\le m} \|\phi_t\| = O_p(m^{1/(4+\delta)})$ under the $(4+\delta)$ moment condition implicit in Assumption 1–3, so $\max_{t\le m} \|\phi_t\|/\sqrt{m} = o_p(1)$. Thus, the integrand in (D.2) can be replaced by $H_m(r) H_m(r)^\top$ at an $o_p(1)$ cost:

$$\|D_m - \int_0^1 H_m(r) H_m(r)^\top dr\| \le \int_0^1 \left\| \frac{S^{\mathrm{tr}}_{\lceil mr \rceil}}{\sqrt{m}} - H_m(r) \right\| \left(\left\| \frac{S^{\mathrm{tr}}_{\lceil mr \rceil}}{\sqrt{m}} \right\| + \|H_m(r)\| \right) dr = o_p(1), \tag{D.3}$$

using $\sup_{r\in[0,1]} \|H_m(r)\| = O_p(1)$ (tightness) and the same for $S^{\mathrm{tr}}_{\lceil mr \rceil}/\sqrt{m}$.

The map $\mathcal{T} : x(\cdot) \mapsto \int_0^1 x(r) x(r)^\top dr$ is continuous from $C([0,1], \mathbb{R}^q)$ endowed with the sup norm

into $\mathbb{R}^{q\times q}$. Since the limit in (i) is continuous a.s., the continuous mapping theorem yields

$$\int_0^1 H_m(r)H_m(r)^\top dr \xrightarrow{d} \int_0^1 \Sigma^{1/2}B_q^0(r)B_q^0(r)^\top\Sigma^{1/2}dr = \Sigma^{1/2}V\Sigma^{1/2}.$$

Combining with (D.3) gives (ii).

By Lemma D.3 below, V is positive definite a.s., hence $\Sigma^{1/2}V\Sigma^{1/2}$ is positive definite a.s. Since the set of singular matrices is closed and matrix inversion is continuous on the open set of invertible matrices, (ii) implies $\mathbb{P}(\det D_m > 0) \to 1$ and, by another application of the continuous mapping theorem, $D_m^{-1} \xrightarrow{d} \Sigma^{-1/2}V^{-1}\Sigma^{-1/2}$, proving (iii). □

Lemma D.2 (Monitoring partial sums)**.** *Under Assumption 6, in $D([0,T],\mathbb{R}^q)$,*

$$\left\{\frac{1}{\sqrt{m}}S_m(\lfloor ms\rfloor)\right\}_{0\le s\le T} \Rightarrow \left\{\Sigma^{1/2}U_q(s)\right\}_{0\le s\le T}, \qquad U_q(s) = B_q(1+s) - (1+s)B_q(1).$$

Proof. For $k = \lfloor ms\rfloor$,

$$\begin{aligned}\frac{1}{\sqrt{m}}S_m(k) &= \frac{1}{\sqrt{m}}\sum_{t=m+1}^{m+k}(\psi_t-\mu) - \frac{k}{m}\cdot\frac{1}{\sqrt{m}}\sum_{t=1}^{m}(\psi_t-\mu)\\ &= \Big(G_m(1+s) - G_m(1)\Big) - sG_m(1) + o_p(1)\\ &= G_m(1+s) - (1+s)G_m(1) + o_p(1),\end{aligned}$$

where the $o_p(1)$ term is uniform in $s\in[0,T]$ and comes only from the floor operation ($\lfloor m(1+s)\rfloor = m + \lfloor ms\rfloor$ and $\sup_{s\in[0,T]}|\lfloor ms\rfloor/m - s| \le 1/m$). The map $x(\cdot)\mapsto x(1+\cdot) - (1+\cdot)\,x(1)$ is continuous at continuous limits, so Assumption 6 and the continuous mapping theorem give

$$\{G_m(1+s)-(1+s)G_m(1)\}_{s\in[0,T]} \Rightarrow \{\Sigma^{1/2}(B_q(1+s)-(1+s)B_q(1))\}_{s\in[0,T]} = \{\Sigma^{1/2}U_q(s)\}_{s\in[0,T]}.$$

This proves the lemma. □

Lemma D.3 (Invertibility of V)**.** *The matrix $V = \int_0^1 B_q^0(r)B_q^0(r)^\top dr$ is almost surely positive definite.*

Proof. Fix $a\in\mathbb{R}^q$ with $a\neq 0$ and consider the real-valued continuous Gaussian process $Z_a(r) := a^\top B_q^0(r)$ on $[0,1]$. Since B_q^0 is a non-degenerate Gaussian bridge, Z_a is not almost surely identically zero. In fact, for any $r\in(0,1)$, $Z_a(r)$ is a centered normal with variance $\mathrm{Var}(Z_a(r)) = r(1-r)\,a^\top a > 0$, so $\mathbb{P}(Z_a(r)=0)=0$. Choose a rational $r^*\in(0,1)$ (countable set) and note that $\mathbb{P}(Z_a(r^*)\neq 0)=1$. On this event, continuity of $Z_a(\cdot)$ implies that $Z_a(r)^2>0$ on a nontrivial neighborhood of r^*, and therefore $\int_0^1 Z_a(r)^2dr > 0$. Hence $a^\top Va = \int_0^1 (a^\top B_q^0(r))^2dr > 0$ almost surely for every $a\neq 0$, i.e. V is positive definite a.s. □

D.2 Proof of Theorem 1

Proof. Assumption 7 implies that replacing the feasible DFT score sequence $\{\psi_t\}$ by its oracle counterpart $\{\psi_t^{(0)}\}$ changes all $\sqrt{m}$–scaled partial sums (both on the training window $[1, m]$ and on the monitoring window $[m+1, m+mT]$) by $o_p(1)$ uniformly on compact time sets. Since D_m and $\mathcal{M}_m^{\mathrm{S}}(\cdot)$ are continuous functionals of these partial sums, the feasible and oracle SSMS processes are asymptotically equivalent. Hence it suffices to establish the limit under Assumption 6 for the oracle scores; to simplify notation we suppress the superscript (0) and work with $\{\psi_t\}$.

We prove the functional convergence of the entire monitoring process $\{\mathcal{M}_m^{\mathrm{S}}(\lfloor ms \rfloor)\}_{s\in[0,T]}$ and then apply the supremum map.

By Lemma D.2,

$$m^{-1/2} S_m(\lfloor ms \rfloor) \Rightarrow \Sigma^{1/2} U_q(s) \quad \text{in } D([0,T], \mathbb{R}^q).$$

By Lemma D.1, $D_m^{-1} \xrightarrow{d} \Sigma^{-1/2} V^{-1} \Sigma^{-1/2}$. Both $m^{-1/2} S_m(\lfloor ms \rfloor)$ and D_m are measurable functionals of the same partial-sum array $\{G_m(r)\}_{r\in[0,1+T]}$. Because the weak limit $\Sigma^{1/2} B_q(\cdot)$ is continuous, the joint map

$$x(\cdot) \;\mapsto\; \Big(\{x(1+s) - (1+s)x(1)\}_{s\in[0,T]},\; \int_0^1 (x(r) - rx(1))(x(r) - rx(1))^\top dr \Big)$$

is continuous at $x = \Sigma^{1/2} B_q(\cdot)$ almost surely. Therefore, by the continuous mapping theorem, we have joint convergence

$$\Big(\{m^{-1/2} S_m(\lfloor ms \rfloor)\}_{s\in[0,T]},\; D_m \Big) \Rightarrow \Big(\{\Sigma^{1/2} U_q(s)\}_{s\in[0,T]},\; \Sigma^{1/2} V \Sigma^{1/2} \Big). \tag{D.4}$$

For $s \in [0, T]$,

$$\mathcal{M}_m^{\mathrm{S}}(\lfloor ms \rfloor) = \frac{\big(m^{-1/2} S_m(\lfloor ms \rfloor)\big)^\top D_m^{-1} \big(m^{-1/2} S_m(\lfloor ms \rfloor)\big)}{(1+s_m)^2 \left(\frac{s_m}{1+s_m}\right)^{2\gamma}}, \qquad s_m := \frac{\lfloor ms \rfloor}{m}.$$

Since $\sup_{s\in[0,T]} |s_m - s| \le 1/m$, we have $(1+s_m)^2 \to (1+s)^2$ and $\left(\frac{s_m}{1+s_m}\right)^{2\gamma} \to \left(\frac{s}{1+s}\right)^{2\gamma}$ uniformly on $[0, T]$. On the event $\{\det D_m > 0\}$ (whose probability tends to one by Lemma D.1(iii)), the map $(y(\cdot), A) \mapsto \left\{ y(s)^\top A^{-1} y(s) \Big/ \big((1+s)^2 \left(\frac{s}{1+s}\right)^{2\gamma} \big) \right\}_{s\in[0,T]}$ is continuous at continuous $y(\cdot)$ and invertible A. Applying this map to the joint limit in (D.4) yields, in $D([0,T], \mathbb{R})$,

$$\mathcal{M}_m^{\mathrm{S}}(\lfloor ms \rfloor) \;\Rightarrow\; \frac{(\Sigma^{1/2} U_q(s))^\top (\Sigma^{-1/2} V^{-1} \Sigma^{-1/2}) (\Sigma^{1/2} U_q(s))}{(1+s)^2 \left(\frac{s}{1+s}\right)^{2\gamma}} = \frac{U_q(s)^\top V^{-1} U_q(s)}{(1+s)^2 \left(\frac{s}{1+s}\right)^{2\gamma}}.$$

The limit process is continuous on $[0, T]$, so the supremum functional $x(\cdot) \mapsto \sup_{0<s\le T} x(s)$ is

continuous (as a map $C([0,T]) \to \mathbb{R}$). Therefore,

$$\sup_{1\le k\le mT} \mathcal{M}_m^{\mathrm{S}}(k) = \sup_{0<s\le T} \mathcal{M}_m^{\mathrm{S}}(\lfloor ms \rfloor) \xrightarrow{d} \sup_{0<s\le T} \frac{U_q(s)^\top V^{-1} U_q(s)}{(1+s)^2 \left(\frac{s}{1+s}\right)^{2\gamma}},$$

which is the desired KS-type null limit. □

D.3 Proof of Theorem 2

Proof. Assumption 7 again allows us to treat the feasible (estimated) DFT scores as asymptotically equivalent to their oracle versions at the $\sqrt{m}$ scale. Because the RSMS statistic depends on the score array only through training and monitoring partial sums and a continuous range functional, the same oracle–feasible equivalence carries over to $\widetilde{\mathcal{M}}_m^{\mathrm{R}}(\cdot)$. We therefore work with the oracle score sequence satisfying Assumption 6, and invoke Assumption 8 to ensure (approximate) diagonalization required for the componentwise range normalizer.

We give a coordinatewise proof in the (approximately) diagonalized system specified in Assumption 8. To keep notation light, we write $\widetilde{\phi}_t$ and $\widetilde{S}_m(k)$ for the scores used by RSMS and omit tildes when no confusion arises. Under Assumption 8, the long-run covariance of the working score vector is diagonal: $\Sigma = \mathrm{diag}(\sigma_1^2, \dots, \sigma_q^2)$.

For each coordinate ℓ, the (scaled) training bridge process

$$H_{m,\ell}(r) = \frac{1}{\sqrt{m}} \sum_{t=1}^{\lfloor mr \rfloor} \phi_{t,\ell}, \qquad r \in [0,1],$$

satisfies $H_{m,\ell}(\cdot) \Rightarrow \sigma_\ell B_\ell^0(\cdot)$ in $D([0,1],\mathbb{R})$ by Lemma D.1(i) applied componentwise.

The adjusted-range self-normalizer is

$$R_{m,\ell} = m^{-1/2}\Big(\max_{1\le t\le m} B_{m,\ell}(t) - \min_{1\le t\le m} B_{m,\ell}(t) \Big), \qquad B_{m,\ell}(t) = \sum_{j=1}^{t} \phi_{j,\ell} - \frac{t}{m} \sum_{j=1}^{m} \phi_{j,\ell}.$$

Noting that $m^{-1/2} B_{m,\ell}(t) = H_{m,\ell}(t/m) + o_p(1)$ uniformly in t, we can rewrite

$$R_{m,\ell} = \Big(\max_{0\le r\le 1} H_{m,\ell}(r) \Big) - \Big(\min_{0\le r\le 1} H_{m,\ell}(r) \Big) + o_p(1).$$

The map $x(\cdot) \mapsto \sup_{r\in[0,1]} x(r) - \inf_{r\in[0,1]} x(r)$ is continuous on $C([0,1])$, and the limit $\sigma_\ell B_\ell^0$ is continuous almost surely. Therefore, by the continuous mapping theorem,

$$R_{m,\ell} \xrightarrow{d} \sigma_\ell R_\ell, \qquad R_\ell := \sup_{0\le r\le 1} B_\ell^0(r) - \inf_{0\le r\le 1} B_\ell^0(r) > 0 \ \text{ a.s.}$$

Consequently $R_m^{-2} \xrightarrow{d} \Sigma^{-1} R^{-2}$, where $R = \mathrm{diag}(R_1, \dots, R_q)$.

By Lemma D.2 (applied to the diagonalized score vector),

$$m^{-1/2} S_m(\lfloor ms \rfloor) \Rightarrow \Sigma^{1/2} U_q(s) \quad \text{in } D([0,T], \mathbb{R}^q).$$

As in (D.4), the pair $\big(\{m^{-1/2} S_m(\lfloor ms \rfloor)\}_{s\in[0,T]},\, R_m\big)$ is a measurable functional of the same partial-sum process and hence converges jointly to $\big(\{\Sigma^{1/2} U_q(s)\}_{s\in[0,T]},\, \Sigma^{1/2} R\big)$. For $s \in (0,T]$, write $s_m = \lfloor ms \rfloor / m$ and note

$$\left(\frac{\lfloor ms \rfloor}{m + \lfloor ms \rfloor}\right)^{2\gamma} = \left(\frac{s_m}{1+s_m}\right)^{2\gamma} \to \left(\frac{s}{1+s}\right)^{2\gamma} \quad \text{uniformly on } [\varepsilon, T] \text{ for any } \varepsilon > 0.$$

On $\{R_\ell > 0 \ \forall \ell\}$ (which holds a.s.), the map that sends $(y(\cdot), R)$ to $y(s)^\top R^{-2} y(s) / \{(1+s)^2 (s/(1+s))^{2\gamma}\}$ is continuous for $s > 0$. Therefore, for each fixed $s \in (0,T]$,

$$\widetilde{\mathcal{M}}^{\mathrm{R}}_m(\lfloor ms \rfloor) = \frac{\big(m^{-1/2} S_m(\lfloor ms \rfloor)\big)^\top R_m^{-2} \big(m^{-1/2} S_m(\lfloor ms \rfloor)\big)}{(1+s_m)^2 \left(\frac{s_m}{1+s_m}\right)^{2\gamma}} \xrightarrow{d} \frac{U_q(s)^\top R^{-2} U_q(s)}{(1+s)^2 \left(\frac{s}{1+s}\right)^{2\gamma}},$$

where the diagonal Σ factors cancel as in the SSMS case.

Because the limit is continuous on $(0,T]$ and finite for every $s > 0$, the supremum over a compact interval $[\varepsilon, T]$ is continuous. Letting $\varepsilon \downarrow 0$ and using $\gamma < 1/2$ ensures the boundary term does not create a spurious divergence at $s \downarrow 0$. Hence,

$$\sup_{1 \le k \le mT} \widetilde{\mathcal{M}}^{\mathrm{R}}_m(k) = \sup_{0 < s \le T} \widetilde{\mathcal{M}}^{\mathrm{R}}_m(\lfloor ms \rfloor) \xrightarrow{d} \sup_{0 < s \le T} \frac{U_q(s)^\top R^{-2} U_q(s)}{(1+s)^2 \left(\frac{s}{1+s}\right)^{2\gamma}}.$$

□

D.4 Proof of Theorem 3

Proof. From Theorem 1 with $\gamma = 0$ we in fact have process-level convergence in $D([0,T], \mathbb{R})$:

$$\mathcal{M}^{\mathrm{S}}_m(\lfloor ms \rfloor) \Rightarrow \mathcal{M}^{\mathrm{S}}(s) \quad \text{in } D([0,T], \mathbb{R}), \qquad \mathcal{M}^{\mathrm{S}}(s) = \frac{U_q(s)^\top V^{-1} U_q(s)}{(1+s)^2},$$

and $\mathcal{M}^{\mathrm{S}}(\cdot)$ is almost surely continuous.

Fix $s \in [0,T]$ and consider

$$\mathcal{I}^{\mathrm{S}}_m(\lfloor ms \rfloor) = \frac{1}{m} \sum_{j=1}^{\lfloor ms \rfloor} w(j/m)\, \mathcal{M}^{\mathrm{S}}_m(j).$$

Define the step-function versions

$$w_m(u) := w(\lceil mu \rceil / m), \qquad \mathcal{M}_m(u) := \mathcal{M}^{\mathrm{S}}_m(\lceil mu \rceil), \qquad u \in [0,T],$$

so that

$$\mathcal{I}_m^{\mathrm{S}}(\lfloor ms \rfloor) = \int_0^{s_m} w_m(u)\, \mathcal{M}_m(u)\, du, \qquad s_m = \lfloor ms \rfloor / m.$$

By boundedness of w and the fact that w is Riemann integrable, $w_m \to w$ in $L^1([0,T])$ and pointwise at continuity points of w. Moreover, $u \mapsto \mathcal{M}_m(u)$ is a discretization of the cadlag process $\mathcal{M}_m^{\mathrm{S}}(\lfloor mu \rfloor)$, so $\sup_{u\in[0,T]} |\mathcal{M}_m(u) - \mathcal{M}_m^{\mathrm{S}}(\lfloor mu \rfloor)| \to_p 0$. Hence, it suffices to study

$$\int_0^s w(u)\, \mathcal{M}_m^{\mathrm{S}}(\lfloor mu \rfloor)\, du.$$

Since $\mathcal{M}_m^{\mathrm{S}}(\lfloor mu \rfloor) \Rightarrow \mathcal{M}^{\mathrm{S}}(u)$ in $D([0,T])$ with continuous limit, we have $\sup_{u\in[0,T]} |\mathcal{M}_m^{\mathrm{S}}(\lfloor mu \rfloor) - \mathcal{M}^{\mathrm{S}}(u)| \to_p 0$. Therefore, for each fixed s,

$$\left| \int_0^s w(u)\, \mathcal{M}_m^{\mathrm{S}}(\lfloor mu \rfloor)\, du - \int_0^s w(u)\, \mathcal{M}^{\mathrm{S}}(u)\, du \right| \le \|w\|_\infty\, s \sup_{u\in[0,T]} |\mathcal{M}_m^{\mathrm{S}}(\lfloor mu \rfloor) - \mathcal{M}^{\mathrm{S}}(u)| \ \to_p \ 0.$$

This yields the stated weak limit $\mathcal{I}_m^{\mathrm{S}}(\lfloor ms \rfloor) \xrightarrow{d} \int_0^s w(u)\mathcal{M}^{\mathrm{S}}(u)\, du$. □

D.5 Proof of Theorem 4

Proof. The argument parallels the proof of Theorem 3, using the process convergence from Theorem 2. Let

$$\mathcal{M}^{\mathrm{R}}(u) := \frac{U_q(u)^\top R^{-2} U_q(u)}{(1+u)^2}.$$

For any fixed $\varepsilon \in (0,T]$, Theorem 2 implies uniform convergence on $[\varepsilon, T]$ in probability, and thus

$$\int_\varepsilon^s w(u)\, \widetilde{\mathcal{M}}_m^{\mathrm{R}}(\lfloor mu \rfloor)\, du \ \xrightarrow{d} \ \int_\varepsilon^s w(u)\, \mathcal{M}^{\mathrm{R}}(u)\, du.$$

It remains to control the contribution from the neighborhood of 0. Since $U_q(0) = 0$ and $u \mapsto (1+u)^{-2}$ is continuous, $\mathcal{M}^{\mathrm{R}}(u)$ is continuous at $u = 0$ with $\mathcal{M}^{\mathrm{R}}(0) = 0$. With bounded $w(\cdot)$, this implies $\int_0^\varepsilon w(u)\mathcal{M}^{\mathrm{R}}(u)du \to 0$ as $\varepsilon \downarrow 0$ almost surely, and the same argument applies to the prelimit integrals, yielding

$$\mathcal{I}_m^{\mathrm{R}}(\lfloor ms \rfloor) = \int_0^s w(u)\, \widetilde{\mathcal{M}}_m^{\mathrm{R}}(\lfloor mu \rfloor)\, du \ \xrightarrow{d} \ \int_0^s w(u)\, \mathcal{M}^{\mathrm{R}}(u)\, du.$$

□

D.6 Proof of Theorem 5

Proof. We present the argument for SSMS; RSMS and the CvM stopping rules follow by identical modifications.

Fix $s^\star \in (0,T)$ and let $k^\star = \lfloor ms^\star \rfloor$ be the change location in monitoring time. Under Assump-

tion 10, for $k \geq k^\star$,

$$\mathbb{E}(\phi_{m+k}) = \mathbb{E}(\psi_{m+k} - \bar{\psi}_m) = \Delta + o(1),$$

because the training mean $\bar{\psi}_m \xrightarrow{p} \mu$ by the law of large numbers on the stable training window. Therefore,

$$\mathbb{E}S_m(k) = \sum_{j=1}^{k} \mathbb{E}(\phi_{m+j}) = \sum_{j=k^\star}^{k} \Delta + o(m) = (k - k^\star)\Delta + o(m).$$

Choose any $s_1 \in (s^\star, T]$ and set $k_1 = \lfloor m s_1 \rfloor$. Then $\|\mathbb{E}S_m(k_1)\| \asymp m$ and, more precisely,

$$\frac{1}{\sqrt{m}}\mathbb{E}S_m(k_1) = \sqrt{m}\,(s_1 - s^\star)\Delta + o(\sqrt{m}),$$

which diverges in norm because $\Delta \neq 0$.

Next write $S_m(k) = \mathbb{E}S_m(k) + \big(S_m(k) - \mathbb{E}S_m(k)\big)$. By the same moment/dependence conditions that yield the FCLT under H_0 (assumed to persist under H_1 in Assumption 10), the centered partial sums satisfy

$$\sup_{1 \leq k \leq mT} \|S_m(k) - \mathbb{E}S_m(k)\| = O_p(\sqrt{m}).$$

Hence, at $k = k_1$,

$$\frac{1}{\sqrt{m}} S_m(k_1) = \frac{1}{\sqrt{m}}\mathbb{E}S_m(k_1) + O_p(1) \;\to\; \infty \quad \text{in probability.}$$

Finally, the self-normalizer D_m is computed entirely from the stable training window, so Lemma D.1 implies $D_m^{-1} = O_p(1)$ and $\mathbb{P}(\det D_m > 0) \to 1$. Therefore,

$$\mathcal{M}_m^{\mathrm{S}}(k_1) = \frac{\big(m^{-1/2} S_m(k_1)\big)^\top D_m^{-1} \big(m^{-1/2} S_m(k_1)\big)}{(1 + k_1/m)^2} \;\xrightarrow{p}\; \infty.$$

Given any fixed boundary $c > 0$, we obtain

$$\mathbb{P}\Big(\sup_{1 \leq k \leq mT} \mathcal{M}_m^{\mathrm{S}}(k) > c \Big) \geq \mathbb{P}\big(\mathcal{M}_m^{\mathrm{S}}(k_1) > c\big) \to 1,$$

which implies $\mathbb{P}(\mathcal{T}_m^{\mathrm{S}} \leq mT) \to 1$.

For the CvM statistic, note that for any $s_2 \in (s_1, T]$,

$$\mathcal{I}_m^{\mathrm{S}}(\lfloor m s_2 \rfloor) \geq \frac{1}{m} \sum_{j=k_1}^{\lfloor m s_2 \rfloor} w(j/m)\, \mathcal{M}_m^{\mathrm{S}}(j).$$

If w is nonnegative and assigns positive mass on $(s_1, s_2]$ (in particular, $w \equiv 1$), then the divergence of $\mathcal{M}_m^{\mathrm{S}}(k_1)$ forces $\mathcal{I}_m^{\mathrm{S}}(\lfloor m s_2 \rfloor) \to_p \infty$ and hence $\mathbb{P}(\mathcal{T}_{m,\mathrm{CvM}}^{\mathrm{S}} \leq mT) \to 1$. □

D.7 Proof of Theorem 6

Proof. We again focus on SSMS; RSMS and CvM variants are analogous.

Under the local alternative in Definition 1, write the score decomposition for $k = \lfloor ms \rfloor$:

$$S_m(k) = \sum_{t=m+1}^{m+k} \big(\psi_t - \mathbb{E}\psi_t\big) \;-\; k(\bar{\psi}_m - \mu) \;+\; \sum_{t=m+1}^{m+k} (\mathbb{E}\psi_t - \mu).$$

The first two terms are exactly those appearing under H_0 and hence satisfy, after scaling by $\sqrt{m}$,

$$\left\{ \frac{1}{\sqrt{m}} \sum_{t=m+1}^{m+\lfloor ms \rfloor} \big(\psi_t - \mathbb{E}\psi_t\big) - s\sqrt{m}(\bar{\psi}_m - \mu) \right\}_{s\in[0,T]} \Rightarrow \{\Sigma^{1/2} U_q(s)\}_{s\in[0,T]}.$$

The mean term contributes a deterministic drift. For $k = \lfloor ms \rfloor$,

$$\frac{1}{\sqrt{m}} \sum_{t=m+1}^{m+k} (\mathbb{E}\psi_t - \mu) = \frac{1}{\sqrt{m}} \sum_{t=m+k^\star+1}^{m+k} \Delta_m + o(1) = \frac{k-k^\star}{\sqrt{m}} \cdot \frac{\delta}{\sqrt{m}} + o(1) \to (s-s^\star)_+ \delta.$$

Combining the stochastic and deterministic parts yields the drifted functional CLT

$$\left\{ \frac{1}{\sqrt{m}} S_m(\lfloor ms \rfloor) \right\}_{s\in[0,T]} \Rightarrow \left\{ \Sigma^{1/2} \big(U_q(s) + (s-s^\star)_+ \delta \big) \right\}_{s\in[0,T]}.$$

Meanwhile, D_m depends only on the (stable) training window, so its limit is unchanged: $D_m \xrightarrow{d} \Sigma^{1/2} V \Sigma^{1/2}$ and $D_m^{-1} \xrightarrow{d} \Sigma^{-1/2} V^{-1} \Sigma^{-1/2}$ (Lemma D.1). Applying the same joint-convergence and continuous-mapping argument as in the proof of Theorem 1 gives, in $D([0,T], \mathbb{R})$,

$$\mathcal{M}_m^{\mathrm{S}}(\lfloor ms \rfloor) \Rightarrow \frac{\big(U_q(s) + (s-s^\star)_+ \delta\big)^\top V^{-1} \big(U_q(s) + (s-s^\star)_+ \delta\big)}{(1+s)^2}.$$

Taking $\sup_{0<s\le T}$ (a continuous functional of the continuous limit process) yields the KS-type local-power limit in Theorem 6. CvM-type drifted limits follow by integrating the drifted limit process against $w(\cdot)$, exactly as in Theorem 3. □

D.8 Proof of Proposition 1

Proof. Write $\bar{\psi}_m^{(0)} = m^{-1} \sum_{t=1}^m \psi_t^{(0)}$ and $\bar{d}_m = m^{-1} \sum_{t=1}^m d_{t,m}$. Because $t = m$ is included in the supremum in (23),

$$\sqrt{m}\, \|\bar{d}_m\| = \frac{1}{\sqrt{m}} \left\| \sum_{t=1}^m d_{t,m} \right\| \;\le\; \sup_{0\le r\le 1} \frac{1}{\sqrt{m}} \left\| \sum_{t=1}^{\lfloor mr \rfloor} d_{t,m} \right\| \;\to\; 0,$$

so $\bar{\psi}_m = \bar{\psi}_m^{(0)} + \bar{d}_m$ satisfies $\sqrt{m}(\bar{\psi}_m - \bar{\psi}_m^{(0)}) \to 0$. Hence the training centering error induced by contamination is $o(m^{-1/2})$.

Define the training-centered arrays $\phi_t = \psi_t - \bar{\psi}_m$ and $\phi_t^{(0)} = \psi_t^{(0)} - \bar{\psi}_m^{(0)}$ for $t \le m$. Then, for $t \le m$,

$$\phi_t = \phi_t^{(0)} + \delta_{t,m}, \qquad \delta_{t,m} := d_{t,m} - \bar{d}_m, \qquad \sum_{t=1}^{m} \delta_{t,m} = 0.$$

Let $H_m(r) = m^{-1/2} \sum_{t=1}^{\lfloor mr \rfloor} \phi_t$ and $H_m^{(0)}(r) = m^{-1/2} \sum_{t=1}^{\lfloor mr \rfloor} \phi_t^{(0)}$ for $r \in [0,1]$. Then $H_m(r) = H_m^{(0)}(r) + \Delta_m(r)$ with

$$\Delta_m(r) = \frac{1}{\sqrt{m}} \sum_{t=1}^{\lfloor mr \rfloor} \delta_{t,m} = \frac{1}{\sqrt{m}} \sum_{t=1}^{\lfloor mr \rfloor} d_{t,m} - \frac{\lfloor mr \rfloor}{m} \cdot \frac{1}{\sqrt{m}} \sum_{t=1}^{m} d_{t,m}.$$

Therefore

$$\sup_{0 \le r \le 1} \|\Delta_m(r)\| \le 2 \sup_{0 \le r \le 1} \frac{1}{\sqrt{m}} \left\| \sum_{t=1}^{\lfloor mr \rfloor} d_{t,m} \right\| \to 0$$

by (23), which yields

$$\sup_{0 \le r \le 1} \|H_m(r) - H_m^{(0)}(r)\| \to 0. \tag{D.5}$$

Because $\{\psi_t^{(0)}\}$ satisfies Assumption 6, Lemma D.1(i) implies $H_m^{(0)}(\cdot) \Rightarrow \Sigma^{1/2} B_q^0(\cdot)$ in $D([0,1], \mathbb{R}^q)$, and hence $\sup_{0 \le r \le 1} \|H_m^{(0)}(r)\| = O_p(1)$. Together with (D.5), this also gives $\sup_{0 \le r \le 1} \|H_m(r)\| = O_p(1)$.

Recall that $D_m = (1/m) \sum_{t=1}^{m} H_m(t/m) H_m(t/m)^\top$ and define $D_m^{(0)}$ analogously from $H_m^{(0)}$. Then, with $\|\cdot\|$ denoting the operator norm,

$$\|D_m - D_m^{(0)}\| \le \frac{1}{m} \sum_{t=1}^{m} \left\| H_m(t/m) H_m(t/m)^\top - H_m^{(0)}(t/m) H_m^{(0)}(t/m)^\top \right\|$$

$$\le \sup_{0 \le r \le 1} \|H_m(r) - H_m^{(0)}(r)\| \cdot \sup_{0 \le r \le 1} \left(\|H_m(r)\| + \|H_m^{(0)}(r)\| \right) = o_p(1),$$

where the last step uses (D.5) and $\sup_r \|H_m(r)\| + \sup_r \|H_m^{(0)}(r)\| = O_p(1)$. Hence $D_m = D_m^{(0)} + o_p(1)$. Since Lemma D.1(ii)–(iii) yields $D_m^{(0)} \xrightarrow{d} \Sigma^{1/2} V \Sigma^{1/2}$ with $\mathbb{P}(\det D_m^{(0)} > 0) \to 1$, we also have $D_m^{-1} - (D_m^{(0)})^{-1} = o_p(1)$ by matrix perturbation and $\mathbb{P}(\det D_m > 0) \to 1$.

Consider first RSMS without prewhitening (the diagonal-Σ case in Assumption 8). Let $B_{m,\ell}(r) = e_\ell^\top H_m(r)$ and $B_{m,\ell}^{(0)}(r) = e_\ell^\top H_m^{(0)}(r)$. Then (D.5) implies $\sup_{r \in [0,1]} |B_{m,\ell}(r) - B_{m,\ell}^{(0)}(r)| \to 0$ for each ℓ. The range functional is Lipschitz under the sup norm: for any $f, g \in C([0,1])$,

$$\left| \left(\sup f - \inf f \right) - \left(\sup g - \inf g \right) \right| \le 2 \|f - g\|_\infty.$$

Therefore, for each ℓ, $\widetilde{R}_{m,\ell} - \widetilde{R}_{m,\ell}^{(0)} \to 0$ in probability, and hence $\widetilde{R}_m = \widetilde{R}_m^{(0)} + o_p(1)$.

If RSMS is implemented with prewhitening, write $\widehat{\Sigma}_{\phi,0} = m^{-1} \sum_{t=1}^{m} \phi_t \phi_t^\top$ and $\widehat{\Sigma}_{\phi,0}^{(0)} = m^{-1} \sum_{t=1}^{m} \phi_t^{(0)} (\phi_t^{(0)})^\top$.

Using $\phi_t = \phi_t^{(0)} + \delta_{t,m}$, we have

$$\widehat{\Sigma}_{\phi,0} - \widehat{\Sigma}_{\phi,0}^{(0)} = \frac{1}{m}\sum_{t=1}^{m}\big(\phi_t^{(0)}\delta_{t,m}^\top + \delta_{t,m}(\phi_t^{(0)})^\top + \delta_{t,m}\delta_{t,m}^\top\big).$$

By Cauchy–Schwarz and the assumption $\frac{1}{m}\sum_{t=1}^{m}\|\psi_t^{(0)}\|^2 = O_p(1)$,

$$\left\|\frac{1}{m}\sum_{t=1}^{m}\phi_t^{(0)}\delta_{t,m}^\top\right\| \le \left(\frac{1}{m}\sum_{t=1}^{m}\|\phi_t^{(0)}\|^2\right)^{1/2}\left(\frac{1}{m}\sum_{t=1}^{m}\|\delta_{t,m}\|^2\right)^{1/2} = o_p(1),$$

and similarly for the transpose term. Moreover,

$$\left\|\frac{1}{m}\sum_{t=1}^{m}\delta_{t,m}\delta_{t,m}^\top\right\| \le \frac{1}{m}\sum_{t=1}^{m}\|\delta_{t,m}\|^2 \le 2\cdot\frac{1}{m}\sum_{t=1}^{m}\|d_{t,m}\|^2 + 2\|\bar{d}_m\|^2 \to 0$$

by (23) and $\sqrt{m}\,\|\bar{d}_m\| \to 0$. Hence $\|\widehat{\Sigma}_{\phi,0} - \widehat{\Sigma}_{\phi,0}^{(0)}\| \xrightarrow{p} 0$. By the assumed continuity of the whitening map, this implies $\|\widehat{W}_m - \widehat{W}_m^{(0)}\| \xrightarrow{p} 0$. Combining this with (D.5) and $\sup_r \|H_m^{(0)}(r)\| = O_p(1)$ yields uniform $o_p(1)$ equivalence of the prewhitened bridge processes and therefore of the adjusted ranges, so again $\widetilde{R}_m = \widetilde{R}_m^{(0)} + o_p(1)$.

For $k \ge 1$, define $S_m(k) = \sum_{t=m+1}^{m+k}(\psi_t - \bar{\psi}_m)$ and $S_m^{(0)}(k) = \sum_{t=m+1}^{m+k}(\psi_t^{(0)} - \bar{\psi}_m^{(0)})$. Since $\psi_t = \psi_t^{(0)}$ for $t \ge m+1$,

$$S_m(k) - S_m^{(0)}(k) = -k(\bar{\psi}_m - \bar{\psi}_m^{(0)}),$$

and hence

$$\sup_{1\le k\le mT}\left\|\frac{1}{\sqrt{m}}\big(S_m(k) - S_m^{(0)}(k)\big)\right\| \le T\sqrt{m}\,\|\bar{\psi}_m - \bar{\psi}_m^{(0)}\| = T\sqrt{m}\,\|\bar{d}_m\| \to 0.$$

(For RSMS with prewhitening, the same bound applies to the transformed partial sums because $\|\widehat{W}_m - \widehat{W}_m^{(0)}\| \xrightarrow{p} 0$.)

The KS- and CvM-type SSMS/RSMS monitoring statistics are continuous functionals of (i) the monitoring partial-sum process $\{m^{-1/2}S_m(\lfloor ms\rfloor) : 0 \le s \le T\}$ and (ii) the training normalizers $(D_m, \widetilde{R}_m)$. These objects are $o_p(1)$ perturbations of their clean counterparts, while the clean counterparts converge jointly to the Brownian-motion functionals in Theorems 1–4. Slutsky's theorem and the continuous mapping theorem therefore yield the claimed invariance of the null weak limits. □

E Additional simulation studies

This appendix provides two complementary sets of simulation evidence beyond the main tables in Section 5. First, Appendix E.1 reports scenario-level power–versus–b plots and additional graphical summaries constructed from the same Monte Carlo output as Tables 1–3 and Tables 4–18. Second,

Appendix E.2 studies robustness to mild Phase-I contamination.

E.1 Graphical summaries: power versus break magnitude and additional diagnostics

Figures E.1–E.4 provide a scenario-level complement to the overall summaries in Figures 1–2 in the main text. Each figure plots the detection probability $\mathbb{P}(k^* < \mathcal{T}_m \leq mT)$ against b separately for each instability design (S1–S5), using a common y-axis scale within the figure. Beyond the universal monotone power–versus–b pattern, the scenario decomposition highlights which instability designs are intrinsically easier or harder to detect. The synchronized designs S1–S3 (abrupt, multiple, or smooth changes shared across the cross section) are relatively easy: power rises rapidly with b and is already high for moderate breaks. In contrast, the cross-sectionally heterogeneous designs S4 (random break magnitudes) and S5 (staggered break dates) dilute the common post-change signal and are therefore more challenging, especially when the change occurs late ($k^*/(mT) = 0.8$) and b is small; among them, S4 is typically the most demanding case. The method ranking is also clearest in these difficult configurations: the adjusted-range self-normalized monitor (RSMS) often forms the upper envelope of the power curves, with SSMS close behind, whereas the HAC benchmark can lag materially for late breaks (most visibly when $\gamma = 0.15$). Finally, compared with the CvM summaries in Figure 2—where late-break power depends strongly on the choice of weight function (U/E/M/L) used to accumulate evidence over time—the KS-type scenario plots emphasize a more uniform gain from self-normalization across instability designs.

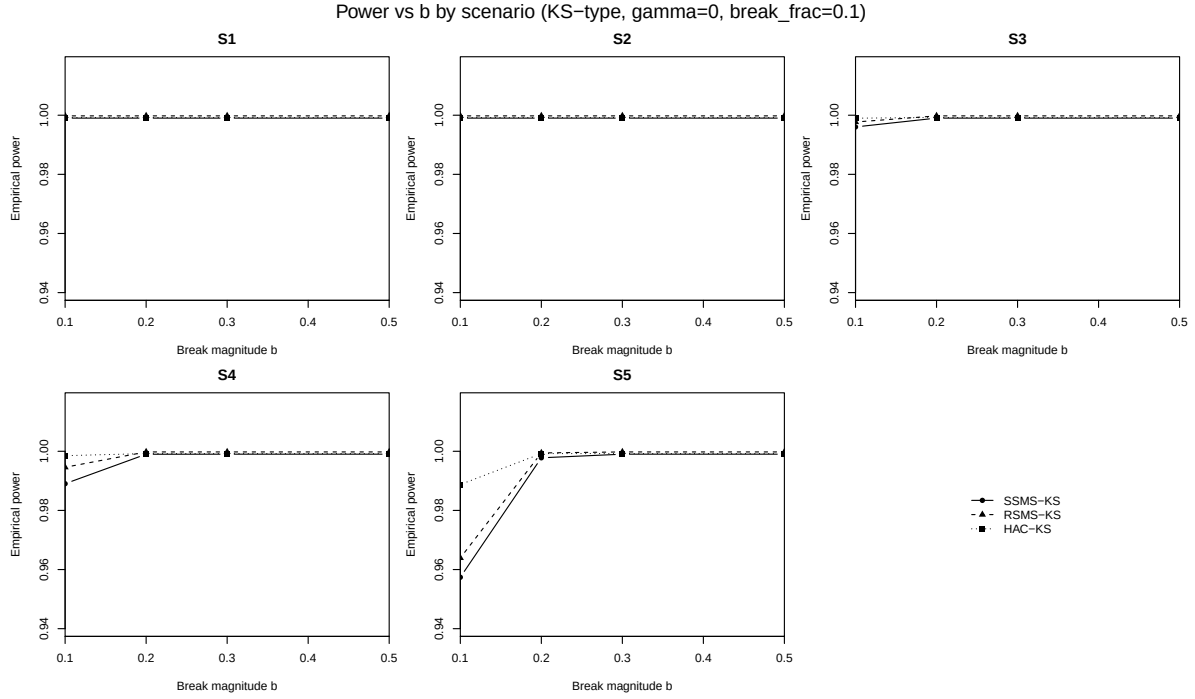

Figure E.1: Scenario-level power versus b (KS-type, $\gamma = 0$, early change $k^*/(mT) = 0.1$).

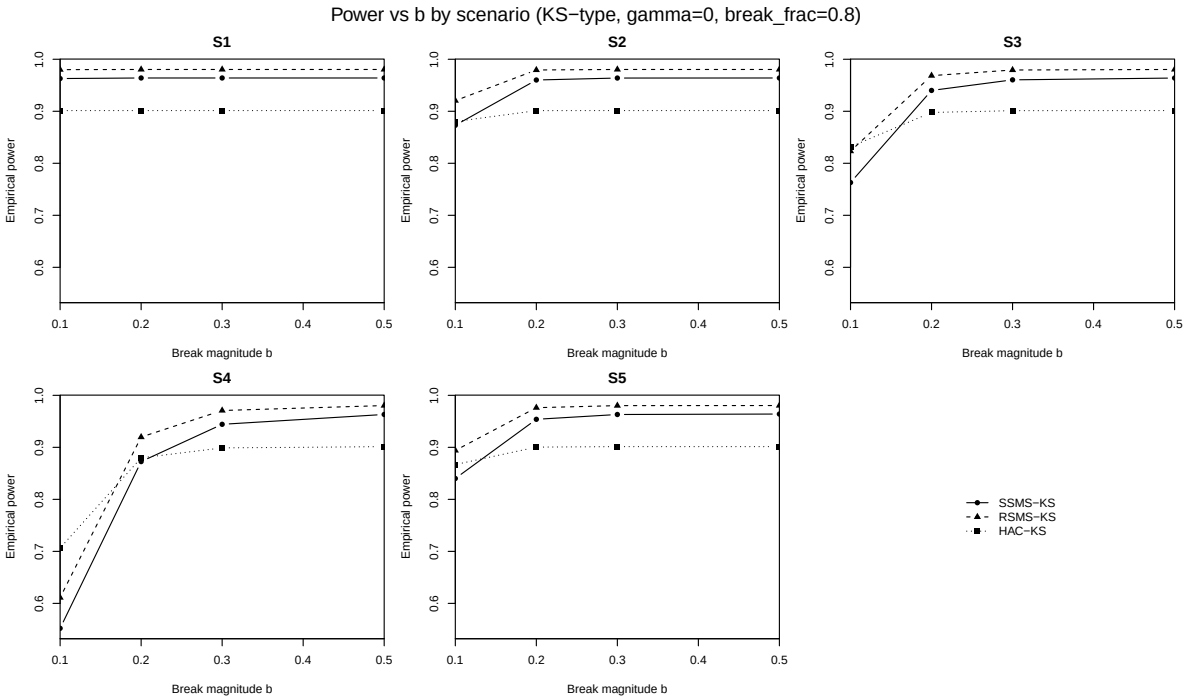

Figure E.2: Scenario-level power versus b (KS-type, $\gamma = 0$, late change $k^*/(mT) = 0.8$).

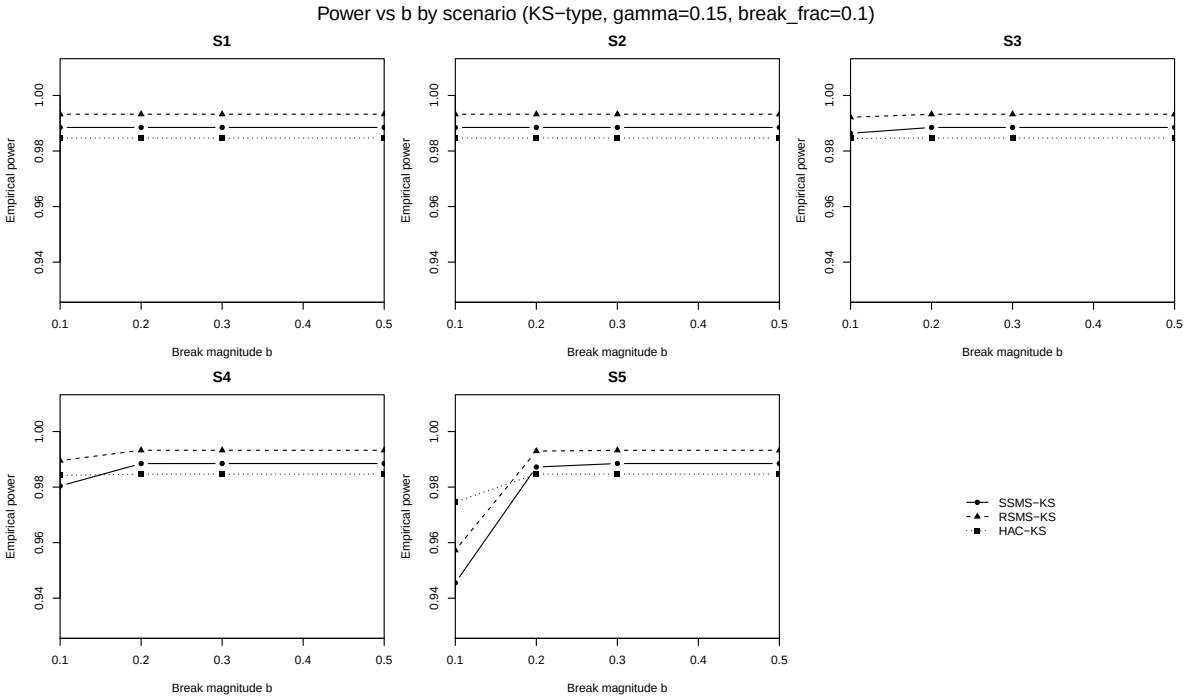

Figure E.3: Scenario-level power versus b (KS-type, $\gamma = 0.15$, early change $k^*/(mT) = 0.1$).

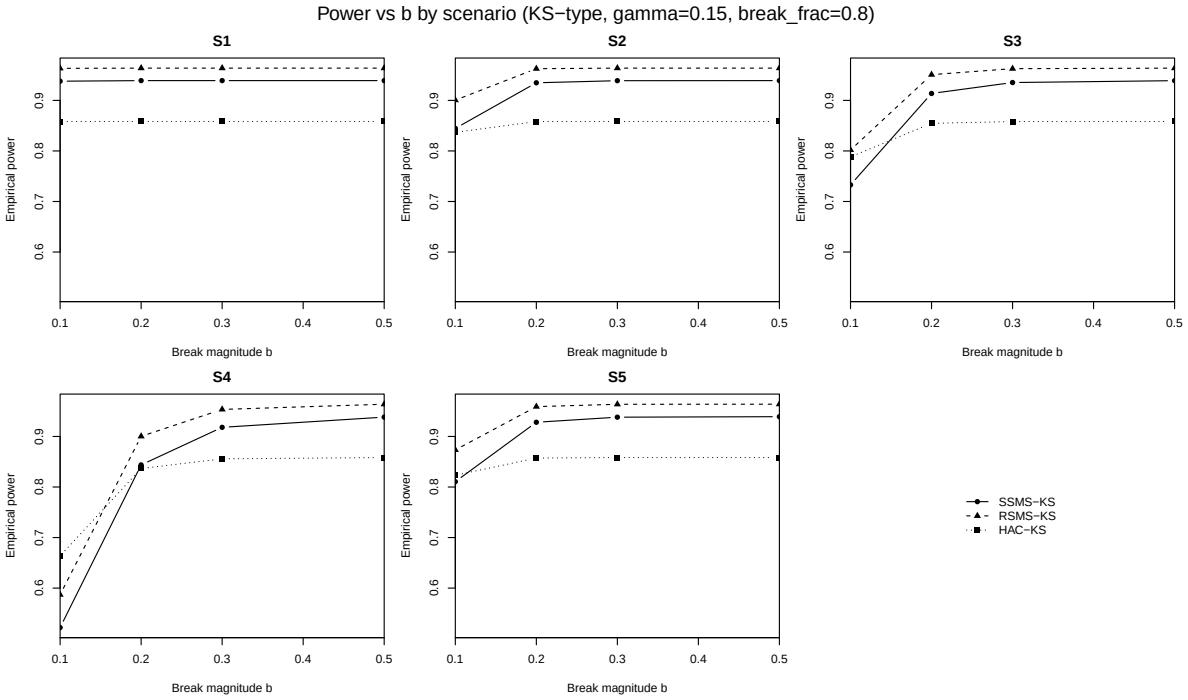

Figure E.4: Scenario-level power versus b (KS-type, $\gamma = 0.15$, late change $k^*/(mT) = 0.8$).

The remainder of this subsection complements the simulation tables in Section 5 with additional figures that highlight two dimensions: the cross-sectional size N and (for CvM-type monitoring) the choice of weight function.

All plotted quantities are computed from the same Monte Carlo output underlying Tables 1–3 and Tables 4–18. For readability, we average within each (N, m, T) cell over the three error designs under H_0; under H_1, we additionally average over break magnitudes $b \in \{0.1, 0.2, 0.3, 0.5\}$. For KS-type plots, we focus on the $\gamma = 0$ boundary; the $\gamma = 0.15$ results are reported in the tables.

Figure E.5 reports the false-alarm probabilities as a function of N for each (T, m). It reinforces the main size-control message from the tables. Across many (T, m) cells, the HAC benchmark exhibits substantial size distortion (often over-rejection), whereas the self-normalized procedures deliver materially more stable false-alarm rates. This distinction is practically important in a sequential setting because liberal size control corresponds to frequent premature stops.

Figure E.6 visualizes how late-change detection varies with N across horizons. Because our power metric is $\mathbb{P}(k^* < \mathcal{T}_m \leq mT)$, procedures that over-reject under the null may also lose late-break power by stopping before the change occurs. Consistent with this, the HAC benchmark (H0) can underperform self-normalized monitoring for late breaks despite sometimes appearing sensitive, reflecting the practical cost of size distortion in sequential monitoring.

Figure E.7 reports the CvM-type late-break detection probability by weight function (U/E/M/L). It is designed to emphasize the weight-induced trade-off for CvM-type monitoring, abstracting from the (T, m)-specific variation shown in the tables. The figure makes clear that late-break performance is highly sensitive to the weight choice: weights that emphasize later monitoring times (L) tend to

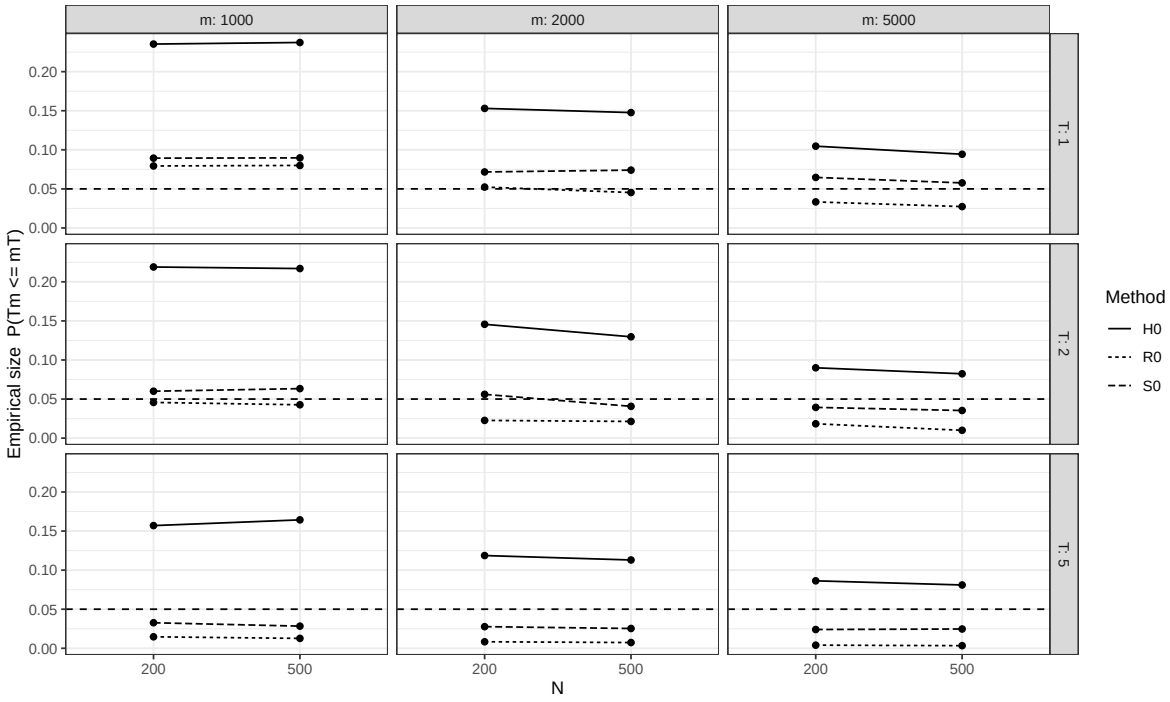

(a) KS-type size under H_0 (S0/R0/H0).

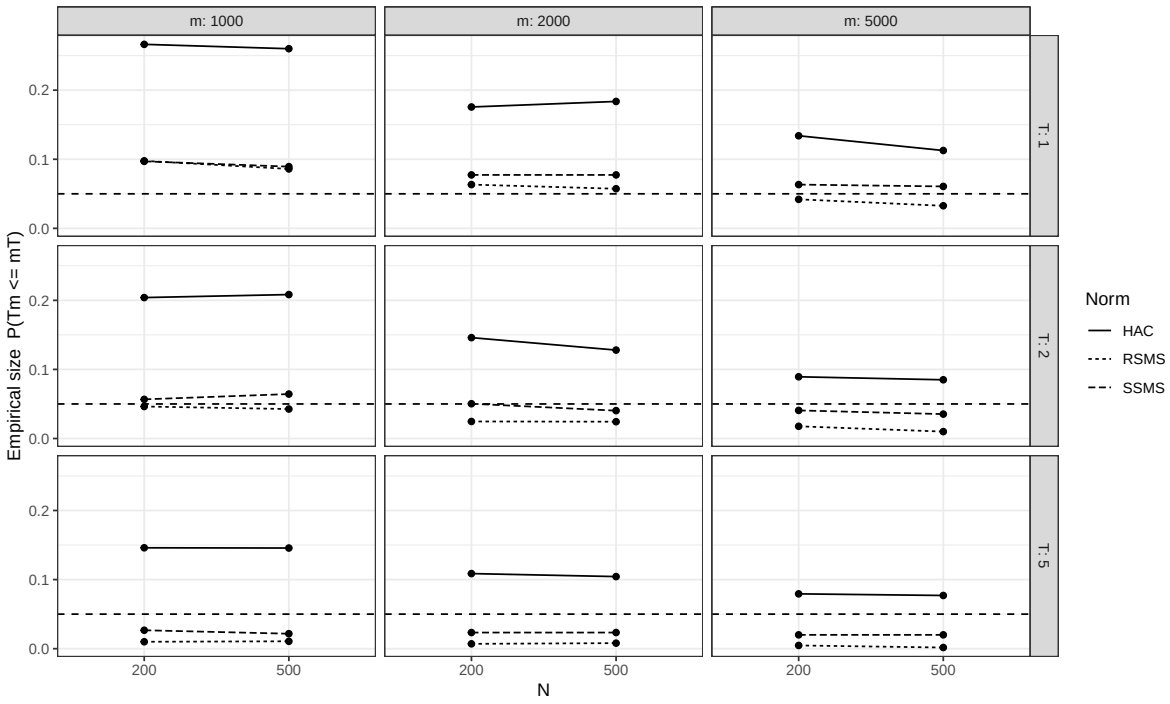

(b) CvM-type size under H_0 with w_{Late} (SSMS/RSMS/HAC).

Figure E.5: Empirical false-alarm probabilities as a function of N for each (T, m). Each point is the Monte Carlo estimate of $\mathbb{P}(\mathcal{T}_m \leq mT)$ based on 1,000 replications, averaged over the three error designs. The dashed line indicates the nominal 5% level. Legend (KS): S0 = SSMS–KS ($\gamma = 0$), R0 = RSMS–KS ($\gamma = 0$), H0 = HAC–KS ($\gamma = 0$). Legend (CvM): SSMS/RSMS are the two self-normalizers and HAC is the LRV benchmark.

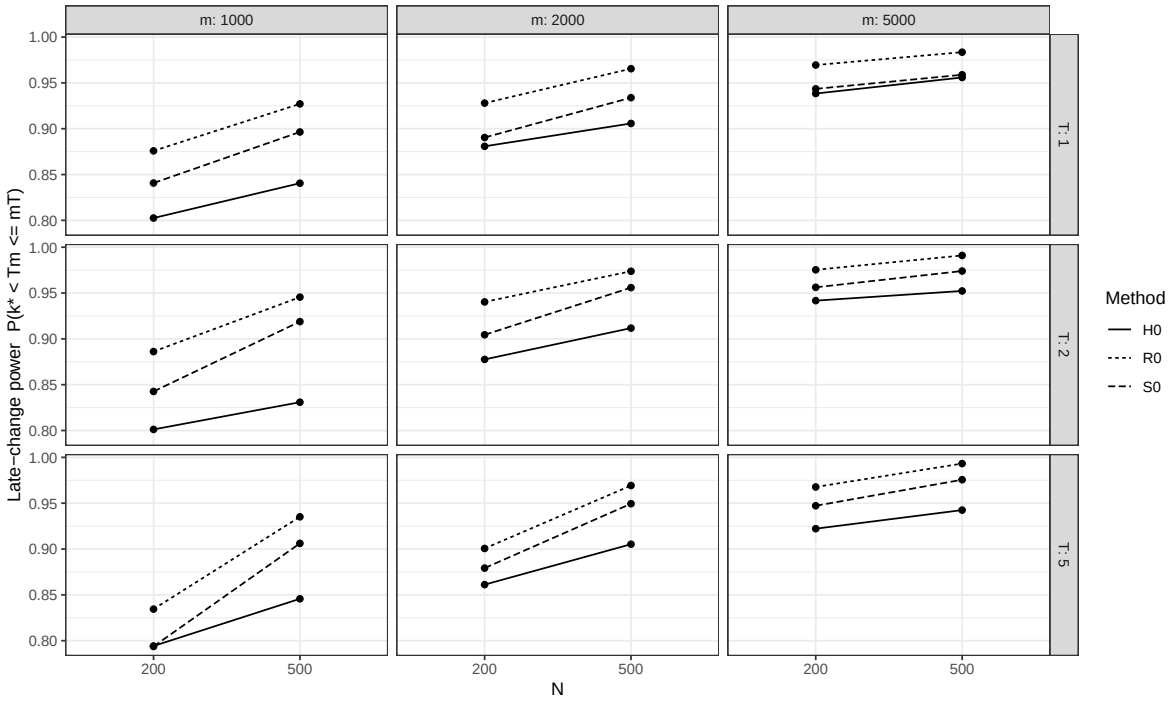

Figure E.6: KS-type late-break detection probability as a function of N for each (T, m) (S0/R0/H0). The y-axis reports $\mathbb{P}(k^* < \mathcal{T}_m \leq mT)$ with $k^* = \lfloor 0.8mT \rfloor$. For each scenario and (N, m, T), detection probabilities are averaged over the three error designs and $b \in \{0.1, 0.2, 0.3, 0.5\}$, and the plotted values then average across scenarios S1–S5 to provide a single, compact summary by (T, m).

deliver substantially higher late-break detection probabilities than early-emphasis weights (E). At the same time, the HAC-CvM benchmark should be interpreted cautiously because its severe size distortion under H_0 (Figure E.5) implies an elevated frequency of false alarms in practice.

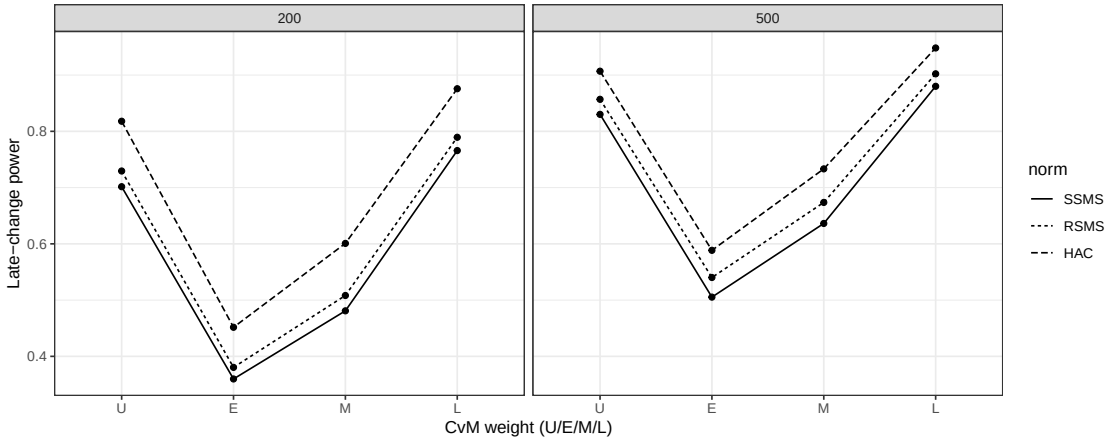

Figure E.7: CvM-type late-break detection probability by weight function (U/E/M/L), shown separately for each N (SSMS/RSMS/HAC). The y-axis reports $\mathbb{P}(k^* < \mathcal{T}_m \leq mT)$ with $k^* = \lfloor 0.8mT \rfloor$. For each scenario and (N, m, T), detection probabilities are averaged over the three error designs and $b \in \{0.1, 0.2, 0.3, 0.5\}$. To highlight the systematic ranking of weights, the plotted values then average across scenarios S1–S5 and across the (T, m) configurations (the tables report each (T, m) cell separately). Legend: U = w_{U}, E = w_{Early}, M = w_{Mid}, L = w_{Late}.

Figure E.8 summarizes the heterogeneity in how late-break power changes when moving from $N = 200$ to $N = 500$ across scenarios and horizons, without aggregating the underlying (T, m) variation into a single number. The distributional view is useful because improvements need not be uniform across all monitoring horizons: the boxplots show whether gains are systematic (shift of the entire distribution above zero) or configuration-specific (wide dispersion around zero). Taken together with Figure E.5, these plots underscore that SN provides a more reliable operating characteristic in this sequential setting, whereas HAC-based monitoring can be dominated by its in-control size distortions.

E.2 Additional simulations: mild Phase-I contamination

This appendix studies a practically relevant regime in which the Phase-I training window is mildly contaminated. The goal is not to model a grossly unclean training sample—which would typically be detected by routine diagnostics—but rather a borderline instability that may plausibly slip into Phase I due to limited power (Type II error) of offline checks.

We keep the baseline configuration fixed at $N = 500$, $m = 1000$, and monitoring horizon $T = 2$ (so that the monitoring period has length mT). We simulate the same factor and error designs as in the main Monte Carlo study, and (for concreteness) report results for the dependent error design. The DFT score construction follows the main simulation setup with $K = 2$ factors and frequency indices $u \in \{2, 4, 6, 8, 10\}$.

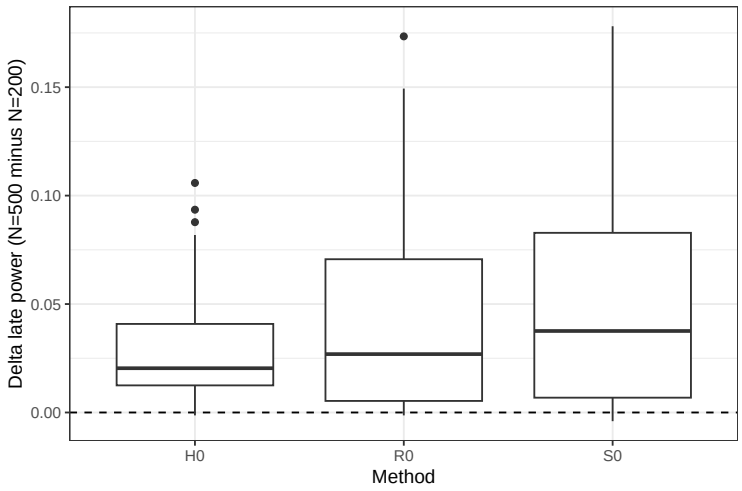

(a) KS-type monitors (S0/R0/H0).

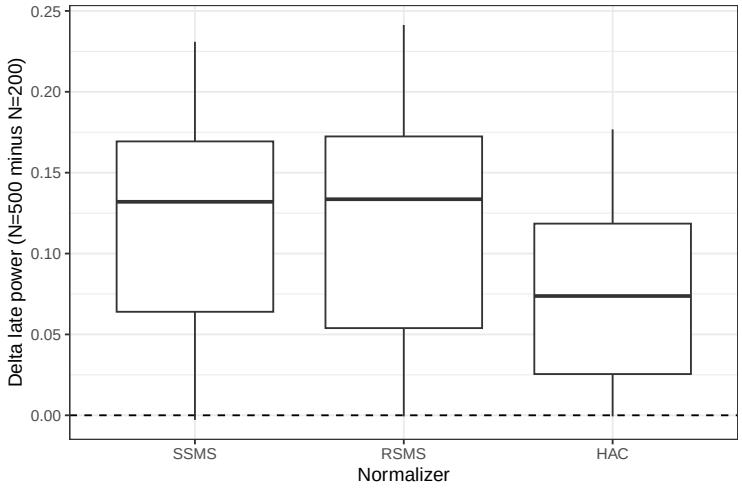

(b) CvM-type monitors with w_{Late} (SSMS/RSMS/HAC).

Figure E.8: Distribution of Δ late power when increasing N from 200 to 500. For each scenario and each (T, m), we compute the cell-average late-break detection probability at $N = 500$ minus the corresponding cell-average at $N = 200$. Boxplots summarize the resulting collection of differences across scenarios and horizons (median and interquartile range (IQR); whiskers use the standard 1.5×IQR rule).

First, for the Phase-I contamination mechanisms, we consider two contamination schemes, each indexed by a contamination magnitude $b_{\text{train}} \geq 0$. In late-break contamination, the loadings undergo a small shift at $t = \lfloor 0.8m \rfloor$ within the training block and the shifted regime persists into Phase II. In drift contamination, the loadings drift linearly over the training window so that the cumulative drift reaches b_{train} at $t = m$, and the end-of-training level persists into Phase II. We vary b_{train} on a fine grid over a local range $[0, 0.03]$, which is comparable to $1/\sqrt{m}$ when $m = 1000$.

Second, for the Phase-II alternative, to isolate the effect of Phase-I contamination on sequential detection, we fix the Phase-II alternative at the same values as in the main simulation tables. Specifically, we use the benchmark loading-instability scenario (S1) with monitoring-break magnitude $b = 0.3$ and two break locations $k^*/(mT) \in \{0.1, 0.8\}$ (early vs. late breaks).

All procedures are calibrated using the simulated decision boundaries reported in Section C (including the HAC-specific critical values reported in that section's HAC subsection, when applicable). For each method we report (i) the post-break detection probability $\mathbb{P}(k^* < \mathcal{T}_m \leq mT)$ (sequential power), and (ii) the pre-break stopping probability $\mathbb{P}(\mathcal{T}_m \leq k^*)$, which diagnoses premature signals and explains power loss when b_{train} increases.

The results (Figure E.9) show a clear transition as the training contamination magnitude increases. First, when b_{train} is very small (so that the Phase-I instability is borderline and may realistically remain in the training set), RSMS is typically more robust: relative to SSMS and the HAC baseline, it maintains higher post-break detection probabilities and exhibits fewer premature stops. This advantage is most pronounced for late Phase-II breaks, where premature stopping before k^* directly translates into a loss of sequential power. Second, as b_{train} moves into a moderate range, the probability of pre-break stopping increases for all methods, and post-break detection becomes increasingly difficult. This regime corresponds to training contamination that begins to be "visible" operationally; in applications one would normally revisit the Phase-I choice (or adopt a restart strategy) rather than proceed with a clearly unstable training block.

To keep the appendix concise, we report representative results for the KS-type monitors with boundary exponent $\gamma = 0.15$ and summarize additional variants (including CvM weights) in a single table (Table E.1). The overall patterns for $\gamma = 0$ and for the other CvM weights are qualitatively similar.

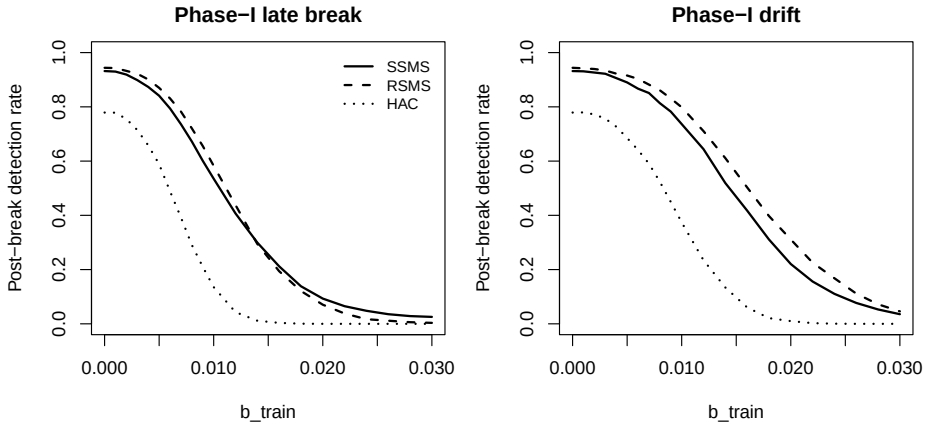

(a) Post-break detection $\mathbb{P}(k^* < \mathcal{T}_m \leq mT)$.

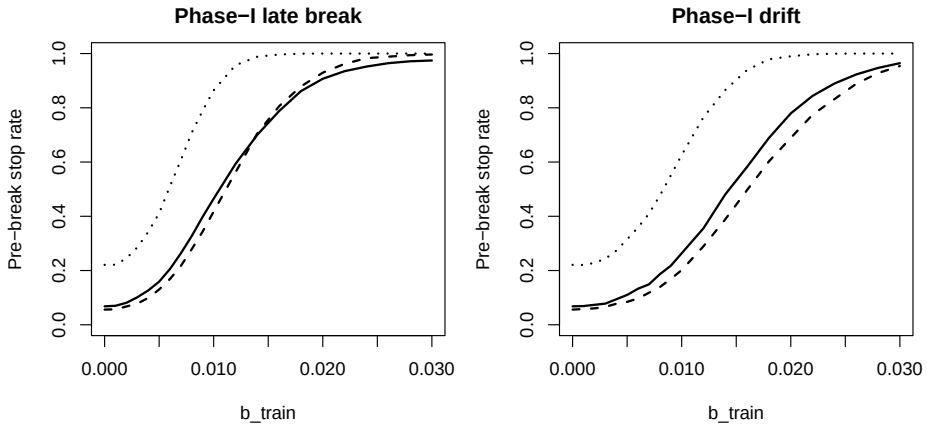

(b) Pre-break stops $\mathbb{P}(\mathcal{T}_m \leq k^*)$.

Figure E.9: Effect of mild Phase-I contamination on sequential detection under a late Phase-II break ($k^*/(mT) = 0.8$). Each panel plots performance against b_{train} for the dependent error design with $(N, m, T) = (500, 1000, 2)$. The left sub-panels correspond to late-break contamination within Phase I, and the right sub-panels correspond to drift contamination. RSMS remains closer to the clean-training benchmark in the borderline regime, while larger b_{train} increases premature stopping and reduces post-break detection.

Table E.1: Effect of mild Phase-I contamination on sequential detection under a late Phase-II break ($k^*/(mT) = 0.8$). Configuration: $(N, m, T) = (500, 1000, 2)$, dependent errors, scenario S1 with monitoring-break magnitude $b = 0.3$, and nominal level $\alpha = 0.05$. Entries report post-break detection probabilities $\mathbb{P}(k^* < \mathcal{T}_m \leq mT)$. Decision boundaries are taken from the clean-training critical values used in the main simulation study.

	KS ($\gamma = 0.15$)			CvM (Late weight)		
b_{train}	SSMS	RSMS	HAC	SSMS	RSMS	HAC
Panel A: late-break contamination in Phase I (break at $t = \lfloor 0.8m \rfloor$)						
0.000	0.932	0.944	0.779	0.998	1.000	0.995
0.002	0.919	0.932	0.755	0.998	1.000	0.992
0.005	0.841	0.870	0.589	0.995	0.999	0.983
0.010	0.535	0.583	0.136	0.981	0.995	0.888
0.020	0.093	0.070	0.000	0.901	0.929	0.182
0.030	0.025	0.004	0.000	0.776	0.783	0.004
Panel B: drift contamination in Phase I (linear drift up to b_{train})						
0.000	0.932	0.944	0.779	0.998	1.000	0.995
0.002	0.926	0.940	0.772	0.997	1.000	0.993
0.005	0.890	0.915	0.685	0.996	1.000	0.990
0.010	0.737	0.798	0.374	0.986	0.997	0.949
0.020	0.221	0.311	0.010	0.881	0.967	0.436
0.030	0.035	0.046	0.000	0.593	0.851	0.020

F Supplementary FHFA empirical results

This appendix provides supplementary evidence for the FHFA application. We report the simulated $(1 - \alpha)$ critical values required for the FHFA design ($q = 30,\ T = 2.10$) and a compact set of representative monitoring-path plots that illustrate how the main SSMS/RSMS procedures (and the HAC benchmark) behave over Phase II.

F.1 Critical values used for $q = 30$ and $T = 2.10$

The FHFA application uses score dimension $q = 30$ and monitoring horizon $T = 2.10$, implied by the Phase-I/Phase-II split. Since our tabulated critical values in Appendix C report only $q \leq 20$ (and a small set of benchmark horizons T), we simulate the required thresholds from the pivotal Brownian-motion limits in Theorems 1–4 (SSMS/RSMS) and Theorems A.1–A.2 (HAC benchmark), using 10,000 replications. For transparency, Table F.1 reports the $(1 - \alpha)$ quantiles used in the FHFA figures for $\alpha = 0.05$; for KS-type monitors we report both $\gamma = 0$ and $\gamma = 0.10$, and for CvM-type monitors we report all four weights. (These same critical values are overlaid as dashed horizontal lines in each monitoring-path plot.)

Table F.1: Critical values used in the FHFA application ($\alpha = 0.05$, $q = 30$, $T = 2.10$). KS critical values are reported for $\gamma \in \{0, 0.10\}$.

	KS		CvM			
Method	$\gamma = 0$	$\gamma = 0.10$	w_{U}	w_{Early}	w_{Mid}	w_{Late}
SSMS	4,576	5,006	5,801	4,485	6,128	7,211
RSMS	25.6	27.9	33.5	26.0	35.4	41.5
HAC	30.9	33.6	40.8	31.5	43.0	50.6

F.2 Monitoring paths

This subsection presents a compact set of representative monitoring-path plots for the FHFA application. In each panel, the monitoring statistic is plotted against the monitoring index k (quarters into Phase II), and the simulated critical value is overlaid as a horizontal dashed line. Although the stopping time is defined by the first boundary crossing, we display the full trajectories for $k \leq mT$ to facilitate diagnostic comparisons.

Because the design space spans many combinations of normalizer, functional (KS/CvM), weight, and boundary exponent, we focus on two informative slices: (i) KS-type SSMS and RSMS paths under both $\gamma = 0$ and $\gamma = 0.10$; and (ii) CvM-type SSMS and RSMS paths under two contrasting weights, the uniform weight w_{U} and the late-emphasis weight w_{Late}. The remaining CvM weights (w_{Early}, w_{Mid}) produce trajectories between these extremes, while the HAC benchmark behaves qualitatively similarly in this application (typically alarming at the very start of Phase II); hence, both are omitted for brevity.

For KS-type monitors, the post-crossing segment helps distinguish alarms driven by transient spikes from those reflecting sustained drift. For CvM-type monitors, the statistic is nondecreasing by construction (a weighted cumulative integral), so post-crossing evolution is primarily informative about the rate and timing of evidence accumulation across weights.

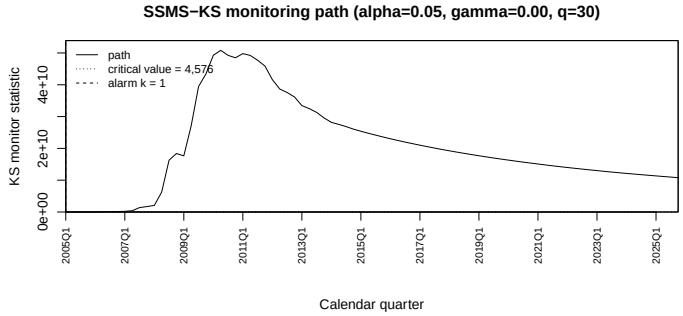

(a) SSMS–KS ($\gamma = 0$).

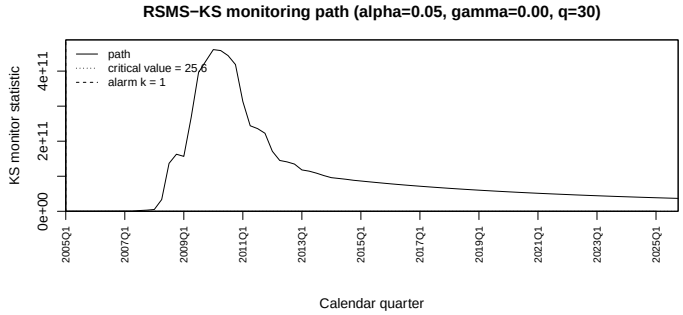

(b) RSMS–KS ($\gamma = 0$).

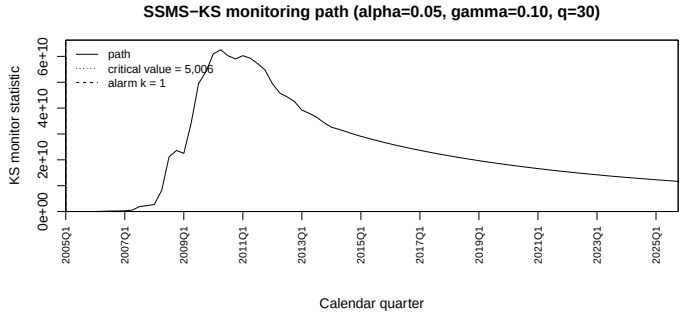

(c) SSMS–KS ($\gamma = 0.10$).

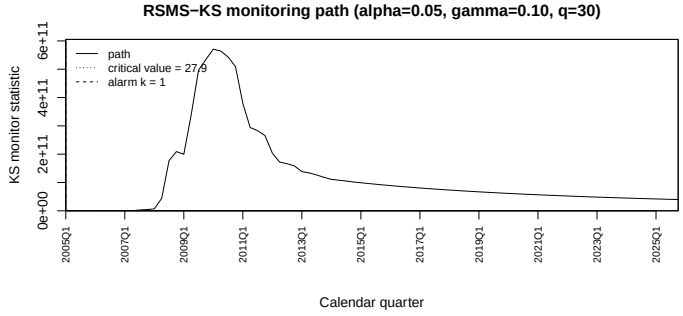

(d) RSMS–KS ($\gamma = 0.10$).

Figure F.1: FHFA monitoring paths: representative KS-type statistics ($\alpha = 0.05$, $q = 30$). The dashed line in each panel is the simulated critical value for the corresponding boundary exponent γ.

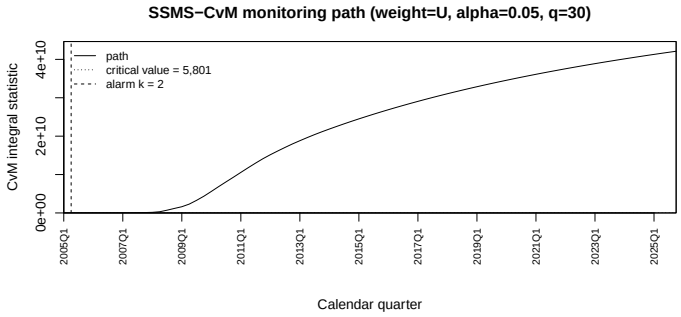

(a) SSMS–CvM (w_{U}).

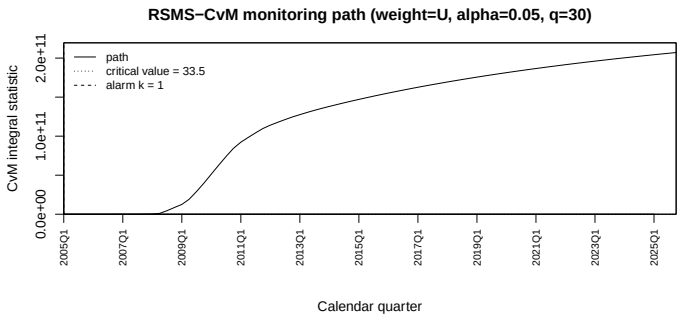

(b) RSMS–CvM (w_{U}).

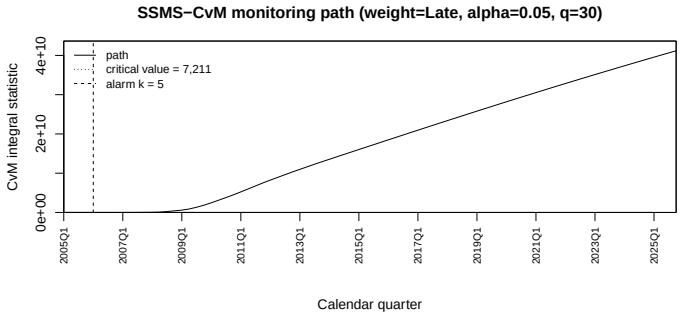

(c) SSMS–CvM (w_{Late}).

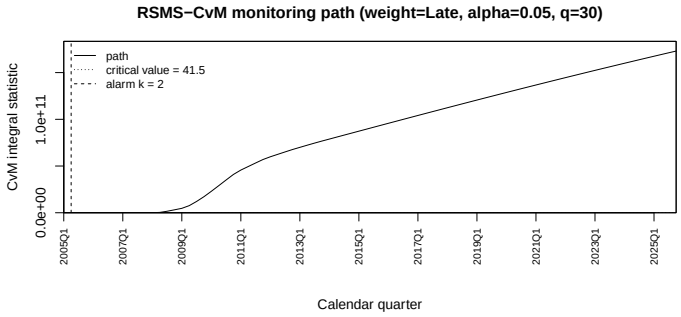

(d) RSMS–CvM (w_{Late}).

Figure F.2: FHFA monitoring paths: representative CvM-type statistics ($\alpha = 0.05$, $q = 30$). CvM-type paths are nondecreasing by construction; the weight choice primarily affects the rate and timing of evidence accumulation.

G Additional empirical illustration: FRED–MD

This appendix provides a second empirical illustration using the monthly FRED–MD U.S. macroeconomic panel. The goal is the same as in Section 6: after estimating a baseline loading space on a clean training window, we monitor the stability of the factor-model loading space in real time using the DFT-based score stream and our sequential stopping rules.

We use the publicly available FRED–MD database released by the Federal Reserve Bank of St. Louis.[3] The monthly dataset/panel contains $N = 126$ monthly U.S. macroeconomic series spanning real activity, labor markets, prices, money/credit, and financial conditions. Each series is transformed according to its published transformation code (levels, differences, log-levels, log-differences, etc.) to promote stationarity before factor extraction.

We construct a balanced panel by retaining only months for which all transformed series are observed (complete cases; no imputation). This yields a balanced sample of $n = 401$ monthly observations from 1992–03 through 2025–09 (with a small number of months dropped due to missing values in the raw panel).

We take the Phase-I training window to end in 2006–12 (a conventional pre-crisis calibration period) and monitor the subsequent stream. In terms of the balanced time index, the split is:

$$\text{Training (Phase I): 1992–03—2006–12 } (m = 178),$$

$$\text{Monitoring (Phase II): 2007–01—2025–09 } (n - m = 223),$$

so the empirical monitoring horizon is $T = (n - m)/m \approx 1.253$.

On the training window we estimate the baseline loading space $\widehat{\Lambda}_0$ by PCA and fix the factor dimension at $\widehat{K} = 3$. For each incoming month in Phase II we project the standardized panel observation onto the frozen loading space to obtain projected factors and residuals as in (5), and we construct the DFT score curve $\eta_t(u)$ in (6). We then form the real score vector $\psi_t \in \mathbb{R}^q$ by evaluating $\eta_t(u)$ on a frequency grid with $J = 5$ Fourier frequencies and stacking real and imaginary parts, so that $q = 2\widehat{K}J = 30$.

We apply the same monitoring families as in Section 6.3: SSMS and RSMS (SN) and an HAC/LRV-standardized benchmark. For KS-type monitoring we report both the classical boundary ($\gamma = 0$) and a mildly increasing boundary ($\gamma = 0.10$), with $\alpha = 5\%$. For CvM-type monitoring we report the uniform weight w_{U} and the early/mid/late emphasis weights (Section 3.3).

Because the score dimension is $q = 30$ and the empirical horizon $T = 1.253$ is not tabulated in Appendix C, we simulate the required critical values from the pivotal Brownian-motion limits (10,000 replications). Each monitoring-path figure overlays its corresponding critical value as a horizontal dashed line.

Table G.1 reports the simulated 0.95 critical value for $q = 30$ and $T = 1.253$. For KS-type monitoring we report both $\gamma = 0$ and $\gamma = 0.10$; for CvM-type monitoring we report all four weights.

[3] FRED–MD and FRED–QD ("Quarterly Database") are available from the St. Louis Fed "FRED databases" page: `https://www.stlouisfed.org/research/economists/mccracken/fred-databases`.

Table G.1: Critical values used in the FRED–MD application ($\alpha = 0.05$, $q = 30$, $T = 1.253$).

	KS		CvM			
Method	$\gamma = 0$	$\gamma = 0.10$	w_{U}	w_{Early}	w_{Mid}	w_{Late}
SSMS	3,718	4,236	2,624	1,958	2,747	3,350
RSMS	20.9	23.7	15.2	11.3	15.8	19.3
HAC	25.3	28.7	18.5	13.7	19.3	23.5

Table G.2 reports the first detection time for each monitoring rule. KS-type monitors flag instability during 2007 (roughly 8–10 months into Phase II), while CvM-type monitors—which accumulate weighted evidence over time—cross their thresholds in early 2008. Across methods, RSMS tends to alarm slightly earlier than SSMS, while HAC is broadly similar to RSMS for this dataset/horizon. Across CvM weights, the four weight functions yield similar detection times, with the late-emphasis weight w_{Late} producing a modest delay (one additional month).

From a macroeconomic perspective, these alarms line up with the transition into the Global Financial Crisis regime: financial and housing indicators began to deteriorate in mid/late 2007, and by early 2008 stress had broadened across credit markets and real activity. The monitoring procedure treats the pre-2007 period as "in control" and therefore interprets the subsequent shift in comovement patterns as a structural change in the loading space.

Table G.2: First detection times for the FRED–MD panel ($\alpha = 0.05$, $q = 30$). "Stop k" is the monitoring index (months into Phase II) at which the statistic first crosses its critical value. For KS-type monitoring we report both $\gamma = 0$ and $\gamma = 0.10$.

Method	Statistic	Weight	γ	Stop k	First alarm (month)
SSMS	KS	–	0.00	10	2007-10
RSMS	KS	–	0.00	8	2007-08
HAC	KS	–	0.00	9	2007-09
SSMS	KS	–	0.10	9	2007-09
RSMS	KS	–	0.10	8	2007-08
HAC	KS	–	0.10	8	2007-08
SSMS	CvM	U	0.00	14	2008-02
RSMS	CvM	U	0.00	14	2008-02
HAC	CvM	U	0.00	14	2008-02
SSMS	CvM	Early	0.00	14	2008-02
RSMS	CvM	Early	0.00	14	2008-02
HAC	CvM	Early	0.00	14	2008-02
SSMS	CvM	Mid	0.00	14	2008-02
RSMS	CvM	Mid	0.00	14	2008-02
HAC	CvM	Mid	0.00	14	2008-02
SSMS	CvM	Late	0.00	15	2008-03
RSMS	CvM	Late	0.00	15	2008-03
HAC	CvM	Late	0.00	15	2008-03

To interpret the detected instability, we compare factor loadings before and after the earliest alarm. Let $\widehat{\Lambda}_{\mathrm{pre}}$ be the PCA loading matrix estimated on the Phase-I training window (ending

2006–12). Starting from the earliest alarm month (2007–08), we re-estimate a post-alarm loading matrix $\widehat{\Lambda}_{\text{post}}$ on a window of length m and align the two loading spaces by an orthogonal Procrustes rotation. The principal angles between the two loading spaces are large (44.5°, 62.9°, 85.3° for $K = 3$), indicating a substantial rotation of the loading space after the 2007 alarm.

Figure G.1 summarizes the distribution of series-level loading changes $\|\widehat{\lambda}_{i,\text{post}} - \widehat{\lambda}_{i,\text{pre}}\|$ and lists the most affected series. The largest shifts are concentrated in monetary/credit and housing indicators (e.g., NONBORRES, M1SL, HOUSTMW, PERMITMW, HOUST, HOUSTW, PERMITW, SRVPRD, HOUSTNE, USTRADE) [4], alongside labor-market variables (e.g., payroll employment and unemployment/claims), consistent with the macroeconomic transmission channels that became dominant during the crisis period. The monitoring paths are similar to those for the FHFA application and are omitted for brevity. They are available from the authors upon request.

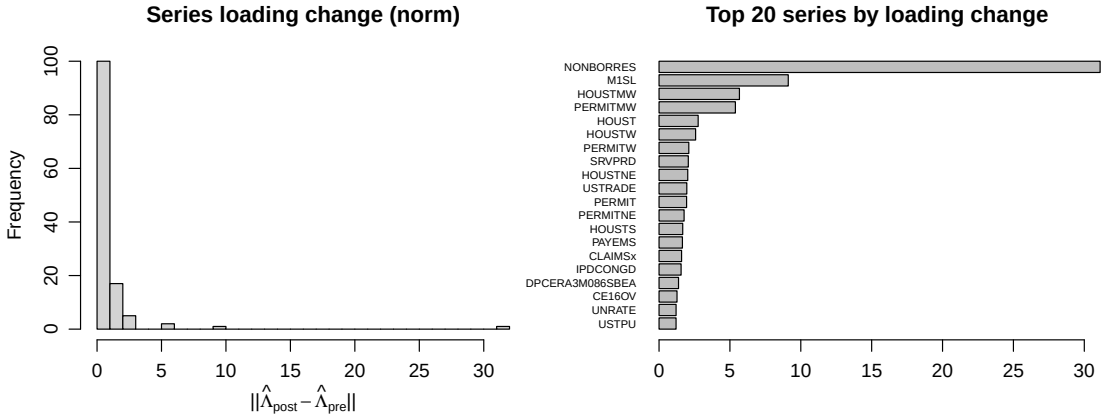

Figure G.1: FRED–MD loading-space diagnostics around the first alarm. Left: distribution of series-level loading-change norms after aligning loading spaces. Right: top series by loading-change norm. The post window begins at the earliest alarm month (2007–08).

[4]The capitalized labels are FRED series mnemonics (as used in FRED–MD): `NONBORRES` = Reserves of Depository Institutions: Nonborrowed; `M1SL` = M1 money stock; `HOUST` = New Privately-Owned Housing Units Started: Total Units (U.S.); `HOUSTMW`/`HOUSTNE`/`HOUSTW` = housing starts (total units) in the Midwest/Northeast/West Census regions; `PERMITMW`/`PERMITW` = housing units authorized by building permits (total units) in the Midwest/West Census regions; `SRVPRD` = All Employees, Service-Providing; `USTRADE` = All Employees, Retail Trade.